NASA CR-54070
TRW ER-5923

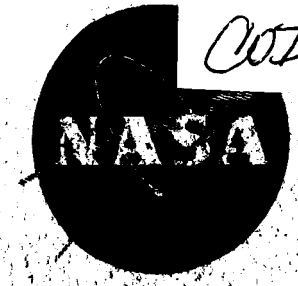

PROPELLANT FLOW METER FOR ION ROCKET SYSTEMS

By
Keith M. Montgomery

Prepared for
NATIONAL AERONAUTICS AND SPACE ADMINISTRATION
CONTRACT NAS 3-2515

TRW ELECTROMECHANICAL DIVISION
THOMPSON RAMO WOOLDRIDGE INC.
CLEVELAND, OHIO

NOTICE

This report was prepared as an account of Government sponsored work. Neither the United States, nor the National Aeronautics and Space Administration (NASA), nor any person acting on behalf of NASA:

A.) Makes any warranty or representation, expressed or implied, with respect to the accuracy, completeness, or usefulness of the information contained in this report, or that the use of any information, apparatus, method, or process disclosed in this report may not infringe privately owned rights; or

B.) Assumes any liabilities with respect to the use of, or for damages resulting from the use of any information, apparatus, method or process disclosed in this report.

As used above, "person acting on behalf of NASA" includes any employee or contractor of NASA, or employee of such contractor, to the extent that such employee or contractor of NASA, or employee or such contractor prepares, disseminates, or provides access to, any information pursuant to his employment or contract with NASA, or his employment with such contractor.

Request for copies of this report should be referred to

National Aeronautics and Space Administration
Office of Scientific and Technical Information
Attention: AFSS-A
Washington, D. C. 20546

NASA CR-54070
TRW ER-5923

FINAL REPORT

PROPELLANT FLOW METER
FOR
ION ROCKET SYSTEMS

by

Keith M. Montgomery

prepared for

NATIONAL AERONAUTICS AND SPACE ADMINISTRATION

June 15, 1964

Contract NAS 3-2515

Technical Management
NASA Lewis Research Center
Cleveland, Ohio
Spacecraft Technology
Procurement Section
R. H. Hieber
and
J. T. Kotnik

TRW ELECTROMECHANICAL DIVISION
Thompson Ramo Wooldridge, Inc.
New Product Research Department
23555 Euclid Avenue
Cleveland, Ohio 44117

FOREWORD

This report was prepared by the New Product Research Department of the Electromechanical Division of Thompson Ramo Wooldridge Inc., Cleveland, Ohio on Contract No. NAS3-2515. The contract was administered by the National Aeronautics and Space Administration, with Messrs. R. H. Hieber and J. T. Kotnik acting as contract monitors.

Studies presented in this report began in January 1963 and were concluded in April 1964. William C. Davis, Senior Engineering Specialist, and Patrick J. Lawlor, Project Engineer, were responsible for the development activity carried on at TRW, Inc. The chief contributors to the program were A. Koestel, thermal analyses, E. J. Yohman, electronic design, K. M. Montgomery, system analyses, design, and test, and E. L. Kubiak, test support.

PROPELLANT FLOW METER

for

ION ROCKET SYSTEMS

by: Keith M. Montgomery

ABSTRACT

23197

A heated fin anemometer vapor flow meter was designed to operate over a flow range of 10^{-4} to 5×10^{-2} gms/sec. with either cesium or mercury vapor at 840° F. A calibration system was developed and consisted of a boiler, superheater, metering orifice, desuperheater, and condenser. The design of the anemometer configuration was accomplished with the aid of a digital computer.

The expected flow rate response of the meter was obtained. In the low flow rate range (10^{-4} to 10^{-3} gms/sec.) the accuracy of the meter was limited by a drift on the meter readout. A discussion of this drift and suggestions for reducing it are included in the report. Author

TABLE OF CONTENTS

LIST OF ILLUSTRATIONS

LIST OF ILLUSTRATIONS (cont.)

PROPELLANT FLOW METER FOR ION ROCKET SYSTEMS

by Keith M. Montgomery

Thompson Ramo Wooldridge, Inc.

SUMMARY

A research and development program to design, build and test a propellant flowmeter for ion propulsion systems was conducted by TRW from January 1963, to April 1964.

Several minimal pressure drop metering concepts including head meters, radiation meters, gate meters, and thermal meters were considered for the application. A heated fin anemometer, with a temperature compensating reference element, was selected for development during the program.

Other thermal flowmeters, including a hot-wire anemometer, calorimeter flowmeter, and a thermocouple flowmeter were considered but rejected on the basis of anticipated insensitive flow response over the lower decade of the design flow rate range of 10^{-4} to 5×10^{-2} gms/sec. of either cesium or mercury vapor. Thermal analysis indicated that the heated fin design was equally applicable to either cesium or mercury service.

The flow sensing element was designed and optimized by an incremental heat balance technique, using a digital computor. The sensing element dimensions were:

Fin length (perpendicular to vapor flow)	= 2.50 in.
Fin width (parallel to vapor flow)	= 0.05 in.
Fin thickness	= 0.250 in.
Support post height	= 0.250 in.
Support post diameter	= 0.188 in.

Nichrome was used for the fin and boron nitride for the support post. Chromel-constantan thermocouples sensed vapor temperature on the heated and reference fins. The electrical input to the flow sensing fin was 0.18 BTU/hr for heating. A constant temperature salt bath was used to maintain the meter assembly at the design temperature of 840°F. The meter test and calibration rig consisted of a boiler, superheater, metering orifice, desuperheater, and condenser. By the proper choice of orifice and temperature setting on the rig components the flowmeter could be calibrated with either mercury or cesium vapor.

Experiments with mercury vapor indicated that the meter responded to changes in flow rate over the entire design flow range. The microvolt output of the system increased from -4 to -560 as the flow changed from 2×10^{-4} to 2×10^{-2} gms/sec. A polarity reversal and voltage deviation from 0 to + 40 to 0 microvolts was observed on the anemometer readout over the 3×10^{-4} to 3×10^{-3} gms/sec. flow rate range. This was accompanied by a no flow drift of 50 microvolts during the course of the calibration. To correct this, modification of the null balance circuitry was recommended.

The appendix of this report contains operating instructions for the calibrator rig, calibrator rig design and orifice calibration procedures.

1.0 INTRODUCTION

On January 1, 1963, Contract NAS3-2515 was awarded to TRW to develop a vapor flow meter suitable for ion engine testing to indicate cesium or mercury mass flow rates in the range of 10^{-4} to 5×10^{-2} gms/sec. The specific design objectives for the meter are listed as follows:

1. Being placed in the feed system line between the phase separator and the ionization chamber without interfering with the vapor flow or operation of the feed system. This would include no vapor-pressure drop across meter.
2. Operating continually for a period of at least 90 days or more without repair or test stoppage.
3. Monitoring a flow rate which might be from 10^{-4} gms/sec. to 5×10^{-2} gms/sec.
4. Operating at a temperature of 450°C (840°F). The operating pressure of the vapor in the feed line is expected to be:
   (1) For cesium, between 1 and 25 torr
   (2) For mercury, between 0.1 and 1.0 torr
5. Operating with an applied potential of 10 kv above ground without danger to the operator.
6. Having a remote read-out of the flow rate on a scale marked in gms/sec.
7. Operating in an atmosphere of 10^{-7} to 750 torr without leakage of the propellant.
8. Operating with an accuracy of five per cent or better of the full scale reading of the remote read-out.
9. This reading should be 90 per cent of the flow rate on remote read-out within twenty seconds after propellant flow reaches full rated flow from a no flow condition and reading total flow within sixty seconds.
10. Simple and quick calibration, with the need for recalibration to be at a miniumum.
11. The remote read-out should cover one order of magnitude of flow per scale and it should have at least three selections of scales to cover the above mentioned range.
12. It is not necessary that the meter be capable of monitoring more than an order of magnitude range of flow for each installation.

This report is a technical discussion of metering concepts in general and the thermal analyses considered in designing the vapor flow meter developed under this contract effort. A review of meter requirements and reasons for choosing a heated fin anemometer as the flow sensing element are presented. Detailed thermal analyses, including a digital computer program for optimizing the anemometer configuration are reviewed. The resulting meter design, test results, and conclusions are subsequently discussed.

The final paragraphs of Section 2 deal with the complete meter configuration and its attendant hardware.

Laboratory results of the systems operations are presented in Section 3. From this, conclusions of the experimental results and recommendations for possible future development effort are discussed.

The appendix of this report contains a description of the calibrator and its operating procedures. Also included are the orifice calibration data which are subsequently used when calibrating the anemometer with mercury or cesium. The design of the calibration rig is also presented. This covers system analyses of the rig boiler, superheater, orifice, desuperheater, and condenser.

2.0 TECHNICAL DISCUSSION - SYSTEM DEVELOPMENT

2.1 Metering Concepts

Several rate metering concepts were considered which could satisfy the design objectives listed in Section 1.0. In rate meters or rate measuring processes, the functioning of the primary metering element depends upon some property of the fluid other than, or in addition to, volume and mass. These properties may include kinetic energy (head meters), radioactive properties (radiation meter), momentum (gate meters), specific heat (thermal meters), and the like. A secondary element is always included which utilizes a change in the property concerned for obtaining an indication of the flow rate and generally embodies some device which draws the necessary inferences automatically, so that the observer can read the result from a dial or chart.

After critically reviewing each of these specific types of flow indicators, a thermal meter was finally chosen as the instrument that would be most likely to meet the design objectives.

2.1.1 Thermal Flow Meter Analysis

In the field of flow measurement the term thermal meter refers to an instrument in which the transfer of heat to or from the fluid constitutes the basic part of the metering action.

Thermal meters are generally classed in two groups:

Group 1 - Meters in which the effect of a fluid stream on a hot body is involved, and

Group 2 - Meters in which the effect of a measurable quantity of heat transferred to or from the fluid stream is involved.

Thermal meters of the first group depend on careful calibration for satisfactory operation. In this group, the hot wire anemometer is a notable example and several forms of this instrument have been developed for the measurement of vapor stream velocities and velocity fluctuations. In this specialized meter, a relatively slight movement of gas and the resulting cooling of the wire effects the wire's electrical resistance.

Correlation of gas velocity with this change in resistance may be made with the use of a constant voltage circuit or a constant resistance circuit.

For meters of the second group to operate satisfactorily it is necessary to have:

1. A knowledge, to the required degree of accuracy, of the specific heat at constant pressure of the fluid stream being measured.
2. Efficient means of transferring heat to the fluid stream and of measuring the heat input.
3. Sufficiently accurate means of measuring or controlling the temperature change of the fluid stream due to the transfer of heat.

The first thermal flow meter to be reviewed is the vapor calorimeter flow meter (Group 2) shown schematically in Figure 2-1 (A). In this design, heat is transferred radially from the vapor stream through a thermopile calorimeter. The calorimeter monitors heat flux and records this flux as a suitable microvolt signal. Thermocouples located at the inlet and discharge of the calorimeter record vapor temperature drop due to the heat transfer. Flow rate and fluctuations in flow rate may be then determined from

$$m = \frac{Q}{C_p \Delta t}$$

where

Q = radial flux

Δt = stream temperature change

C_p = vapor specific heat

(A complete list of symbols and their appropriate units is presented as Appendix E of this report).

A disadvantage to the calorimeter design is the difficulty of obtaining reproducible temperature readings in the downstream thermocouple.

The insert in Figure 2-1(A) shows a typical boundary layer effect in the laminar regime. This boundary is caused by the cooling effect of the calorimeter. Obtaining meaningful downstream temperatures requires positioning the thermocouple in the laminar boundary at a point where time-wise constancy of temperature readings can be assured.

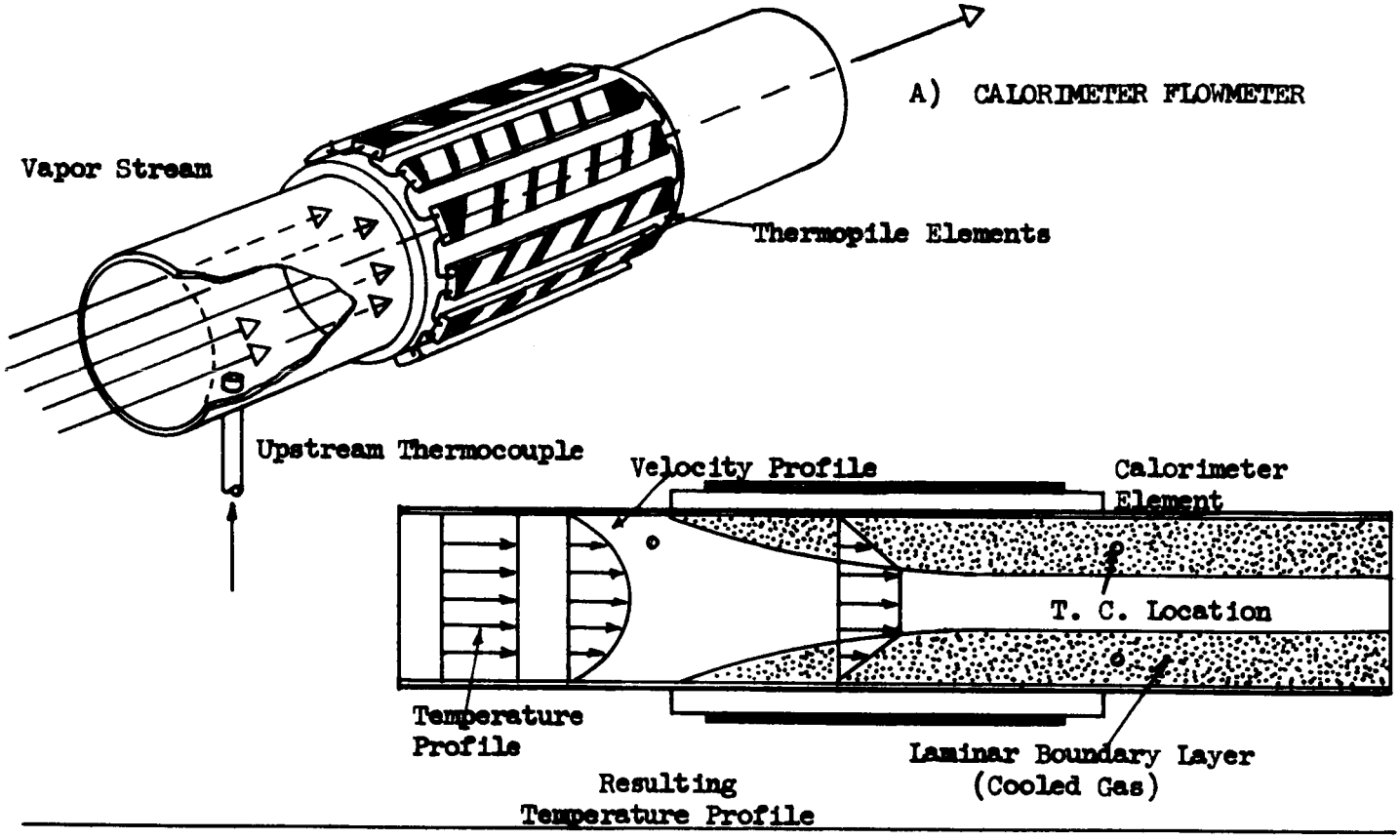
A) CALORIMETER FLOWMETER
Vapor Stream
Thermopile Elements
Upstream Thermocouple
Velocity Profile
Calorimeter Element
T. C. Location
Temperature Profile
Laminar Boundary Layer (Cooled Gas)
Resulting Temperature Profile

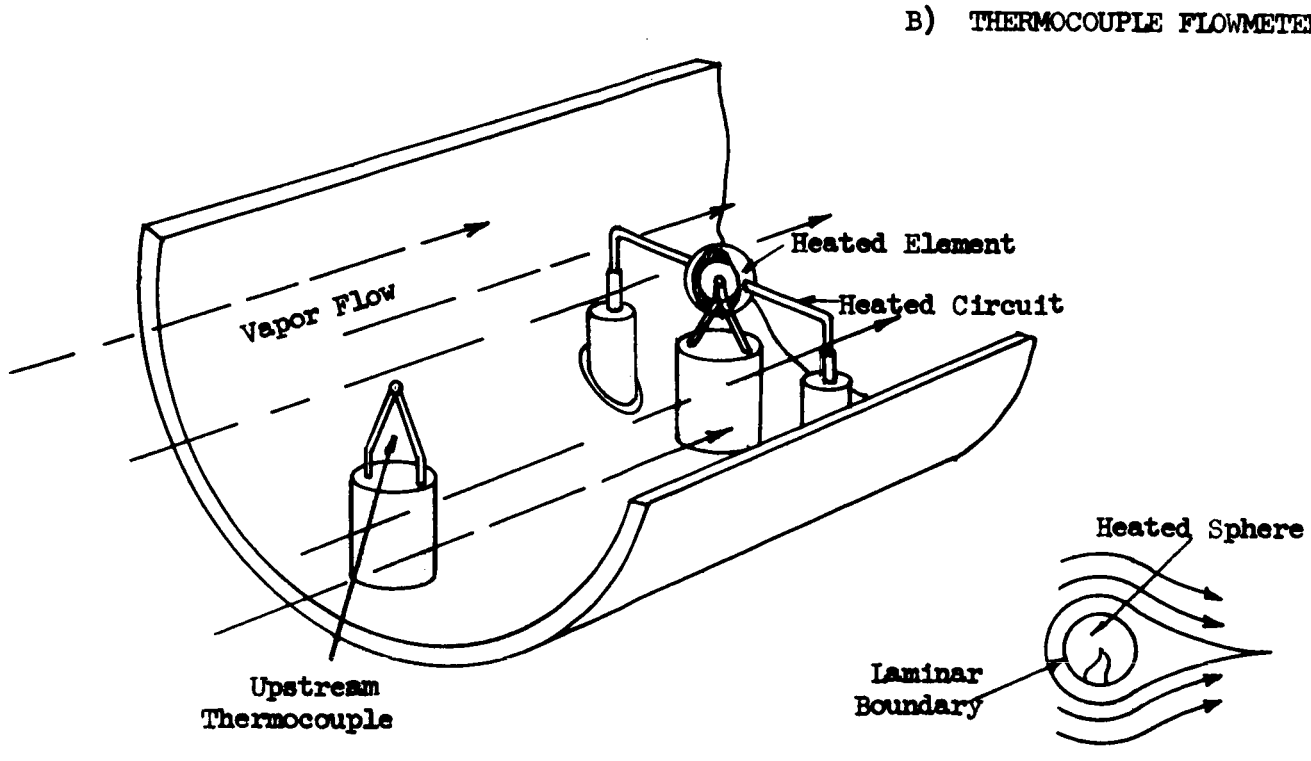
B) THERMOCOUPLE FLOWMETER
Vapor Flow
Heated Element
Heated Circuit
Upstream Thermocouple
Heated Sphere
Laminar Boundary

Figure 2-1

The calorimeter thermopile itself has been shown to be an accurate device, capable of registering small heat fluxes (90 BTU/hr) and monitoring small flow rates (1×10^{-6} lbs/sec). It is, however, a complex device and could suffer reliability drawbacks in unattended operation for ninety days.

One final disadvantage involves the effect of the calorimeter on the engine system. The thermopile operates on a steady radial heat flux from vapor line to surroundings. In effect this flux cools the vapor stream. To minimize transient effects from the surrounding it would be necessary to include a system of guard heaters, thereby establishing a steady environmental temperature.

Another precision thermal meter which was seriously considered is the heated thermocouple (Figure 2-1(B)). In this approach, a thermocouple is heated externally by an appropriate circuit. This couple, together with an unheated one upstream, is placed into the flow path. Heater current is adjusted so that the measuring thermocouple is a few degrees higher in temperature than the tube environment.

In operation, changes in the flow rate cause the vapor to remove more or less heat from the thermocouple. This fluctuation in the heat transferred to the flowing vapor is reflected by a change in thermocouple output. The unheated thermocouple upstream acts as a compensating device for changes in vapor temperature. Should this temperature change without a change in flow, the adjusted reading of the upstream couple would be used in an appropriate compensating circuit to correct an otherwise erroneous meter output.

The serious drawback to this design can be best seen by examining the thermodynamic relationships involved:

$$Q_{in} - Q_{out} = Q_{storage} \qquad (1\text{-}2)$$

$$Q_{in} - \pi d^2 h\Delta t = \frac{\pi d^3}{6} \rho_m C_m \frac{dT}{d} \qquad (1\text{-}3)$$

$$Q_{in} = \frac{\pi d^3}{6} \rho_m C_m \frac{dT}{d\theta} + \pi d^2 \frac{hd}{K_v} \Delta t \qquad (1\text{-}4)$$

where

Q_{in} = required heater circuit power

Q_{out} = heat transferred to flowing vapor

$Q_{storage}$ = heat required to bring thermocouple up to operating temperature (this is a transient term)

d	= diameter of heater sphere
ρ_m	= electrical resistivity of sphere
$dT/d\theta$	= change in sphere temperature with time
h	= heat transfer coefficient; sphere to gas
K_v	= thermal conductivity of streaming vapor

The drawback becomes apparent in reviewing Figure 2-2. Here Reynolds number has been plotted against the Nusselt number for a sphere (Nusselt number = hd/K_v). The values plotted are not theoretical but actually observed experimental results. It is seen in this figure that as the Reynolds number approaches a lower limit of 9 the relationship changes radically and the heat transfer coefficient becomes insensitive to changes in Reynolds number. This flattening out of the curve means that at lower velocity ranges the hd/K_v term of equation 1-4 is essentially velocity insensitive. Unfortunately for the intended meter application forced convection of heat, sensitive to velocity fluctuations, is the primary basis for meter operation. Calculation indicates that the "flattening out" of the curve in Figure 2-2 occurs well above the lower limit of the required velocities. This eliminates the instrument from further evaluation.

The hot wire anemometer has been used successfully in applications similar to the intended one. Unfortunately it suffers from the same insensitivity characteristic described in the thermocouple meter. The data of Figure 2-3 is similar to 2-2; it is a plot of observed Nusselt number versus Reynold's number for a cylinder in gas flow. These results appear to apply analogously for gas flow axial or normal to the wire axis. As in Figure 2-2, the curve tends to flatten at lower values of velocity. Analyses indicate that at the lower velocity ranges specified in the application, an area of insensitivity will result.

The flow meter to be developed is shown schematically in Figure 2-4. This unit is properly classed as a thermal device which measures the effect of the fluid stream on a hot body. It consists of a heated fin or plate placed axial to the vapor flow. A thermocouple is attached to the fin body. When in operation, the fin is carefully maintained at some nominal temperature above the environment to reduce radiation losses to a minimum.

EXPERIMENTAL DATA RESULTS

NUSSELT NUMBER vs REYNOLDS NUMBER

SPHERICAL CONFIGURATION

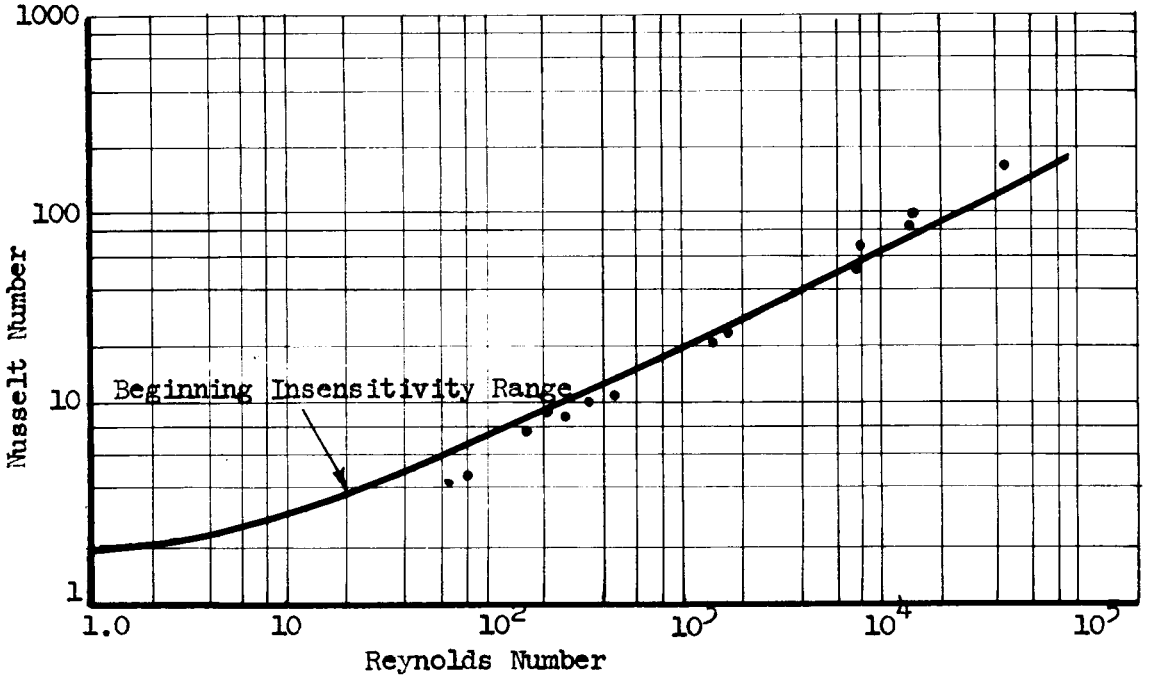

Figure 2-2

EXPERIMENTAL RESULTS
NUSSELT vs REYNOLDS NUMBERS
FOR FLOWING FLUIDS NORMAL
TO A SINGLE CYLINDER

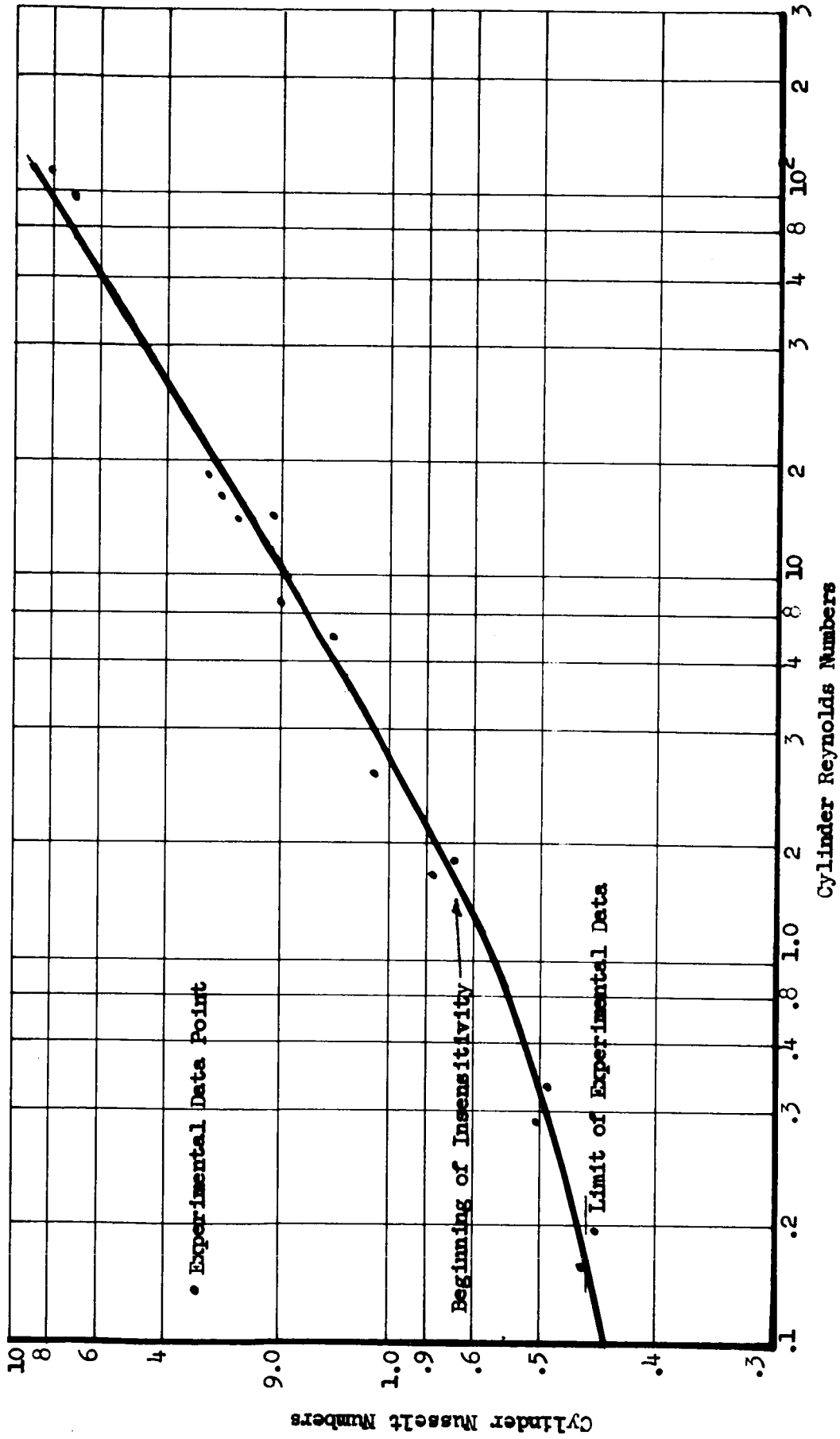

Figure 2-3

HEATED FIN FLOWMETER

SCHEMATIC

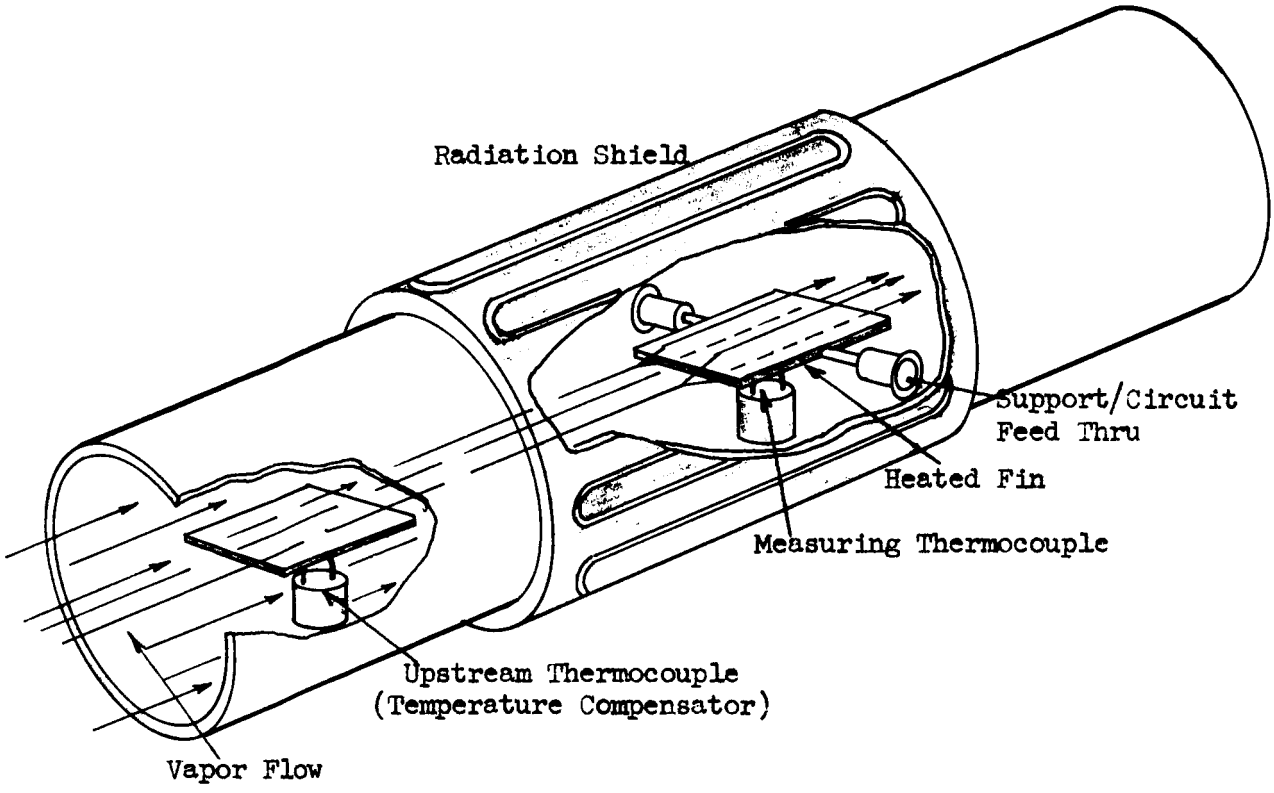

Figure 2-4

As the vapor flow fluctuates the heat transfer conditions from the fin surface, across the boundary layer to the vapor, produce a change in fin temperature which is recorded by the surface thermocouple. Upstream of the hot fin a second fin and thermocouple have been mounted in the vapor transfer line. This fin remains unheated except by the effects of the system environment.

This upstream fin and thermocouple acts as a vapor temperature compensating device. Should vapor superheat temperature change without a flow rate fluctuation the cooling (or heating) effects of the gas passing over this fin is measured by the attached thermocouple. This millivolt output is used to compensate for any erroneous reading of the fin thermocouple arising from the vapor temperature variation.

A radiation shield is added to reduce inaccuracies due to radiation changes. This shield is shown in the illustration as a heater placed at the tube wall and is held at the same temperature as the reference fin surface. The shield is so placed that its boundary layer does not interfere with the critical heat transfer occurring at the fin surfaces.

The heated fin meter was chosen for development principally because the convection heat transfer coefficient for this geometry varies linearly with vapor velocity over the entire design flow rate range. The overall heat transfer coefficient in terms of the Nusselt number for a fin configuration is shown in Figure 2-5. This illustration plots heat transfer data versus Reynolds number. As a point of illustration the same plot for a sphere has been superimposed in the illustration. As mentioned earlier, experimental data for the sphere has shown that as vapor velocity decreases a limit is reached beyond which heat transfer rates are essentially insensitive to velocity changes. At this point the thermal device can no longer meter flow accurately. This insensitivity is shown as the definite flattening out of the curve at lower Reynolds numbers. It is noted that this insensitive range occurs within the low flow rate meter design specifications thereby eliminating the spherical and cylindrical configuration from further consideration.

EXPERIMENTAL DATA RESULTS
FOR NUSSELT NUMBER vs REYNOLDS NUMBER
FIN HEAT EXCHANGER

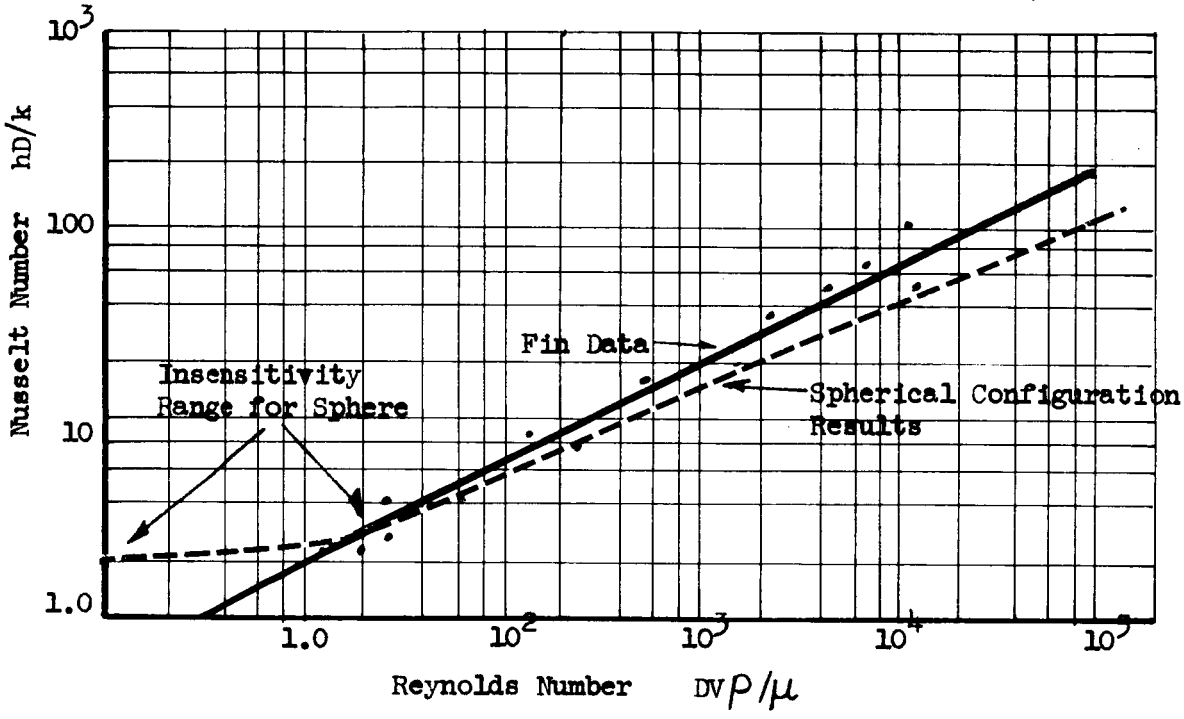

Figure 2-5

The flat fin meter however is definitely linear (curve of Nusselt versus Reynolds numbers) to well below the lowest specified velocities.

In fact, this heat transfer correlation curve theoretically has no lower velocity limit. It is this ability to transfer heat at extremely low velocities which has led to the recommendation of the fin configuration.

2.2 Anemometer Sensing Fin Design

The objectives in designing the anemometer fin are listed as follows:

1. Acceptable performance in either mercury or cesium environment.
2. Maximum thermal output change from minimum vapor velocity change.

The following discussion is presented to indicate how each of these objectives were met.

2.2.1 Establishment of Meter Performance Characteristics

Referring to Figure 2-5, the heat transfer coefficient (h) in the Nusselt number is the prime factor measured by the anemometer fin. In the insensitive range of the sphere the h values remain essentially constant, while they tend to decrease linearly with flow for the fin data. The number h is calculated from the relation

$$Nu_x = (3.31 \times 10^{-1}) \quad \sqrt[3]{Pr} \quad \sqrt{Re_x} \qquad (1) \qquad (1\text{-}5)$$

where Nu_x = the Nusselt number with the characteristic linear dimension parallel to the direction of flow.

Pr = Prandtl number

Re_x = the Reynolds number with the characteristic linear dimension parallel to the direction of flow.

For both cesium and mercury at 840°F and 1.0 torr flowing at 10^{-4} gms/sec through a one inch I.D. tube, the following values were calculated. A fin width (x) of 0.05 inches was used for the calculations.

---

(1) TRW Report No. ER-5078

Flowing Media	Pr	Re_x (1)	Nu_x	(BTU/hr ft^2 F)
Mercury	6.53×10^{-1}	3.56×10^{-3}	1.73×10^{-2}	2.70×10^{-2}
Cesium	4.22×10^{-1}	2.03×10^{-2}	3.58×10^{-2}	2.28×10^{-2}

$Pr = C_p \mu/k$ (1-6) $Re_x = xv \rho/\mu$ (1-7)

Because the magnitude of the heat transfer coefficient is the same for both mercury and cesium vapors (under similar flow conditions) the anemometer concept is equally applicable to either of the specified vapors. For this reason all design calculations were performed for the data with cesium vapor. The calculations could have been performed equally as well with the data for mercury vapor.

2.2.2 Meter Design Procedure

Referring to Figure 2-4, a design procedure was formulated to establish the following meter parameters:

1. anemometer fin length
2. anemometer fin width
3. anemometer fin thickness
4. support post diameter
5. support post height

In addition, compatible materials of construction were considered. The design objective was to maximize the anemometer output (the net microvolt signal from the thermocouple system) for a selected combination of geometric and metallurgical meter parameters.

Because of the magnitude of the Reynolds numbers encountered in the flow systems, all three forms of heat transfer ---- conduction, convection, and radiation ---- had to be considered.

(1) Data taken from WADC Technical Report 59-598

Furthermore, natural as well as forced convection was included in the calculations. Therefore, the design technique was formulated on the basis of a digital computer program where the input data were the anemometer parameters and vapor velocity and the output the anemometer response (vapor velocity versus degree of fin cooling).

The diagram in Figure 2-6 was used as the mathematical model for the computer study. Each of the numbered points located within the increments are referred to as nodal points. A heat balance is written for each nodal point with the temperature as the unknown. This results in twenty simultaneous algebraic equations with twenty unknowns. The solution of these equations provides the necessary data to plot vapor velocity versus fin temperature.

These equations are listed as follows:

1) $(T_o - T_1)\psi_{1A} + (T_2 - T_1)\psi_1 + (T_6 - T_1)\psi_2 + Q_{w\ gen} = 0$
2) $(T_3 - T_2)\psi_1 + (T_1 - T_2)\psi_1 + (T_7 - T_2)\psi_2 + Q_{w\ gen} = 0$
3) $(T_4 - T_3)\psi_1 + (T_2 - T_3)\psi_1 + (T_8 - T_3)\psi_2 + Q_{w\ gen} = 0$
4) $(T_5 - T_4)\psi_1 + (T_3 - T_4)\psi_1 + (T_9 - T_4)\psi_2 + Q_{w\ gen} = 0$
5) $(T_{16} - T_5)\psi_{11} + (T_4 - T_5)\psi_1 + (T_{10} - T_5)\psi_2 + Q_{w\ gen} = 0$
6) $(T_o - T_6)\psi_{3A} + (T_7 - T_6)\psi_3 + (T_1 - T_6)\psi_2 + (T_{11} - T_6)\psi_4 = 0$
7) $(T_6 - T_7)\psi_3 + (T_2 - T_7)\psi_2 + (T_8 - T_7)\psi_3 + (T_{12} - T_7)\psi_4 = 0$
8) $(T_7 - T_8)\psi_3 + (T_9 - T_8)\psi_3 + (T_3 - T_8)\psi_2 + (T_{13} - T_8)\psi_4 = 0$
9) $(T_8 - T_9)\psi_3 + (T_{10} - T_9)\psi_3 + (T_4 - T_9)\psi_2 + (T_{14} - T_9)\psi_4 = 0$
10) $(T_{16} - T_{10})\psi_{10} + (T_9 - T_{10})\psi_3 + (T_5 - T_{10})\psi_2 + (T_{15} - T_{10})\psi_4 = 0$
11) $(T_6 - T_{11})\psi_4 + K_1 (T_o - T_{11})\psi_5 + (T_v - T_{11})\psi_6 = 0$
12) $(T_7 - T_{12})\psi_4 + K_1 (T_o - T_{12})\psi_5 + (T_v - T_{12})\psi_6 = 0$
13) $(T_8 - T_{13})\psi_4 + K_1 (T_o - T_{13})\psi_5 + (T_v - T_{13})\psi_6 = 0$
14) $(T_9 - T_{14})\psi_4 + K_1 (T_o - T_{14})\psi_5 + (T_v - T_{14})\psi_6 = 0$
15) $(T_{10} - T_{15})\psi_4 + K_1 (T_o - T_{15})\psi_5 + (T_v - T_{15})\psi_6 = 0$

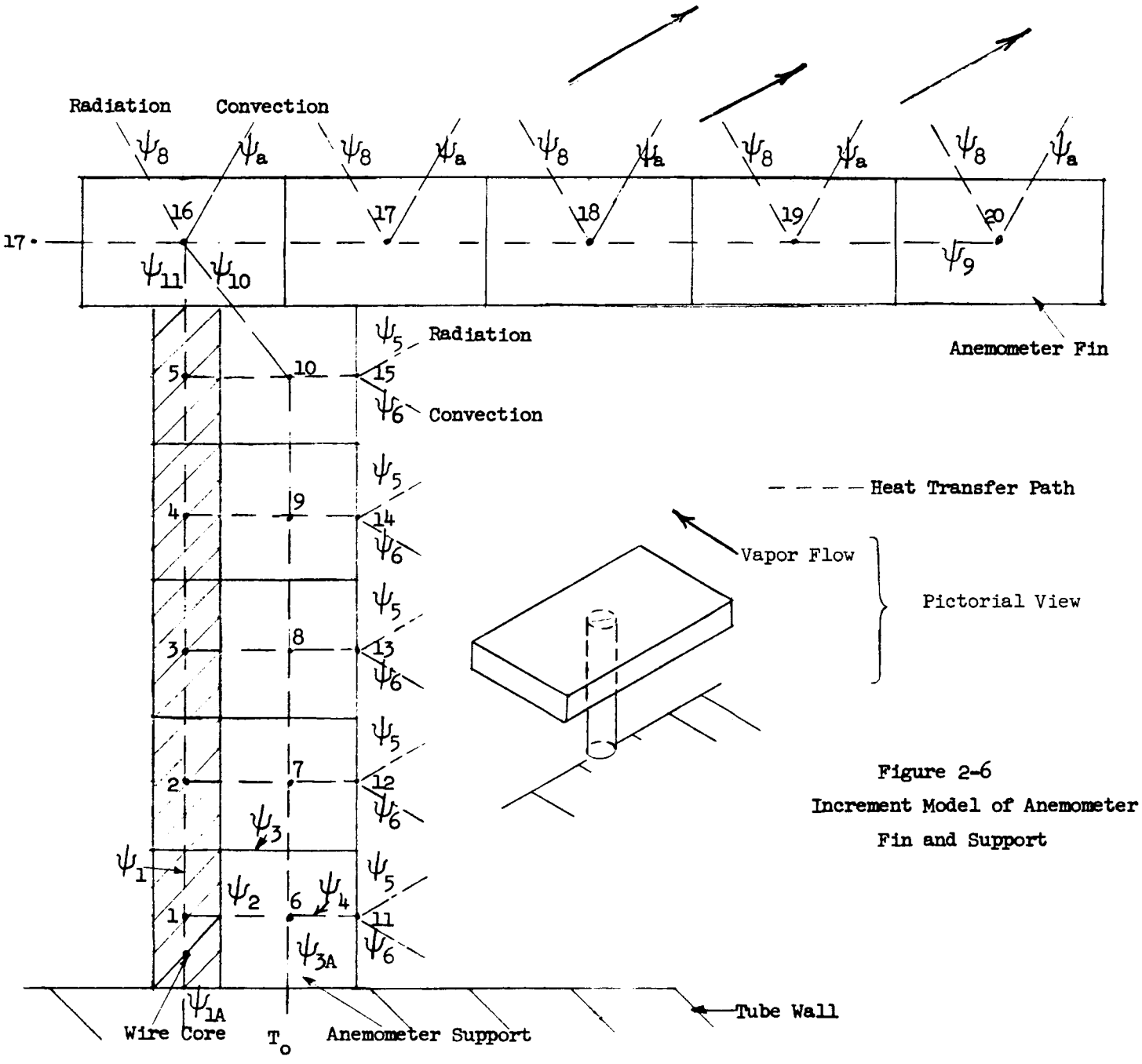

Figure 2-6
Increment Model of Anemometer
Fin and Support

16) $2\,(T_{17} - T_{16})\psi_9 + K_1\,(T_o - T_{16})\psi_8 + (T_v - T_{16})\psi_a + (T_5 - T_{16})\psi_{11} + (T_{10} - T_{16})\psi_{10} + Q_{gen} = 0$

17) $(T_{16} - T_{17})\psi_9 + (T_{18} - T_{17})\psi_9 + K_1\,(T_o - T_{17})\psi_8 + (T_v - T_{17})\psi_a + Q_{gen} = 0$

18) $(T_{17} - T_{18})\psi_9 + (T_{19} - T_{18})\psi_9 + K_1\,(T_o - T_{18})\psi_8 + (T_v - T_{18})\psi_a + Q_{gen} = 0$

19) $(T_{18} - T_{19})\psi_9 + (T_{20} - T_{19})\psi_9 + K_1\,(T_o - T_{19})\psi_8 + (T_v - T_{19})\psi_a + Q_{gen} = 0$

20) $(T_{19} - T_{20})\psi_9 + K_1\,(T_o - T_{20})\psi_8 + (T_v - T_{20})\psi_a + Q_{gen} = 0$

The ψ equations (defined as heat flux product equations) are further defined as:

$$\psi_1 = \frac{k_w\,\pi d_w^2}{4h}$$

$$\psi_{1A} = \frac{k_w\,\pi d_w^2}{2h}$$

$$\psi_2 = \frac{\pi k_s\,h\,(D + 3d_w)}{D - d_w}$$

$$\psi_3 = \frac{\pi k_s\,(D^2 - d_w^2)}{4h}$$

$$\psi_{3A} = \frac{\pi k_s\,(D^2 - d_w^2)}{2h}$$

$$\psi_4 = \pi h\,k_s\,\frac{(3D + d_w)}{(D - d_w)}$$

$$\psi_5 = \sigma F \pi Dh$$

$$\psi_6 = B\pi Dh; \quad B = \phi\left(\frac{DB}{k_f}, \frac{D v_f \rho_f}{\mu_f}\right)$$

$$\psi_a = 4N \left(\frac{1}{\sqrt{w}} \pm R\sqrt{w}\right) xw$$

$$N = M\sqrt{v_f \rho_f / \mu_f}$$

$$M = k_f (3.31 \times 10^{-1}) (Pr)^{1/3}; \quad Pr = \frac{C_p \mu_f}{k_f}$$

$$R = \frac{g\beta \Delta TC}{3 v_f^2}$$

$$C = \phi(pr)$$

$$\psi_8 = 2 F wx$$

$$\psi_9 = \frac{k_p wz}{x}$$

$$\psi_{10} = \frac{k_s \pi (D^2 - d_w^2)}{2h}$$

$$\psi_{11} = \frac{2k_w xw}{h}$$

Summing the terms in equations 1 to 20 and equating them to zero defines the equalibrium or steady state rather than the transient operating conditions of the anemometer.

T_x $(0 < x \leq 20)$ = Nodal temperature at point x.

T_o = Meter wall temperature (840°F).

ψ = A mathematical term defined as the heat flux product. This ψ term is the product of the heat transfer coefficient at the nodal point times the area through which heat transfer occurs. The path of heat conduction along with the appropriate ψ value representing the heat conduction is shown in Figure 2-6.

$Q_{w\ gen}$ = Internal heat generation by current passing through the lead wires to the anemometer fin.

K_1 = Radiation constant.

T_v = Vapor temperature. (840°F)

Q_{gen} = Heat generation in the anemometer fin.

k_w = Thermal conductivity of the heater and lead wire.

d_w = Lead wire diameter.

h = Incremental height of the anemometer support member

D = Support member diameter.

k_s = Thermal conductivity of support member.

σ = Stefan-Boltzman radiation constant.

F = Radiation view factor.

B = Convection heat transfer coefficient (Reference: Figure 2-8)

k_f = Thermal conductivity of flowing vapor.

v_f = Linear velocity of flowing vapor.

ρ_f = Density of flowing vapor.

μ_f = Viscosity of flowing vapor.

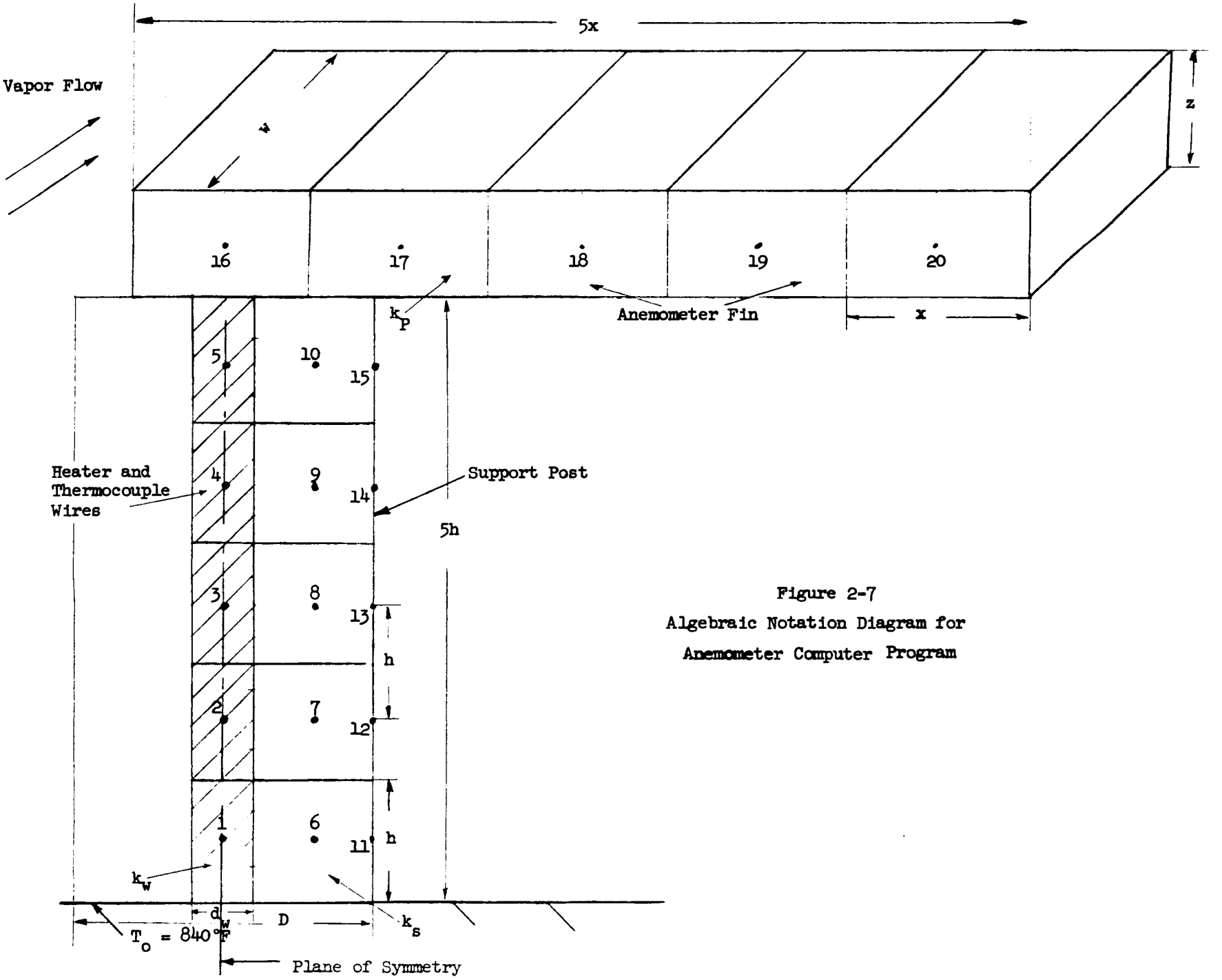

Figure 2-7
Algebraic Notation Diagram for
Anemometer Computer Program

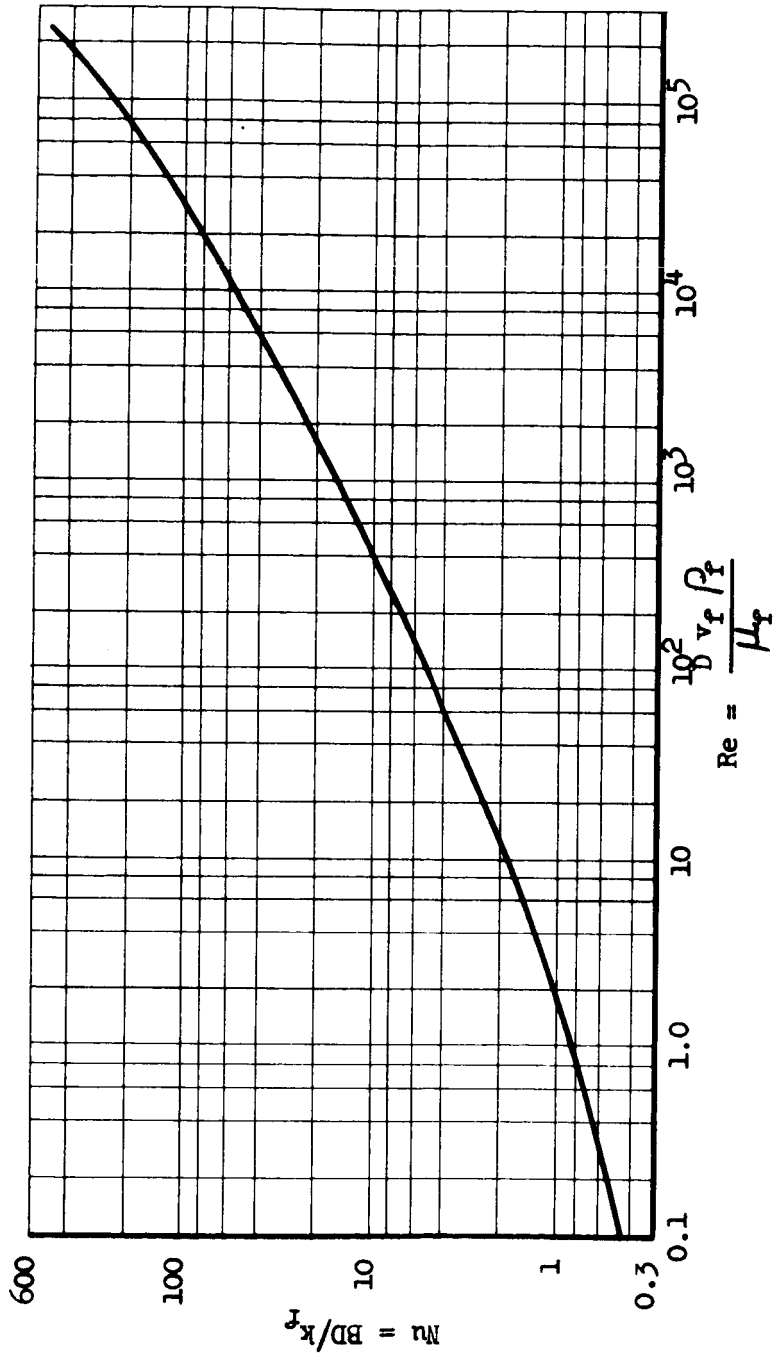

Figure 2-8

Average Nusselt number vs. Reynolds number for a circular cylinder in air, placed normal to the flow. (From McAdams (1954)).

w = Anemometer fin width.

x = Incremental anemometer fin length.

Pr = Prandtl number.

C_p = Specific heat of flowing vapor.

g = Dimensional constant (32.2 ft lb_m/lb_f sec^2).

β = Thermal expansion coefficient or bulk modulus.

ΔT = Temperature difference between the heated anemometer fin and the flowing vapor.

C = A number that is a function of the Prandtl number. (Reference: Figure 2-9).

z = Anemometer fin thickness.

k_p = Anemometer fin thermal conductivity.

At steady state conditions for each of the increments, the heat transferred into the nodal point plus the heat generated at the nodal point is equal to the heat being transferred away from the nodal point. All heat transfer modes (conduction, convection, and radiation) are considered. Terms with ψ_1, ψ_{1A}, ψ_2, ψ_3, ψ_4, ψ_9, ψ_{10}, and ψ_{11} are conduction terms. Radiation terms contain ψ_5 and ψ_8 and convective terms contain ψ_6 and ψ_a. The heat transfer path over which each of these ψ terms apply is shown in Figure 2-6.

The radiation constant (K_1) is determined by the following consideration.

Heat transfer by radiation from point 16 to the tube wall may be expressed as

$$(T_o^4 - T_{16}^4) \sigma F A = h_r (T_o - T_{16}) A \qquad (1\text{-}8)$$

h_r = Radiation heat transfer coefficient

A = Surface area from which radiation is occurring

Radiation is assumed to occur only between the anemometer fin and the meter walls and not between the fin and the vapor.

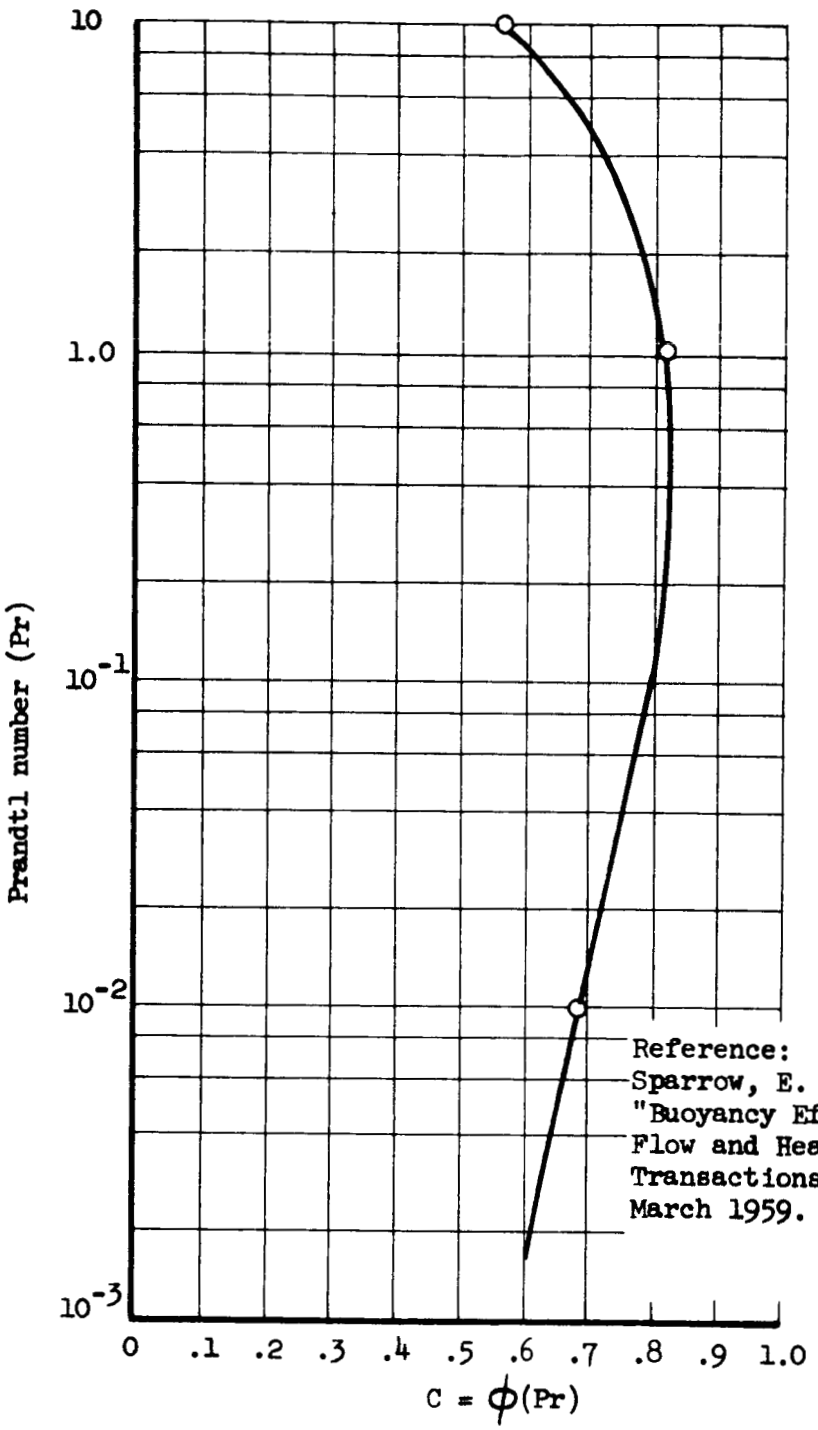

Reference:
Sparrow, E. M., and Gregg, J. L., "Buoyancy Effects in Forced Convection Flow and Heat Transfer", Jl of Appl Mech. Transactions of the ASME, p. 133, March 1959.

Figure 2-9
Prandtl Number Function Plot

Equation 1-8 can be simplified to read:

$$h_r / \sigma F = (T_o^2 + T_{16}^2)(T_o + T_{16}) \qquad (1\text{-}9)$$

The temperature relationship (the right side portion of Equation 1-9) is defined to be K_1. Assuming plate temperature (T_{16}) to be in the vicinity of 890°F (1350°R) and the wall temperature to be 840°F (1300°R), K_1 equals

$$K_1 = \left[(1300)^2 + (1350)^2\right] \quad \left[(1300) + (1350)\right]$$

$$K_1 = 9.3 \times 10^9 \ °R^3$$

Applying this constant to the radiation terms of the calculations reduces the order of the unknown temperatures from the fourth power to the first power, and thereby establishes a series of simultaneous linear first order equations. The assumption is made that the fin temperature will always be 890°F -- an assumption verified by computer results. The degree to which this assumption is in error is a measure of the inaccuracy of the computer solution.

The term ψ_a considers the convective heat transfer effects resulting from the vapors flowing over the anemometer fin. The basic relations for the heat transfer coefficient were taken from a paper by Sparrow and Gregg[1]. When the flow of heat is opposite to the direction of the gravity vector the plus term is used in the ψ_a formulation. When the flow of heat is parallel to the gravity vector the minus term is used.

The heat generation terms (Q_{gen} and $Q_{w\ gen}$) in the computer equations were calculated from electrical resistance heating relationships. The term Q_{gen} (the heat generation in the anemometer fin) is calculated as:

$$Q_{gen} = i^2 R_p \qquad (1\text{-}10)$$

---

[1]Sparrow, E. M., and Gregg, J. L., "Buoyance Effects in Forced Convection Flow and Heat Transfer", JI. of Appl. Mech., Transactions of the ASME, p. 133, March 1959.

where

i = The current flowing through the anemometer fin.

R_p = The resistance of the anemometer fin.

For $Q_{w\ gen}$ (the heat generation in the heater lead wires)

$$Q_{w\ gen} = i^2 R_w$$

where

R_w = The resistance of the heater lead wires within the support post.

Equations (1-1) through (1-20) were solved with an IBM 7070 digital computer.

2.2.3 Computer Program Results

In designing an optimum anemometer configuration, the following geometric variables were to be specified:

x (fin length)
w (fin width)
z (fin thickness)
D (support post diameter)
h (support post height)

To optimize the flow meter, a set of values for the variables was chosen. Then the temperature magnitudes at each of the nodal points were calculated for different vapor velocity values over the flow rate range. Next, an average fin temperature was determined for each velocity point. From this data, a plot was made of average fin temperature minus vapor temperature (the cooling effect of the vapors) versus vapor velocity. The greater the slope of this curve, the more sensitive is the meter to indicate vapor velocity changes. This sensitivity curve was plotted for different combinations of geometric variables until a maximum sensitivity was obtained.

The following results were obtained from the computer studies. Referring to Figures 2-6 and 2-7, the numerical values used in the calculations were:

Support post diameter	= 0.0625 inches (D)
Support post height	= 0.5 inches (5h)
Fin thickness	= 0.005 inches (z)
Fin width	= 0.05 inches (w)
Fin length	= 3.14 inches (9x)

In addition, the thermocouple and heater lead wires were 0.005 inches in diameter and were considered to have the thermal conductivity of constantan (15.5 BTU/hr ft °F). Here it was intended to use the fin as the thermocouple itself. Later it was decided to attach a thermocouple wire directly to a nichrome fin; thereby eliminating the necessity of a bimetallic piece. For this calculation the wall temperature and vapor temperature were respectively 879°F and 840°F. Later it was determined that the wall temperature and vapor temperature should be identical. This minimized vapor temperature fluctuations within the meter.

Throughout the entire flow range (10^{-4} to 5×10^{-2} gms/sec.) the heater input to the fin was constant and equal to 1.21×10^{-3} BTU/hr. All calculations were performed for cesium vapor. Magnesium oxide was used as the fin support in the calculations. Boron nitride because of its machineability was used in the final meter design.

Because of the low flow rate requirements in the design specifications, it is necessary to minimize or control all extraneous heat losses. Therefore, in the radiation calculations the emissivity of the fin and post support was taken as 0.1. To accomplish this physically, it was necessary to have a highly reflective surface over the anemometer fin. This was accomplished by polishing the fin to a high degree of surface reflectivity.

For a cesium flow rate of 5×10^{-2} gms/sec. the following temperatures were calculated:

T_1 = 875.91801 °F		T_{11} = 875.44625	
T_2 = 871.95732		T_{12} = 871.63491	
T_3 = 869.57080		T_{13} = 869.34322	
T_4 = 868.29762		T_{14} = 868.12058	
T_5 = 867.89524		T_{15} = 867.72305	
T_6 = 875.78432		T_{16} = 867.89654	
T_7 = 871.86180		T_{17} = 867.96317	
T_8 = 869.50326		T_{18} = 868.00927	
T_9 = 868.24488		T_{19} = 868.03825	
T_{10} = 867.83581		T_{20} = 868.05222	

Note: Subscripts apply to nodal point numbers in Figure 2-6.

Even though the number of significant figures in the answer are more than those used in the input data, the difference between many of these values (i.e., $T_{19} - T_{18}$) is sufficiently small that all of the figures must be used in order to obtain an accurate answer.

These calculations were repeated for four different flow rates (given both as mass and linear velocity through a one inch tube).

$\dot{m}$ (cesium) (gm/sec)		v (ft/sec)
5×10^{-2}	$\approx$	3.86
5×10^{-3}		2.98
10^{-3}		1.35
10^{-4}		0.193

The calculated sensitivity curve for an anemometer fin of this geometry over the design flow rate range is shown in Figure 2-10.

Figure 2-10

ANEMOMETER SENSITIVITY CURVE

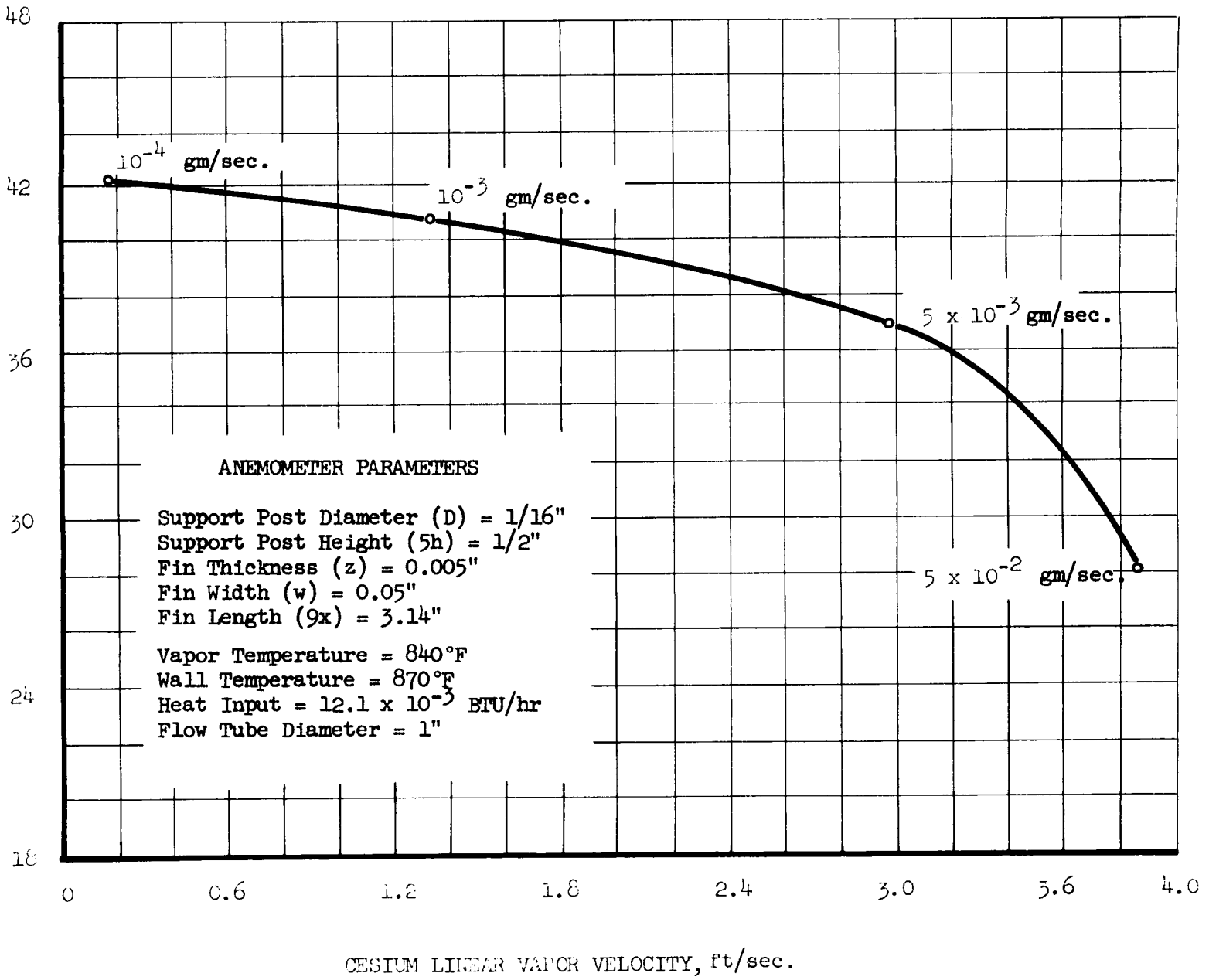

These computed results indicate that the meter sensitivity is significantly different over the flow range. At a flow near 10^{-4} gm/sec, a one degree temperature change indicates a vapor velocity change of approximately 1.2 ft/sec. At a flow near 5×10^{-2} gm/sec, a one degree temperature change indicates a vapor ΔV of less than 0.1 ft/sec.

The accompanying graphs in Figures 2-11 through 2-15 are optimization curves in which only one geometric parameter was varied at a time. With the exception of the fin width calculations, the velocity levels were all in the 10^{-4} to 10^{-3} gm/sec flow rate range. The fin width studies were in the 5×10^{-3} to 5×10^{-2} gm/sec flow rate range. As for the data plotted in Figure 2-10, all calculations were made for cesium vapor.

The slope of the curves (linearized for calculation simplicity) is a measure of the anemometer sensitivity. The more negative the slope, the more sensitive the anemometer will be. With a meter of maximum sensitivity a larger electrical thermocouple output will be obtained per unit change in vapor velocity.

Examining Figure 2-11 indicates that the longer the fin length is made, the more negative is the slope and the more sensitive is the meter. The data in Figure 2-12 indicate that the smaller the support post diameter, the more sensitive is the meter. As shown in Figure 2-13, increasing the anemometer fin thickness from 0.005 inches to 0.010 inches does not change the meter sensitivity. A one-quarter inch height support post renders a more sensitive anemometer than a one-half inch support post -- Figure 2-14. And from Figure 2-15, a fin width of 0.08 inches was more responsive to vapor velocity changes than a fin width of 0.10 inches.

From these calculations the following parameters were used in building the anemometer.

fin width	= 0.05 inches	support post height	= 0.250 inches
fin thickness	= 0.005 inches	support post diameter	= 0.063 inches
fin length	= 2.50 inches	(Later, because of fabricational difficulties, this diameter was increased to 0.188 inches).	

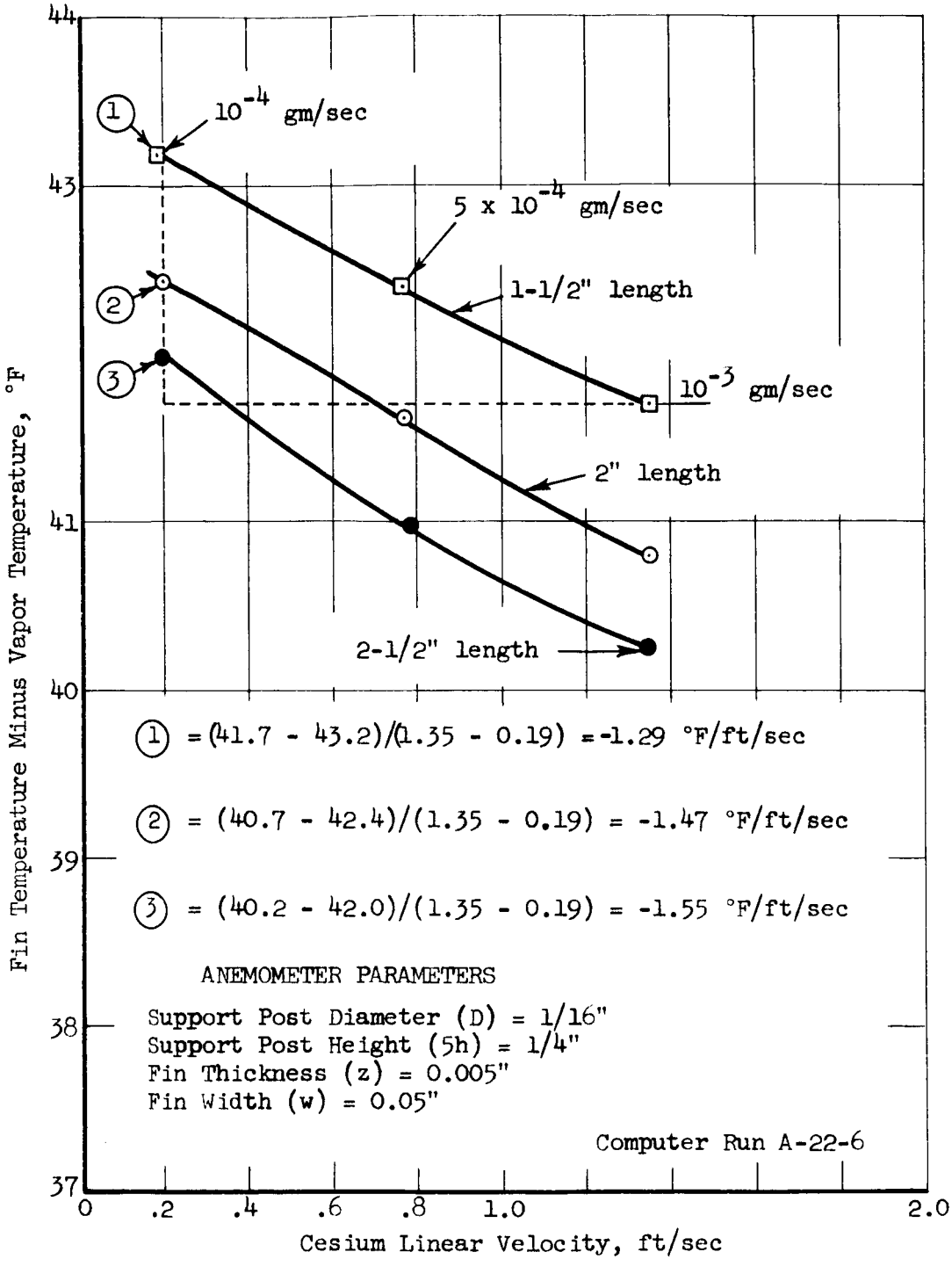

Figure 2-11

Anemometer Fin Sensitivity Optimization Curve

(Fin Length Variation)

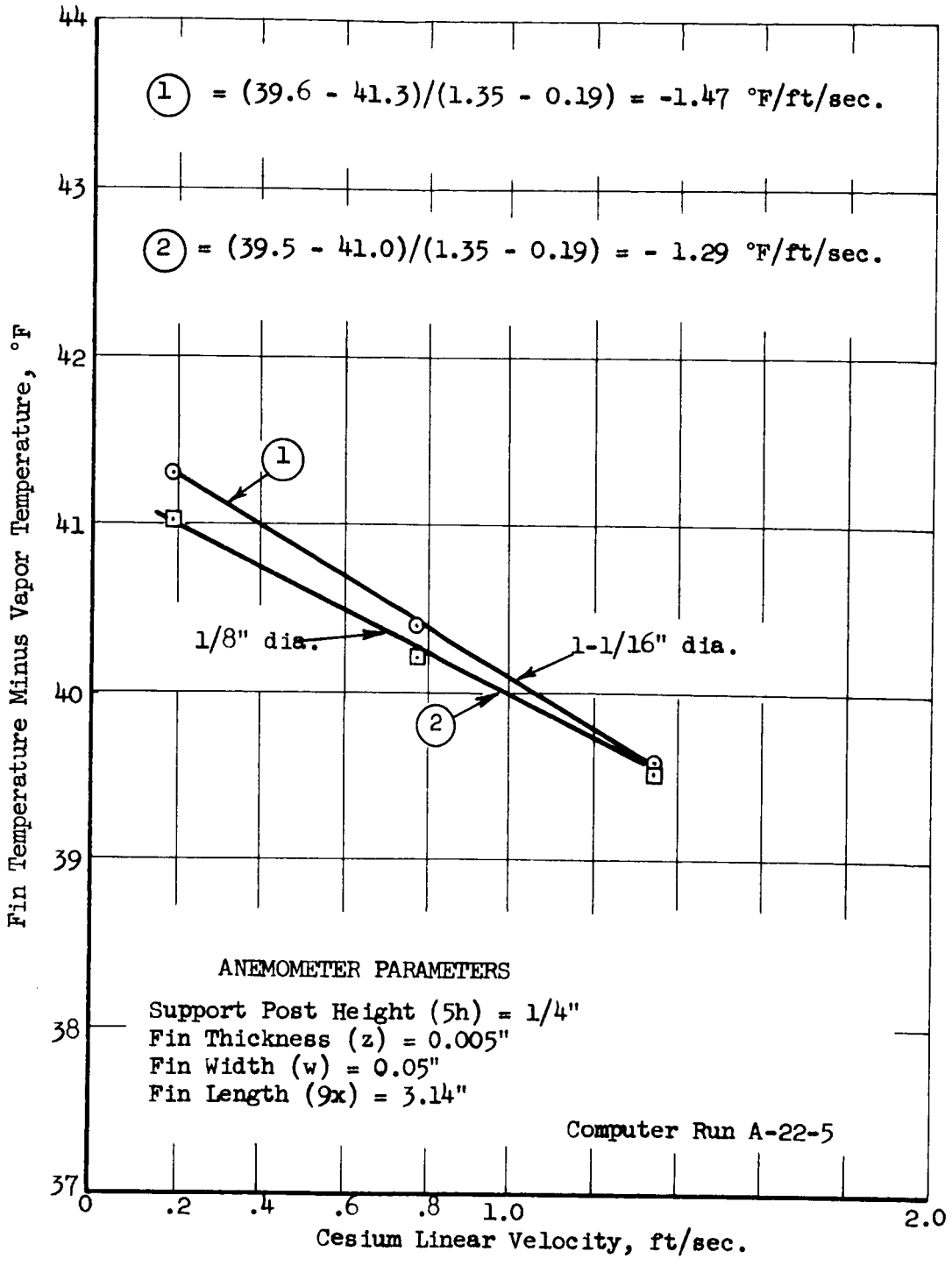

Figure 2-12

Anemometer Fin Sensitivity Optimization Curve

(Support Post Diameter Variation)

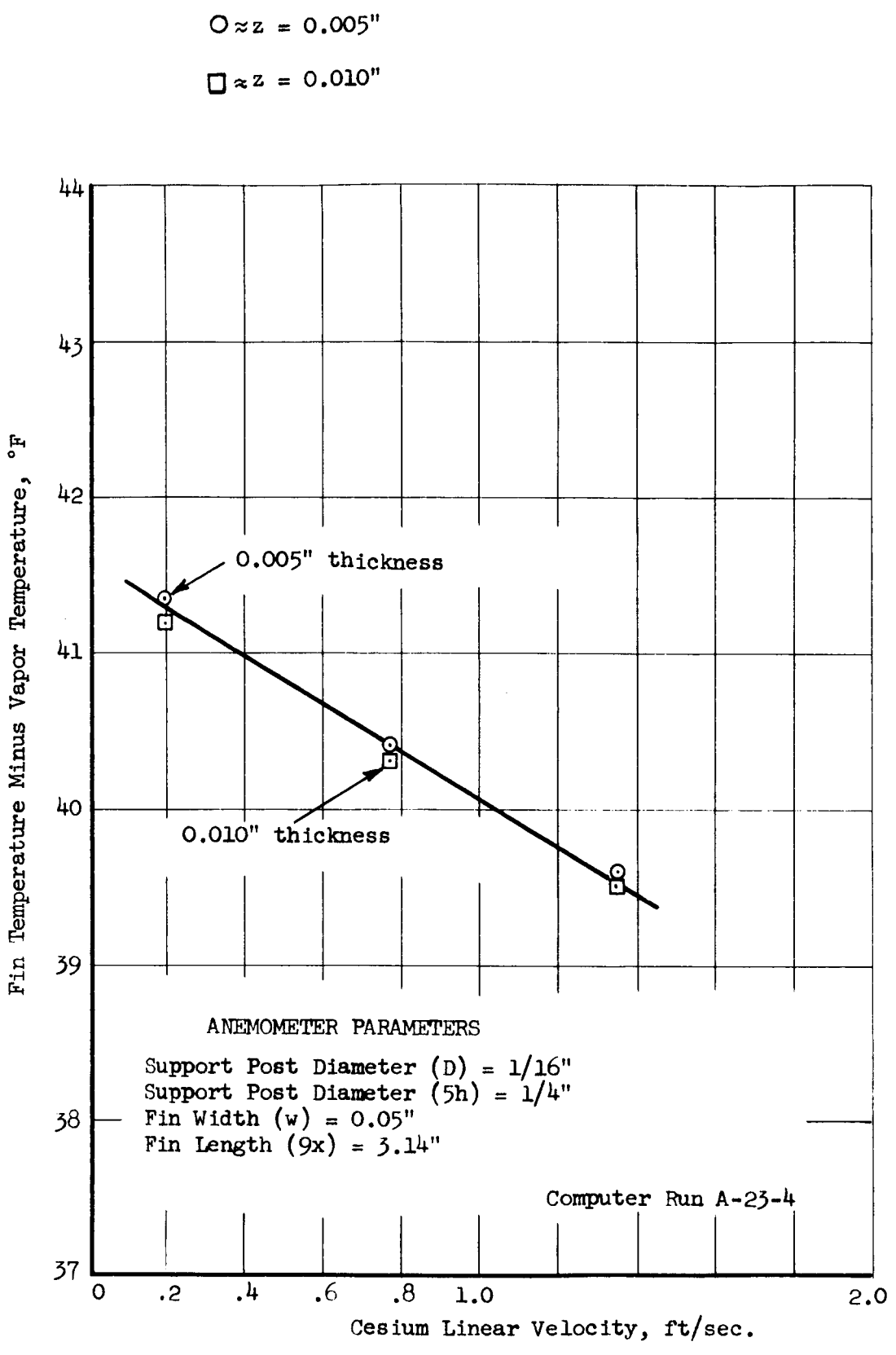

Figure 2-13

Anemometer Fin Sensitivity Optimization Curve

(Thickness Variation)

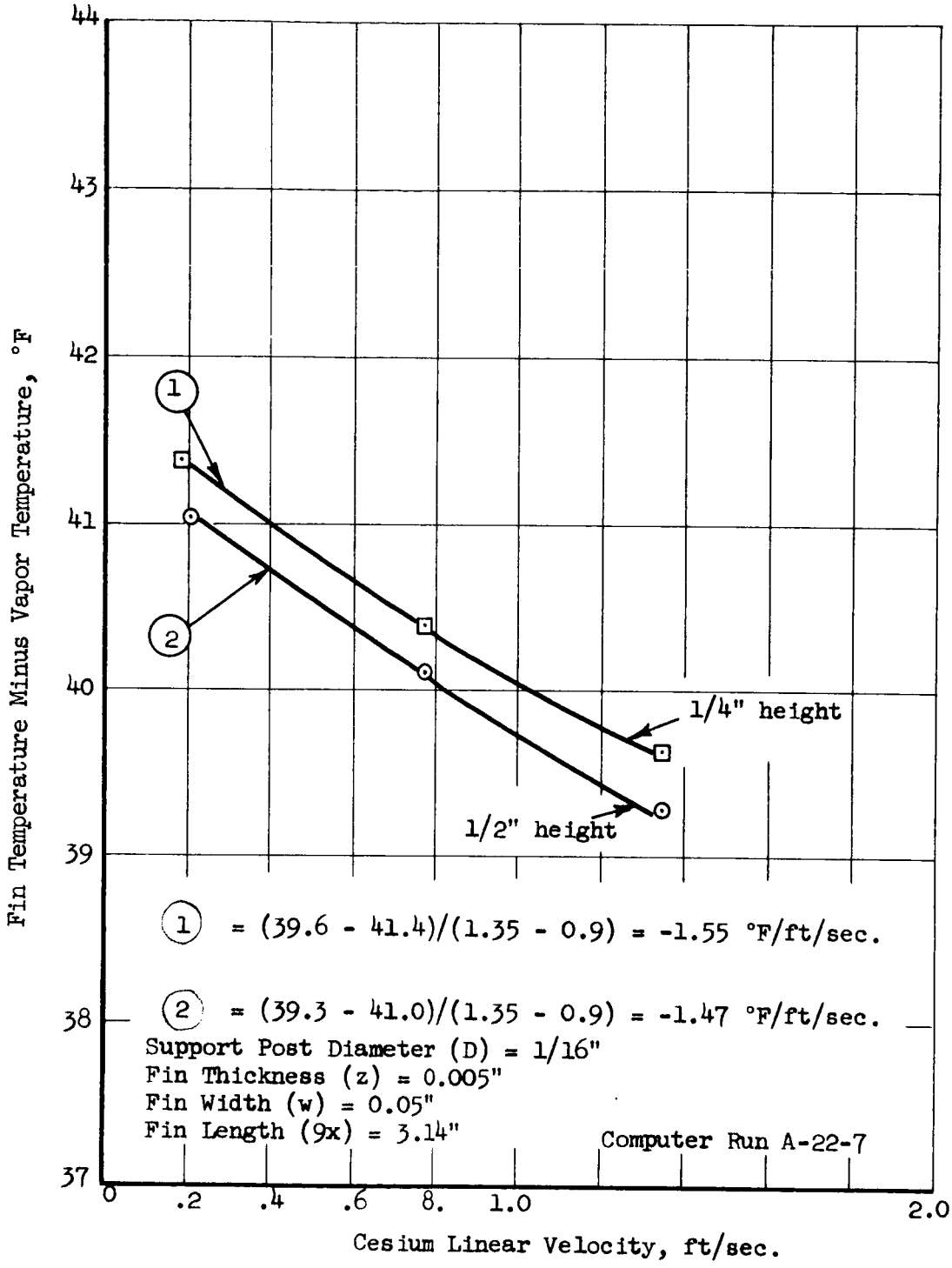

Figure 2-14

Anemometer Fin Sensitivity Optimization Curve

(Support Post Height Variation)

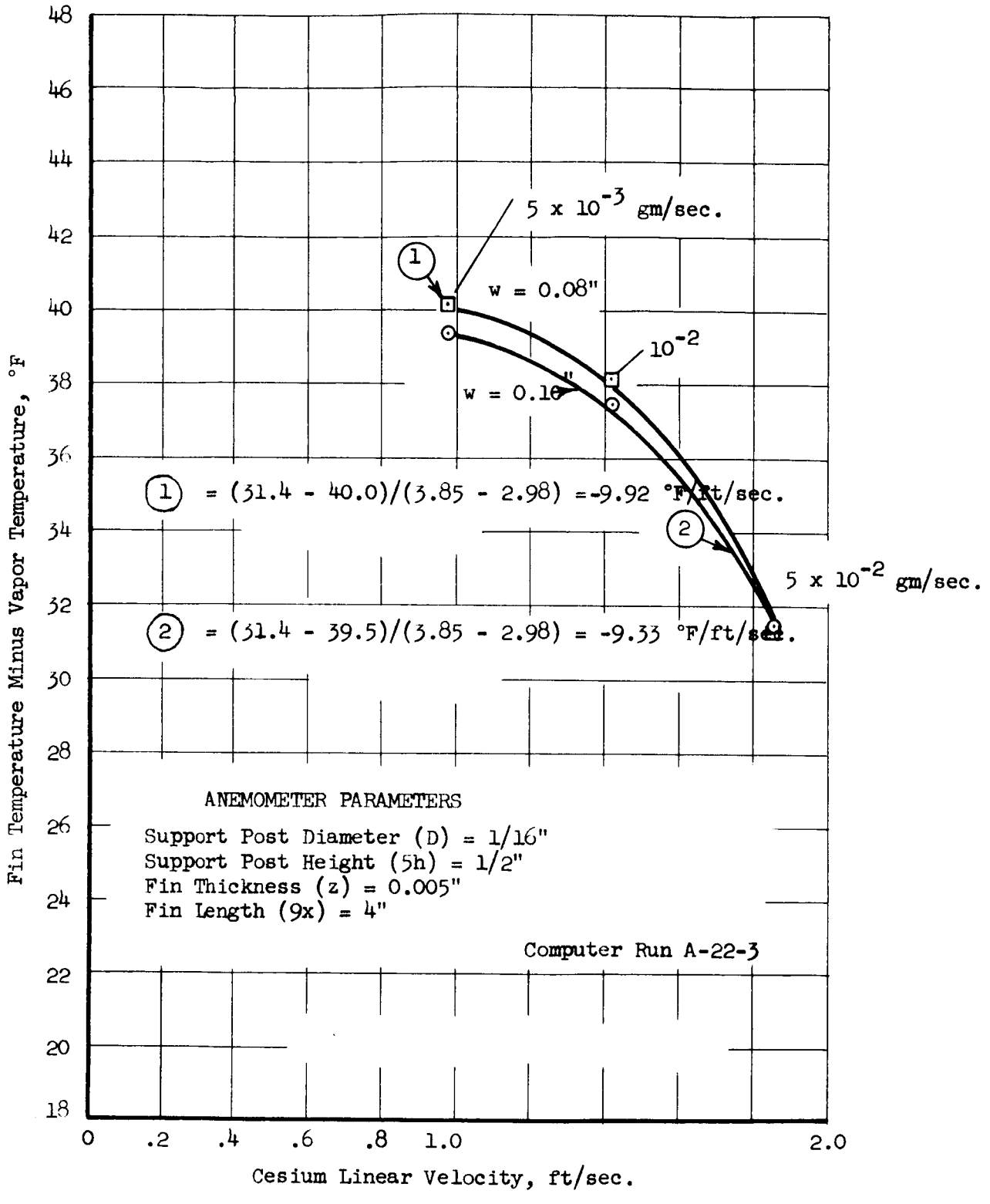

Figure 2-15
Anemometer Fin Sensitivity Optimization Curve
(Width Variation)

The reason for the trends in performance of the anemometer fin or sensing element can be explained by the heat transfer modes experienced by the meter. In the convection terms both forced and natural convection are experienced. Forced convection is more velocity dependent than natural convection. Therefore, by making the fin as long as possible (length direction being defined as that direction perpendicular to vapor flow) the heat transfer by forced convection is maximized and the heat transfer by natural convection is minimized. The practical limit in choosing the length was limited by how much material can be conveniently fitted into the inside diameter of the flow tube.

In order to minimize the heat conduction losses from the fin down through the support post the sensing element should be as thin as possible in both its width direction and fin thickness. However, as shown in Section 2.1, it is still necessary that fin characteristics be maintained. A fin is defined as a geometric configuration in which the thickness is one-tenth or less of the width. Therefore, in making the width 0.05 inches and the thickness 0.005 inches, this fin concept is maintained.

Minimizing the support post diameter also minimizes the heat conduction losses through the post. The practical limit on the post diameter is based upon what size wire feed through holes can be made in it for accommodating the heater and thermocouple leads.

The final computer run with the optimum set of geometric variables is shown as Figure 2-16. As in Figures 2-11 through 2-14, the flow rate is in the 10^{-4} to 10^{-3} gm/sec. range. Heat input to this fin was 1.8×10^{-1} BTU/hr. The heat input to the fin in the calculations for Figures 2-11 through 2-15 was 1.2×10^{-2} BTU/hr.

Increasing the heat input to the fin only raised the average temperature level of the anemometer surface. It did not alter anemometer sensitivity. Varying fin and support post parameters more directly changed the slope of the velocity versus fin temperature curves.

Slope = (67.0 - 70.0)/(1.35 - 0.19) = -2.58 °F/ft/sec.

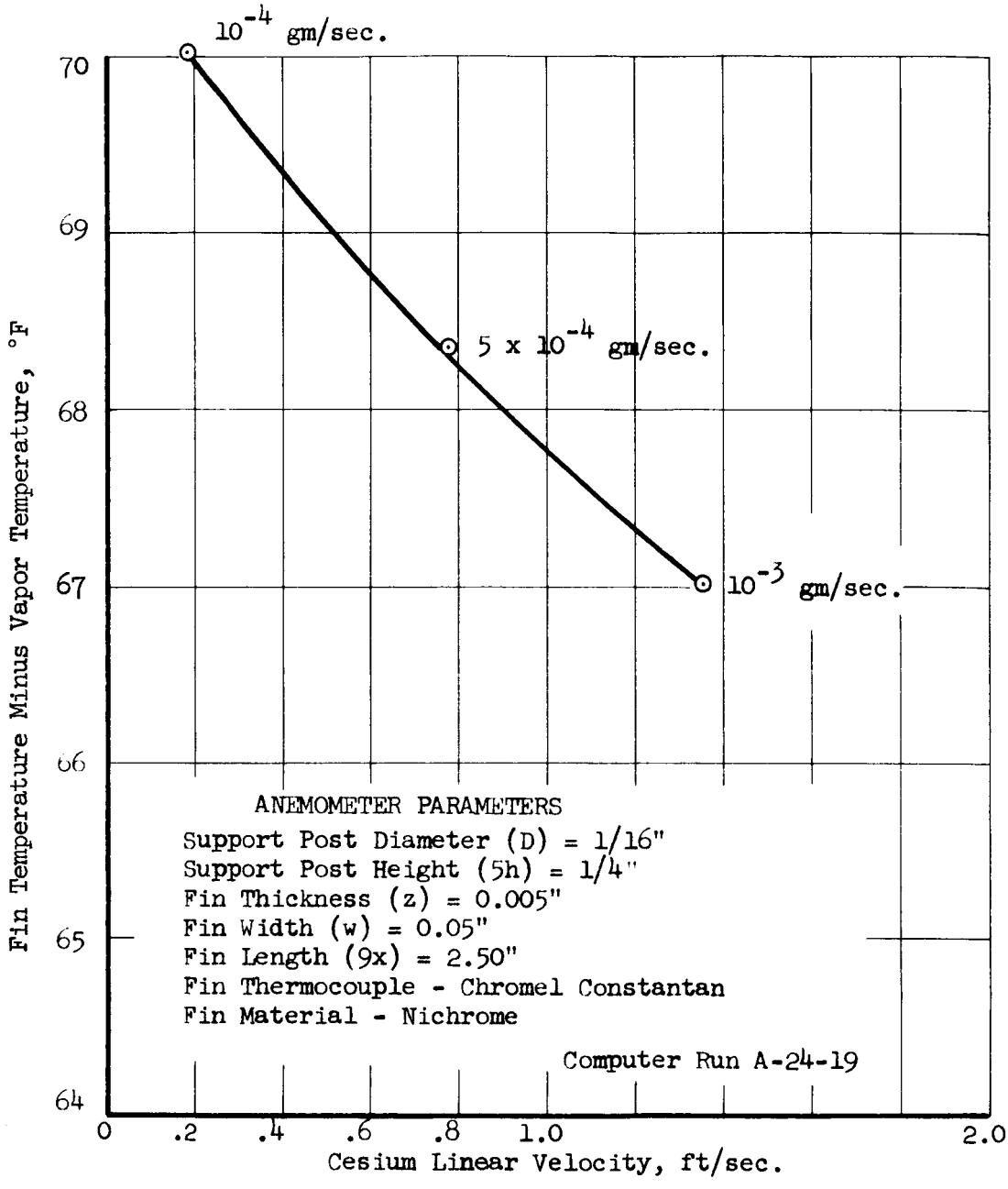

Figure 2-16

Theoretical Anemometer Operating Curve

Optimizing the meter configuration increased the sensitivity slope from an average -1.5 °F per ft/sec. value (in curves 2-11 through 2-14) to -2.6 °F per ft/sec. in Figure 2-16.

2.3 Anemometer Design

The pictorial drawing shown in Figure 2-4 was the first concept of the flow meter configuration. After the computer program had been completed and optimum values for the sensing fin and support member geometric parameters were chosen, there still remained the task of assembling the system with its attendant hardware into an integral unit.

As shown in Section 2.2, the dimensions of the fin and support member were:

1. Fin length (direction perpendicular to vapor flow path) = 2.5 inches
2. Fin width (direction parallel to vapor flow path) = .05 inches
3. Fin thickness = 0.005 inches
4. Fin support height = 0.25 inches
5. Fin support diameter = 0.063 inches

A schematic diagram of how the configuration was assembled into a final unit is shown in Figure 2-17. To assure a constant uniform temperature around the sensing fin, a salt bath was used to heat the meter. The salt was a mixture of potassium and sodium nitrates with a liquid range of 300 to 1800°F.

The salt bath temperature was maintained by a TRW designed controller unit. A Winsco Instrument Control type 2404-APB temperature transducer and an iron-constantan thermocouple were inserted into the salt bath. The iron-constantan couple was used to indicate the bath temperature, while the transducer was connected to the control bath unit. A circuit diagram for this assembly is shown in Figure 2-18.

The controller supplies a proportioning signal rather than an on or off signal to the salt bath heaters, and will maintain the bath temperature at 840°F $\pm$ 5°. With the adjustable potentiometers shown in Figure 2-18, the controller unit will function over a 500° to 1000°F temperature range. Changing the values of these potentiometers could make the unit workable over a 70° to 1000°F temperature range.

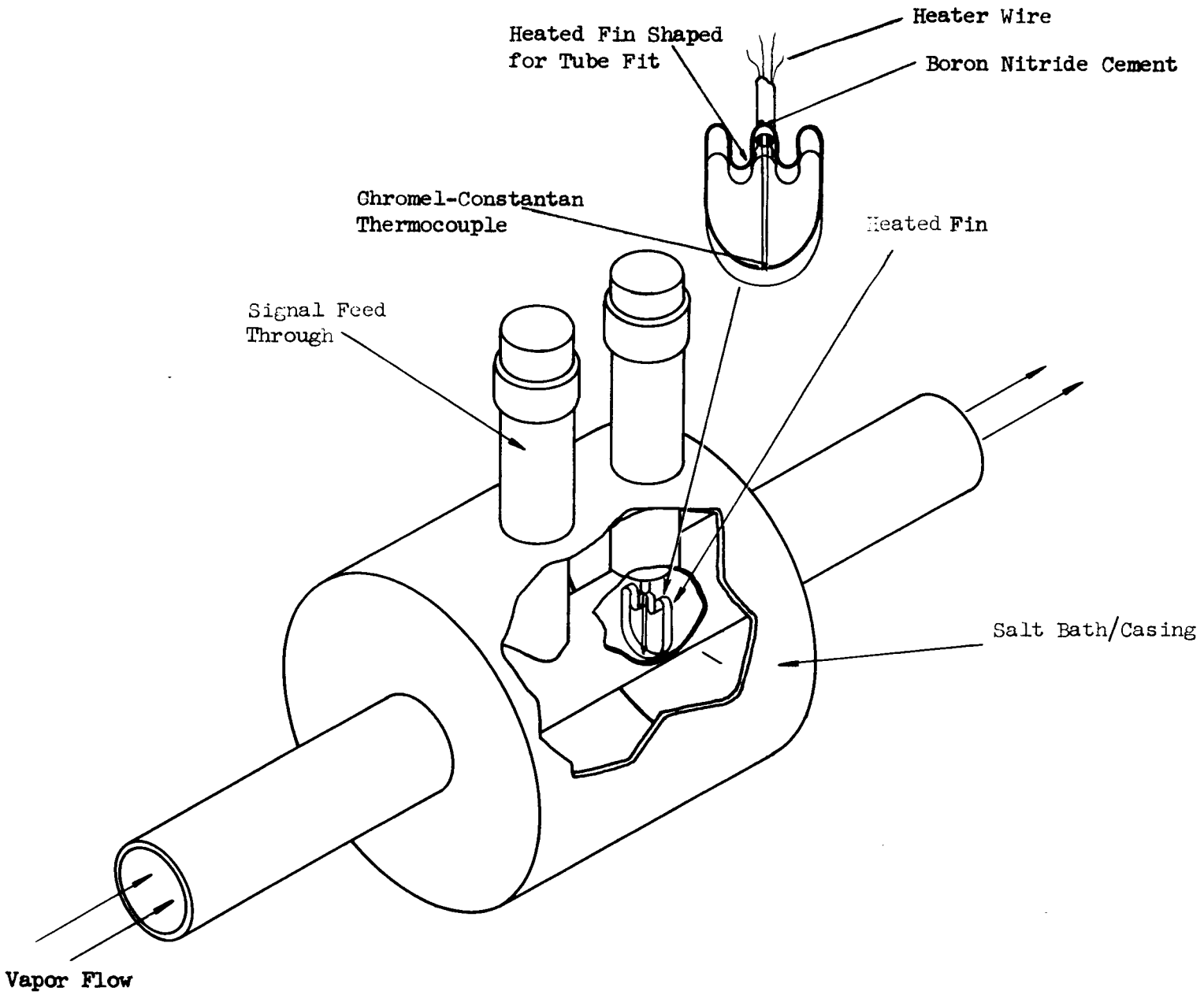

Figure 2-17

Anemometer Assembly

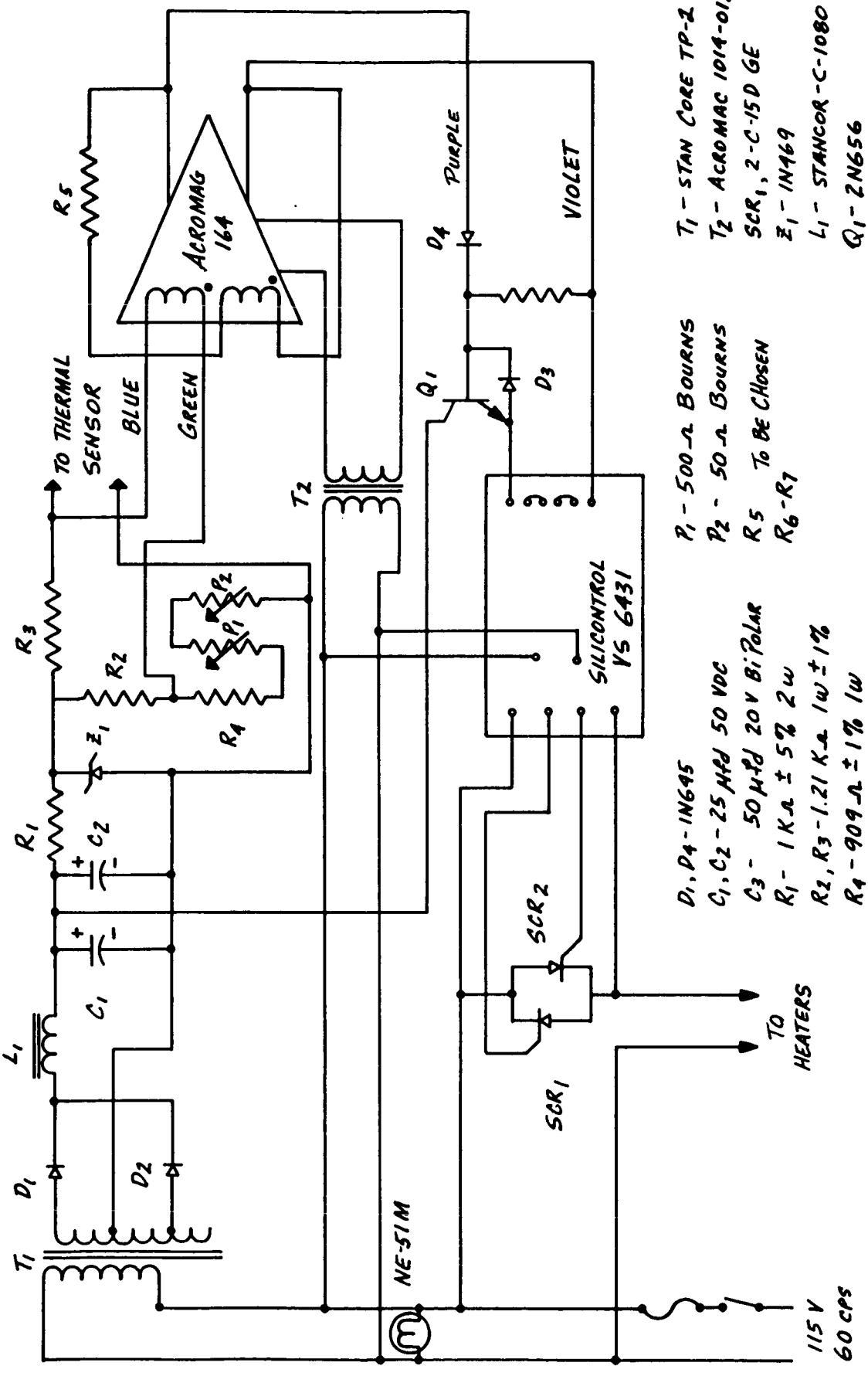

Figure 2-18
Circuit Diagram of Control Unit for Constant Temperature Bath

The heat sources for the bath were two 100 watt type A-23 Watlow immersion heaters.

2.3.1 Fin Design and Feed Through Assembly

Several attempts to build the heated anemometer failed before it was finally decided to shape the fin from 0.005 inch nichrome strip and attach the heater wires directly to the fin -- making the anemometer the heater element. The thermocouples were spot welded to the center of the fin. This concept is shown schematically in the insert of Figure 2-17.

The feed through mechanism used to hermetically seal the thermocouple and heater lead wires is shown schematically in Figure 2-19. A Teflon sealant gland within the Conax fitting is compressed against the wire leads and the inside of the fitting body until a hermetic seal is obtained. The Conax fitting is in turn welded into a Swagelok connector which fits over the tube containing the boron nitride fin support.

Because the seal is at the Teflon compression gland, rather than at the support member itself, there is no need for a nonporous support piece. Therefore, boron nitride which is an easily machineable high temperature electrical insulator was used as the fin support piece. The anemometer fin was attached to the boron nitride by means of boron nitride cement.

Care must be taken to maintain the sealant temperature between limits. Excessive temperatures will cause sealant decomposition. An excessively low temperature would permit mercury condensation to occur at the Teflon sealant gland, thereby causing an electrical short between the heater and thermocouple wires.

The extension length of the anemometer feed through was calculated on the basis of heat conduction through a solid rod with one end immersed in an infinite heat source. (Figure 2-20).

Figure 2-19

Schematic Diagram of Anemometer Feed Through

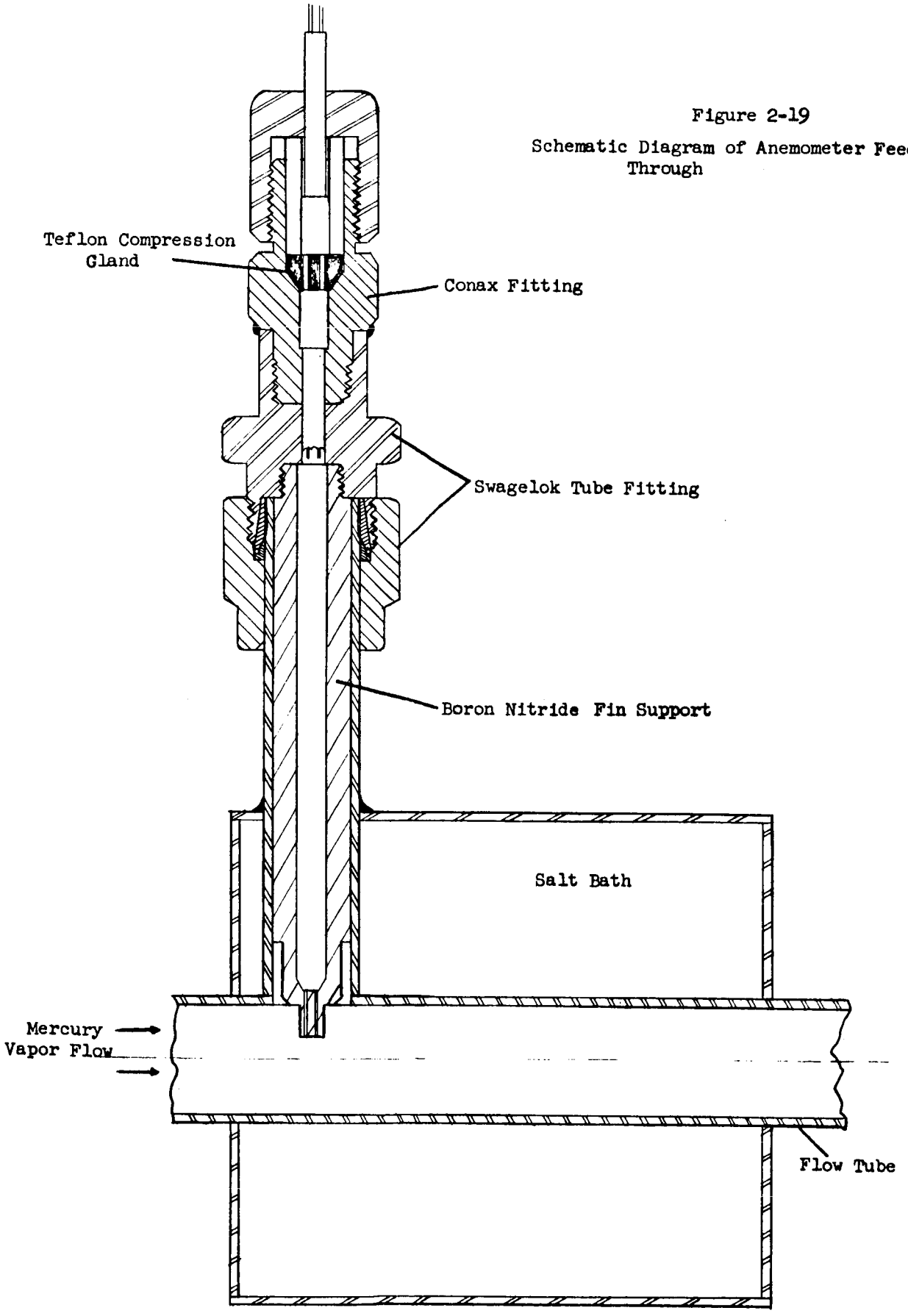

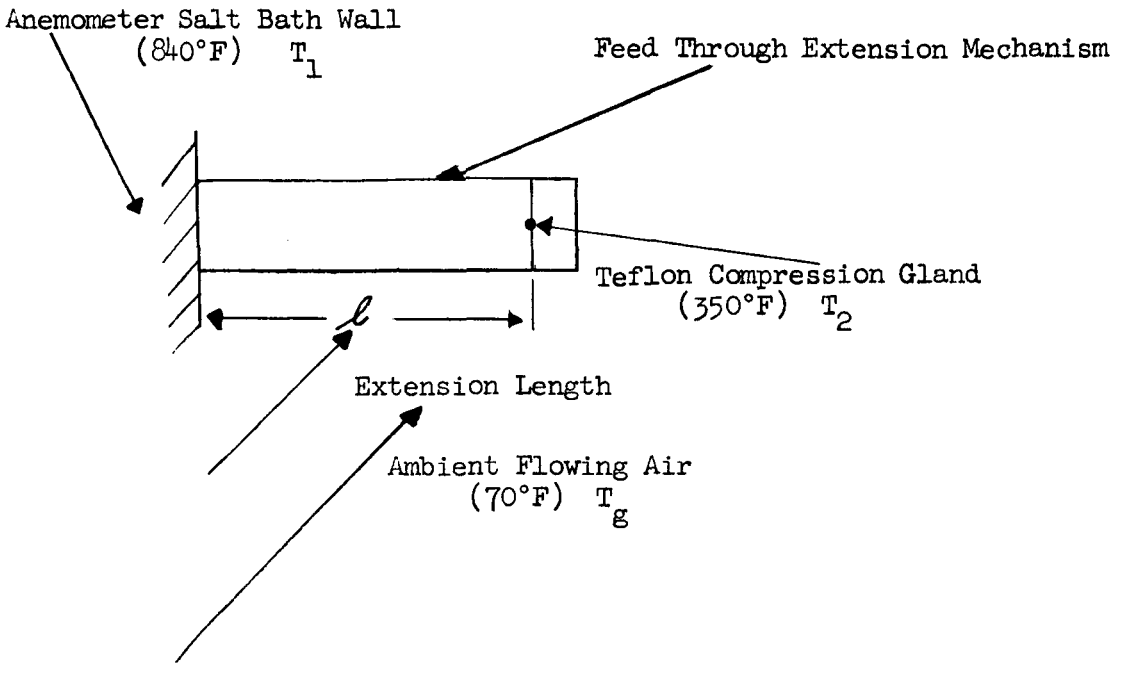

Figure 2-20
Mathematical Model of Anemometer
Feed Through Extension

Assuming that the extension is a hollow circular tube, Eckert[1] has shown that the temperature profile along the tube is described as:

$$\frac{\Delta T_1}{\Delta T_2} = \cosh m\ell \qquad (1\text{-}11)$$

$$\Delta T_2 = T_2 - T_g$$

$$\Delta T_1 = T_1 - T_g$$

---

[1]Eckert, E. R. G., "Introduction to the Transfer of Heat and Mass", McGraw-Hill Book Company Inc., New York, New York, p. 27, 1950.

$$m = \sqrt{hc/kA}$$

The cross section of the extension tube has the configuration shown as:

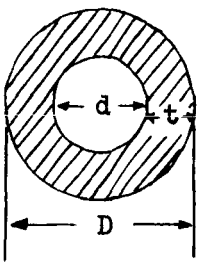

D = 0.75 in.

t = 0.065 in.

$c = 1.96 \times 10^{-1}$ ft

k = 12.4 BTU/hr ft °F (for type 316 stainless steel)

$A = 9.72 \times 10^{-4}$ ft^2

h is assumed to be = 2 BTU/hr ft^2 °F

$$m = \sqrt{hc/kA} = \sqrt{\frac{(2)(1.96 \times 10^{-1})}{(1.24 \times 10)(9.72 \times 10^{-4})}} = 5.71$$

$\Delta T_2 = 250 - 70 = 180$

$\Delta T_1 = 840 - 70 = 770$

Therefore, using Equation 1-11

$\ell = 0.292$ ft = 3.5 inches

This was the length the Teflon compression gland was extended away from the anemometer salt bath wall.

In order to eliminate extraneous conduction heat losses away from the anemometer fin, the heater lead wires and thermocouple wires were made as small in diameter as practical. Wire of 0.005 in. diameter was chosen for both the heater leads and thermocouple wires.

From the computer results, it was shown that a heat input of 1.8×10^{-1} BTU/hr or 530 milliwatts was sufficient to power the anemometer heater. The current required to power the nichrome fin is 366 milliamps.

A constant voltage source was used to supply this current. Because of the probability of resistance change in the anemometer fin and lead wires as the temperature changes in the meter, a 120 ohm wire wound precision resistor was put in series with the anemometer heater element. This increased the total resistance of the circuit to 150 ohms.

Any resistance change in either the heater or lead wires is negligible in comparison with the resistance of the overall circuit. This assures the constancy of the heater element current.

2.3.2 Thermocouple Selection

The choice of a thermocouple combination for the anemometer was based upon the thermocouple electrical output and upon thermocouple location. Of the common thermocouple combinations, the chromel-constantan junction produces the highest millivolt output per degree of temperature change. This may be observed by examining the data in the following table.

THERMOCOUPLE ELECTRICAL OUTPUTS

Thermocouple Junction	Microvolts/°F (at 800°F)
Iron Constantan	28.8
Chromel Alumel	21.9
Platinum-Platinum with 10% Rhodium	4.4
Platinum-Platinum with 13% Rhodium	4.6
Tungsten-Tungsten with 26% Rhenium	4.7
Chromel-Constantan	39.0

Because of the small change in anemometer fin temperature in the lowest portion of the flow rate range (i.e., 10^{-4} to 10^{-3} gms/sec.), the higher the millivolt output from the couple, the easier it is to distinguish and measure these changes.

The thermocouple materials most inert to either cesium or mercury are the refractory metals. Using tungsten-tungsten rhenium as an example, an 800°F temperature would generate a 3.72 millivolt output. For a chromel constantan junction, this same output would be 31.09 millivolts.

Some thought was given to making the anemometer fin the thermocouple itself. In this way a closer approximation to the average fin temperatue could be measured. However, during the computer studies, it was noted that the localized temperature (for example, at point 16 in Figure 2-6 and 2-7) changed in the same amount as did the average fin temperature. Therefore, it was decided to spot weld the thermocouples on the fins of both the reference and heated anemometers. This manner of attachment is shown schematically in Figure 2-17.

The materials selected for thermocouples were chromel and constantan because of high thermoelectric effects associated with this material combination. To what degree long term vapor exposure will alter these electrical output characteristics has not been determined. Therefore, it is suggested that the vapor flow meter be periodically recalibrated over a several month period to determine if any cesium or mercury alloying has occurred and if this has changed the electrical output characteristics of the thermocouples.

The function of the reference or nonheated fin was to compensate for expected temperature variations in vapor as it passed through the meter. Without this reference, a change in vapor temperature as well as a change in vapor velocity would cause an output variation on the readout equipment and hence indicate a false flow rate. The thermocouple signal of the reference unit was bucked against the heated anemometer signal at zero vapor flow by means of a null balance system. Any change from this null output would only be due to cooling resulting from vapor velocity convection effects. The extent of anemometer cooling arising from vapor temperature variation would be duplicated on each of the anemometer vanes with the net result that the meter readout could be altered only by vapor velocity variation and not by vapor temperature variation.

A diagram of the nulling system used in this operation is shown as Figure 2-21.

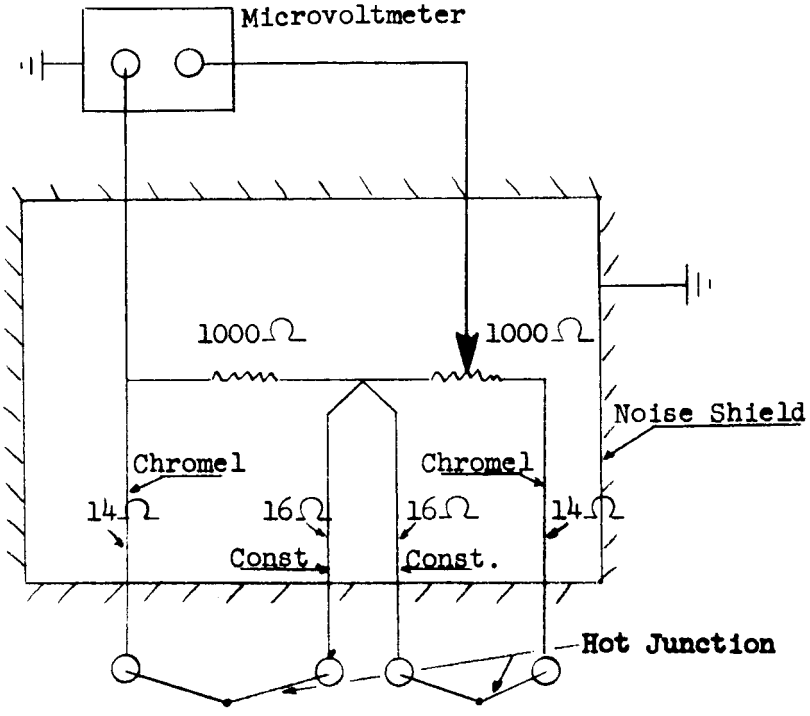

Figure 2-21
Anemometer Nulling System

3.0 TECHNICAL DISCUSSION - EXPERIMENTAL INVESTIGATION

A description of the testing used to calibrate the anemometer meter and the procedure for operating the rig are presented in Appendices A and B of this report. This section contains a discussion of the experimentally determined operating characteristics of the vapor flow meter and its attendant circuitry.

3.1 Calibration Results

The following results were obtained from calibration experiments with the anemometer vapor flow meter.

1. A calibration plot relating microvolt output to mercury mass flow rate is presented in Figure 3-1.
2. The zero point of the indicating voltmeter drifted from 0 to +50 microvolts during the course of the calibration. In the flow rate range of 10^{-4} to 10^{-3} gms/sec., this magnitude of this drift could be interpreted as a false flow rate change of 5×10^{-4} gms/sec.
3. From a no flow condition to a mercury flow of 2×10^{-4} gm/sec, the response for the meter and rig to indicate an equilibrium flow condition was approximately one minute.

3.2 Discussion of Data

From the plot shown in Figure 3-1, the operating characteristics of the anemometer vapor flow meter can be observed. Within the flow rate range of 10^{-4} to 2×10^{-2} gms/sec. the anemometer readout first indicated a positive output and then a negative output as the flow rate increased. This polarity reversal can best be explained by considering the shift in the zero point of the indicating system during the course of the experiment (shown graphically in Figure 3-1). Initally, with the anemometer heater powered, the null system was so adjusted as to supply a zero differential output from the reference and heated anemometer thermocouples. In doing this, all exterior leads were shielded, and the cold junctions of the thermocouples were insulated. Without the lead shielding, the voltmeter could not be brought to a zero reading within a range of less than plus or minus 20 microvolts. Background noise and general electrical interference in the laboratory was sufficient to prevent a more precise nulling of the meter.

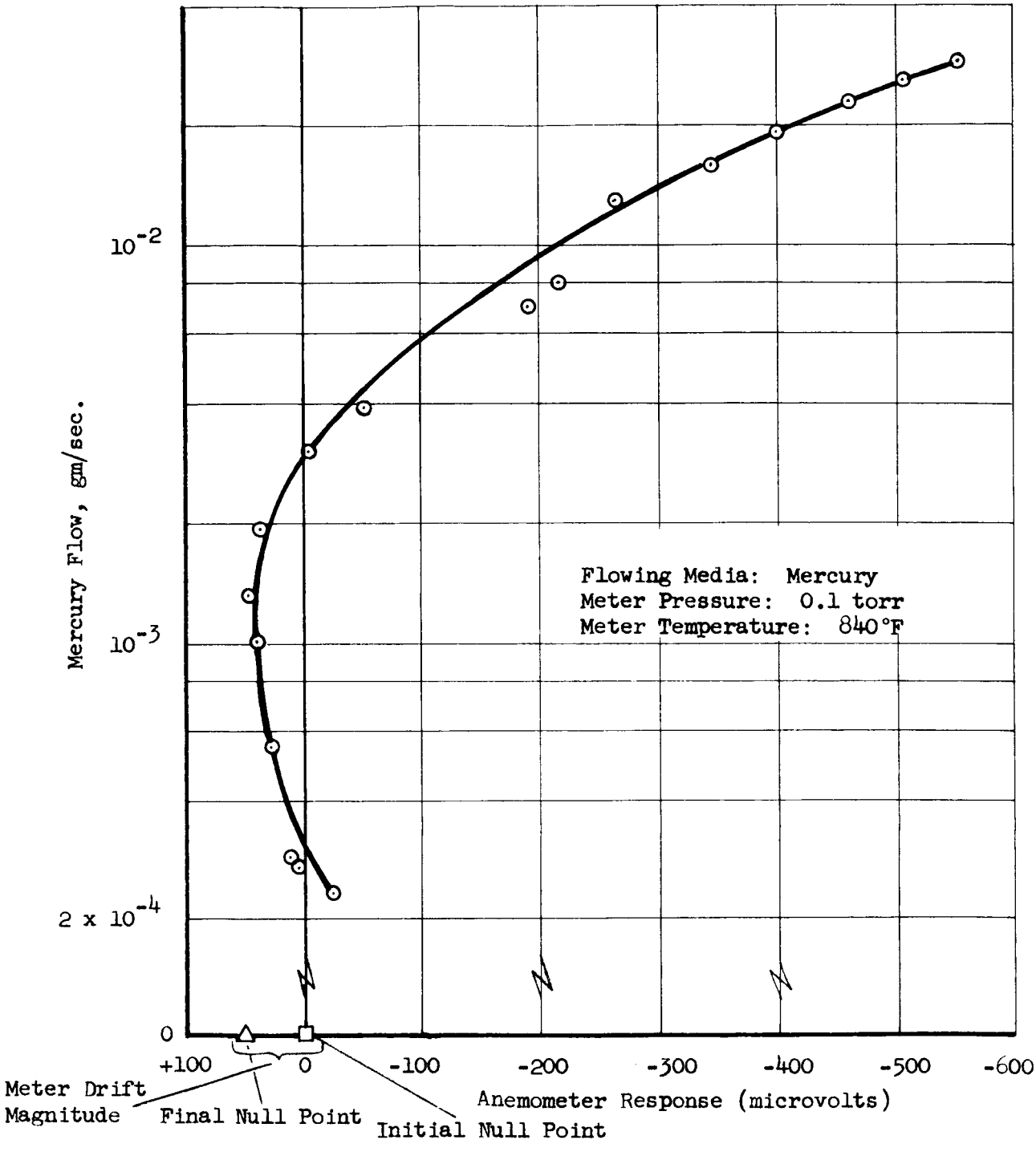

Figure 3-1

Vapor Flow Anemometer Calibration Curve

In the upper range of the flow rate (i.e., 5×10^{-3} to 5×10^{-2} gms/sec.) the anemometer fin temperature changes by one or more Fahrenheit degrees when the vapor velocity changes by a unit factor (e.g., from 4 to 5×10^{-2} gms/sec.).

In the low flow range (10^{-4} to 10^{-3} gms/sec.) a unit factor of mass flow rate change corresponds to a few hundredths of a degree temperature change on the fin and is equivalent to a differential thermocouple output of only a few microvolts.

A change in hot junction temperature, cold junction temperature or a combination of these will cause a change in the thermocouple output. When the temperature change to be sensed produces only a few microvolts, it is necessary that only the hot junction and never the cold junction should change in temperature.

During the calibration effort the cold junction was insulated with Kaowool. However, temperature variations of a few hundredths of a degree may still have occurred. This is one possible reason for the observed null point drift.

A second reason for the occurrence may be associated with the fin heater input current. If the thermocouples (Reference: Figure 2-17, Section 2) was attached only by a single contact point on the anemometer fin, the heater current should increase the thermocouple output due to resistance heating only. However, if the two thermocouple wires are separated from each other by a finite distance a current passing through the fin will be detected by the voltmeter attached to the thermocouples.

When the anemometer salt bath had attained an equilibrium temperature, 840°F, and at a no flow condition the output at the heated fin thermocouple (prior to bucking it against the reference thermocouple) was 31.2 millivolts. After passing 366 milliamperes of current through the fin, the output immediately increased to 32.8 microvolts, an increase of 1600 microvolts. A current fluctuation of only 11 milliamperes would be sufficient to change this imposed current output by 50 microvolts. Thus, a small change in the fin heater current could cause a microvolt drift of the null point on the readout meter. Because of the readability of the heater current meter a change of several milliamps design value of 366 could not be readily detected.

Nevertheless, a possible variance in the heater fin input current is a partial cause for the observed drift read on the output microvolt meter.

Figure 2-10, Section 2 is a theoretical plot of the expected anemometer response to cesium vapor velocity changes over the design flow range. This data was recalculated and plotted on the basis of a chromel-constantan thermocouple output versus cesium flow rate. Superimposed on this same plot is the experimental data from the calibration effort with mercury. This is shown as Figure 3-2.

While it should not be expected that the two sets of data coincide exactly with each other, the trends for the two sets of data should be similar. This is shown in Section 2 where the convection coefficients for both cesium and mercury (under the same flow conditions) are calculated. Since the coefficients are approximately equal the degree of heat transfer and subsequently the response characteristics of the anemometer should be approximately the same for both cesium and mercury.

This trend is borne out by the data in Figure 3-2. The anemometer microvolt output increases in nearly the same proportion as does the predicted data. Following correction of the null point shift the two curves should have even more similar characteristics.

The time response of the vapor flow meter was tested by measuring the time required for the system to indicate an equilibrium microvolt output from a no flow condition. After a nominal flow had passed through the meter, the supply valve was closed and all mercury was removed from the flow system. The supply valve was again opened, and the time interval to reach the same flow rate a second time was recorded. From 0 to 2×10^{-4} gms/sec. mercury flow rates, an equilibrium reading was attained about one minute after flow began. At higher flow rates this time should be shorter and at lower flow rates this time should be longer. This recorded interval included the meter and rig response time.

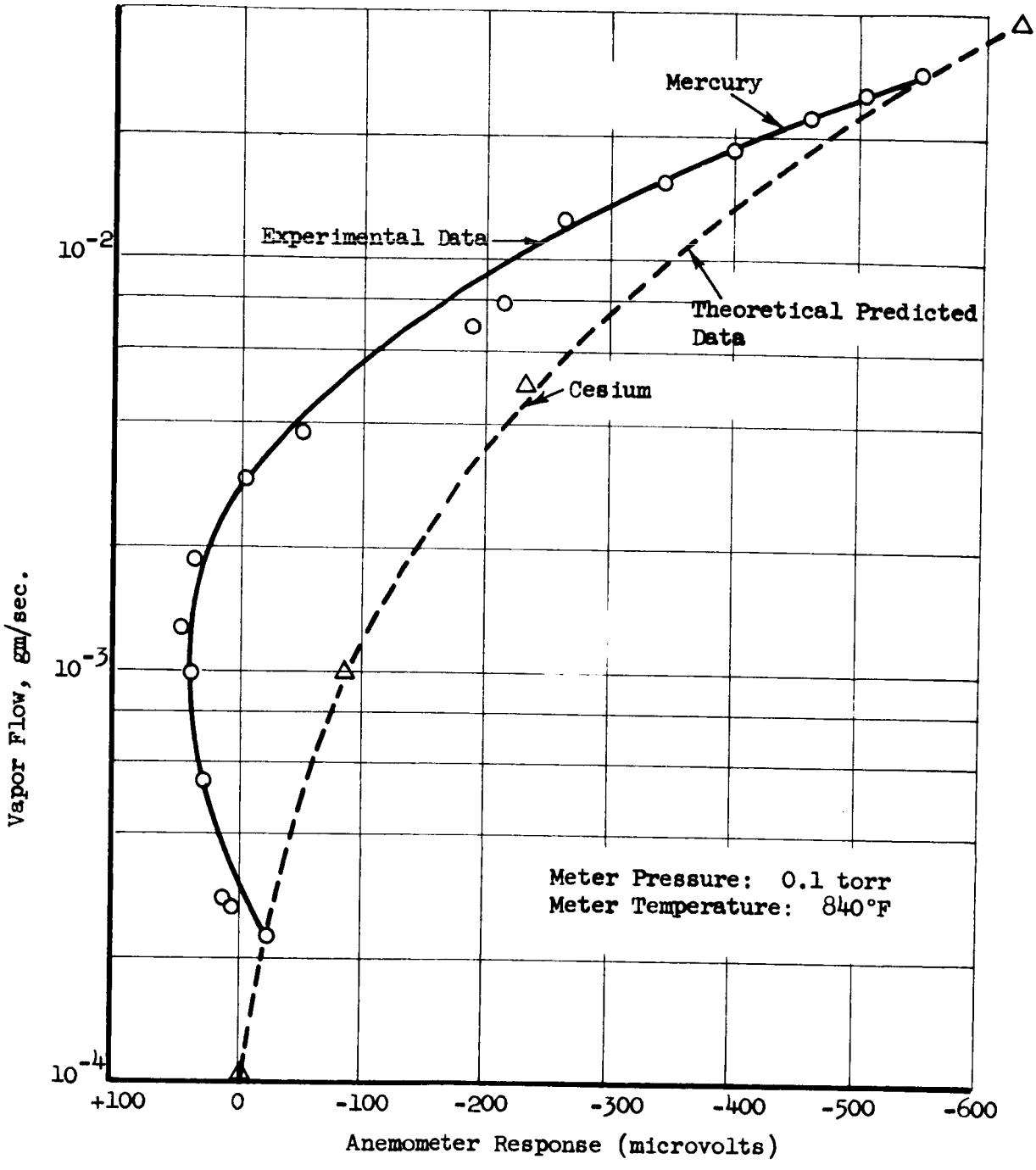

Figure 3-2

Experimental Compared to Theoretical
Anemometer Calibration Data

3.2.1 Operating Features of the Anemometer

One of the design objectives of the anemometer development effort was to assure that the flow meter could be placed in the vapor feed system line of an ion engine without interfering with the vapor flow or operation of the feed system. This imposes two main restrictions on the meter design.

1. That a very minimal pressure drop occurs across the meter.
2. That the meter and its attendant circuitry must be so designed that they can operate with a several thousand volt applied potential without danger to the operator.

The basic design of the anemometer meets requirement one. Since there are no restrictions or flow channels in the meter configuration, line loss would be the only pressure drop encountered by the anemometer design. However, because line loss is a direct function of vapor velocity (which is minimal in the meter design requirements) pressure drop due to line loss will also be minimal.

The operation of the anemometer system is not dependent upon the applied voltage. The performance characteristics shown in Figure 3-1 would not be altered by placing the anemometer in a high potential field. While this is true for the sensing circuit, the readout, temperature controller, and heater fin current source should all be suitably modified in order that they can be operated at a high electrical potential without being injurious to personnel. This can easily be accomplished by heavily isolating each of the units from ground and suitably modifying the control features in order that they can be operated at a distance, by means of insulator rods. All the control equipment, including the constant temperature bath regulator and the microvolt meter readout can be modified to incorporate this feature.

The vapor flow anemometer is designed to operate over a pressure range of 0.1 to 1 torr for mercury and 1 to 25 torr for cesium. In performing the calibration at any one pressure level, the effect of varying the meter pressure level on the accuracy of the calibration was considered.

As shown in Section 2, the varying parameter that the anemometer senses is the convection heat transfer coefficient. This is considered in a plot of Nusselt number versus Reynolds number (Figure 2-2). The terms in the Nusselt number are:

$$Nu = \frac{hx}{k}$$

The number x (characteristic linear dimension) and k (thermal conductivity) are not pressure dependent.

The Reynolds number is expressed as:

$$Re = \frac{xv\rho}{\mu}$$

The linear velocity (v) is related to the mass velocity by the expression

$$\dot{m} = v\rho_A \quad \text{or} \quad v\rho = \dot{m}/A$$

Therefore, the Reynolds number can be rewritten as

$$Re = \frac{x\dot{m}}{\mu A}$$

All these terms (the characteristic linear dimension -- s, mass flow rate -- $\dot{m}$, viscosity -- μ, and flow area -- A) are not pressure dependent. The Reynolds number, like the Nusselt number, is independent of system pressure.

From this analysis, it can be concluded that a calibration made at any one pressure level is equally applicable over all pressure levels specified in the design. To use the flow meter in actual practice, it is not necessary to measure the meter pressure level, as long as it is within design specifications.

3.3 Conclusions and Recommendations

From this course of studies, it was concluded that the anemometer vapor flow meter, met in principle the design objectives of the contract. The meter responded to changes in flow rate over the entire specified flow range.

Design calculations showed the meter to be equally as applicable to cesium as to mercury. The pressure, temperature, and compatibility requirements specified by the contract have been experimentally attained during meter testing.

To improve the meter further and make it a more reliable laboratory instrument, there still remains some points of experimental investigation. These are:

1. The possible changing of anemometer thermocouple composition and emf output with time after prolonged exposure to cesium or mercury.

2. Appropriate modification of the null balance circuitry to eliminate the present drifting tendency of the anemometer during the course of calibration.

APPENDIX A

CALIBRATOR RIG AND TEST SYSTEM COMPONENTS

The photograph shown as Figure A-1 is an overall view of the anemometer-calibrator test rig. The anemometer salt bath temperature control (whose circuit diagram is shown in Figure 2-18, Section 2) is positioned below the microvolt meter.

The power controls for the rig and the thermocouple readouts used to indicate component and vapor temperatures are in the test panel to the left of the calibrator rig.

A close up of the vapor flow meter itself, properly positioned in the test rig without the insulation in place, is shown as Figure A-2. The meter is designed to be used in a vertical position with the reference anemometer fin upstream of the heated anemometer fin.

Figure A-3 is a pictorial drawing of the calibration system depicting the location of each of the thermocouples in the system. The temperature indicators are positioned as:

1. Lower salt bath temperature at boiler.
2. Upper salt bath temperature at boiler.
3. Boiler vapor temperature.
4. Vapor temperature at boiler exit and superheater entrance.
5. Lower salt bath temperature at superheater.
6. Upper salt bath temperature at superheater.
7. Vapor temperature at entrance to orifice.
8. Lower salt bath temperature at desuperheater.
9. Upper salt bath temperature at desuperheater.
10. Vapor temperature at entrance to meter.
11. Meter salt bath temperature.
12. Lower oil bath temperature at condenser.
13. Middle oil bath temperature at condenser.
14. Upper oil bath temperature at condenser.
15. Vapor temperature at top of condenser.
16. Vapor temperature at bottom of condenser.
17. Condenser inlet surface temperature.

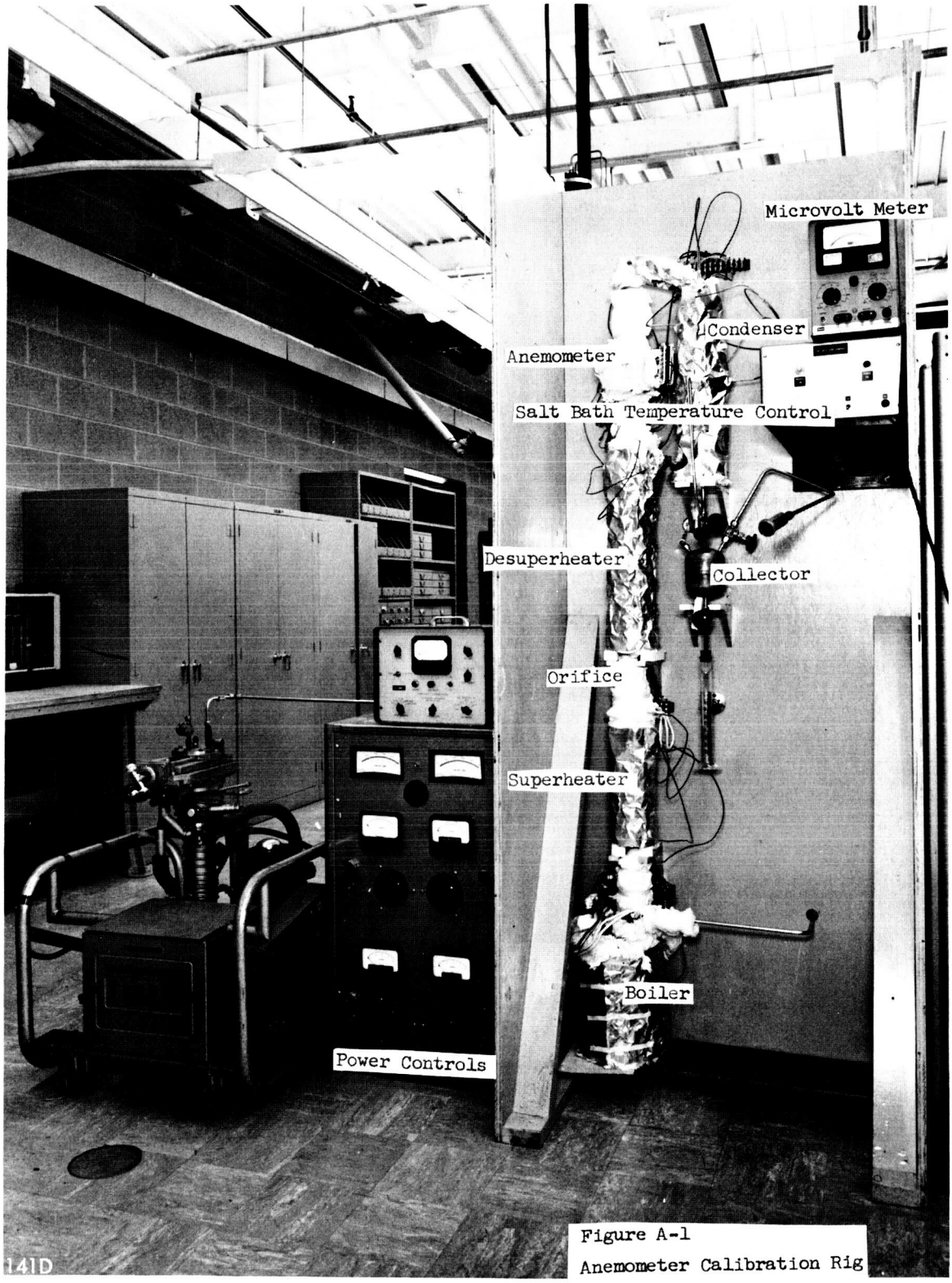

Figure A-1
Anemometer Calibration Rig

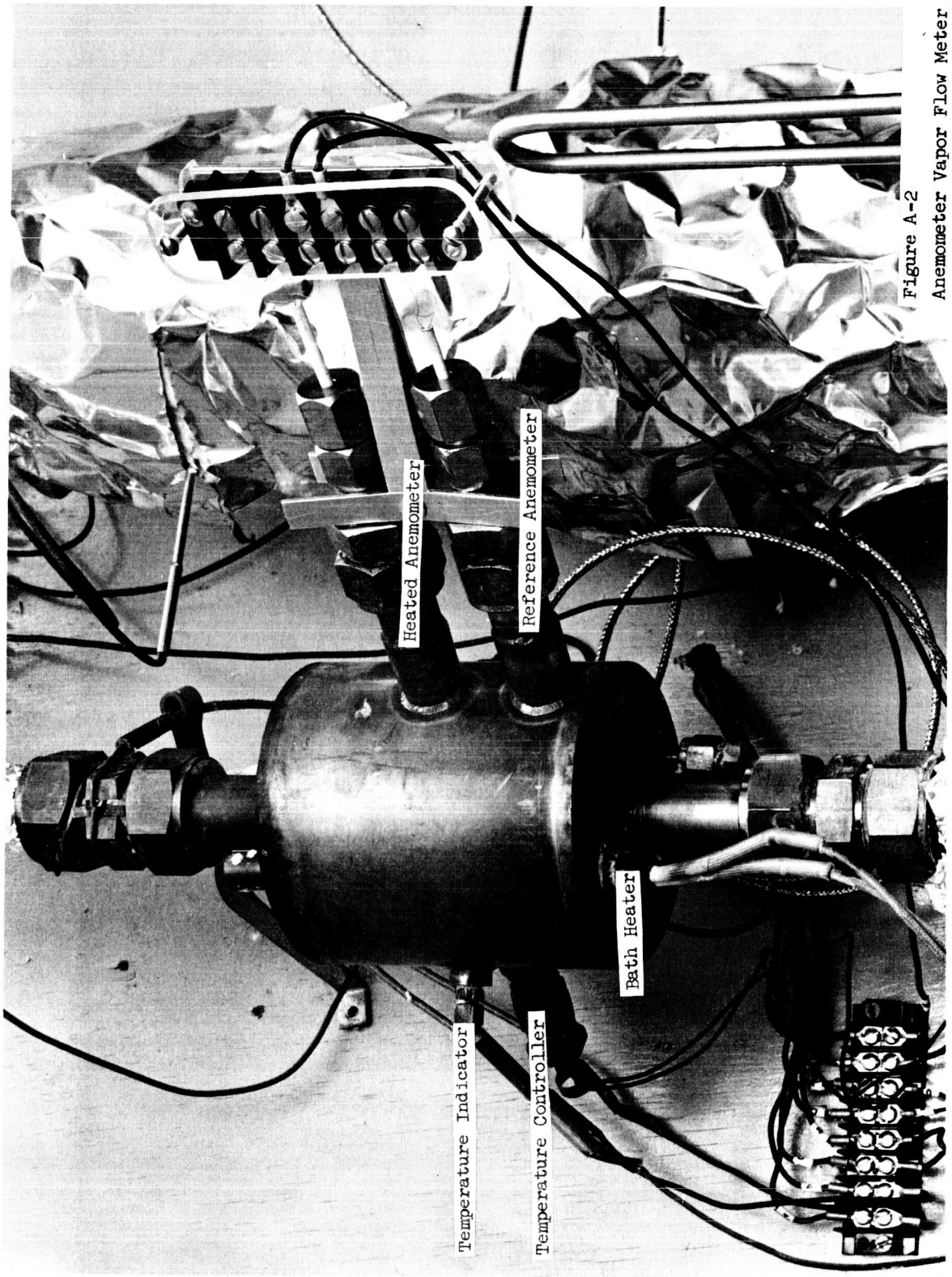

Figure A-2
Anemometer Vapor Flow Meter

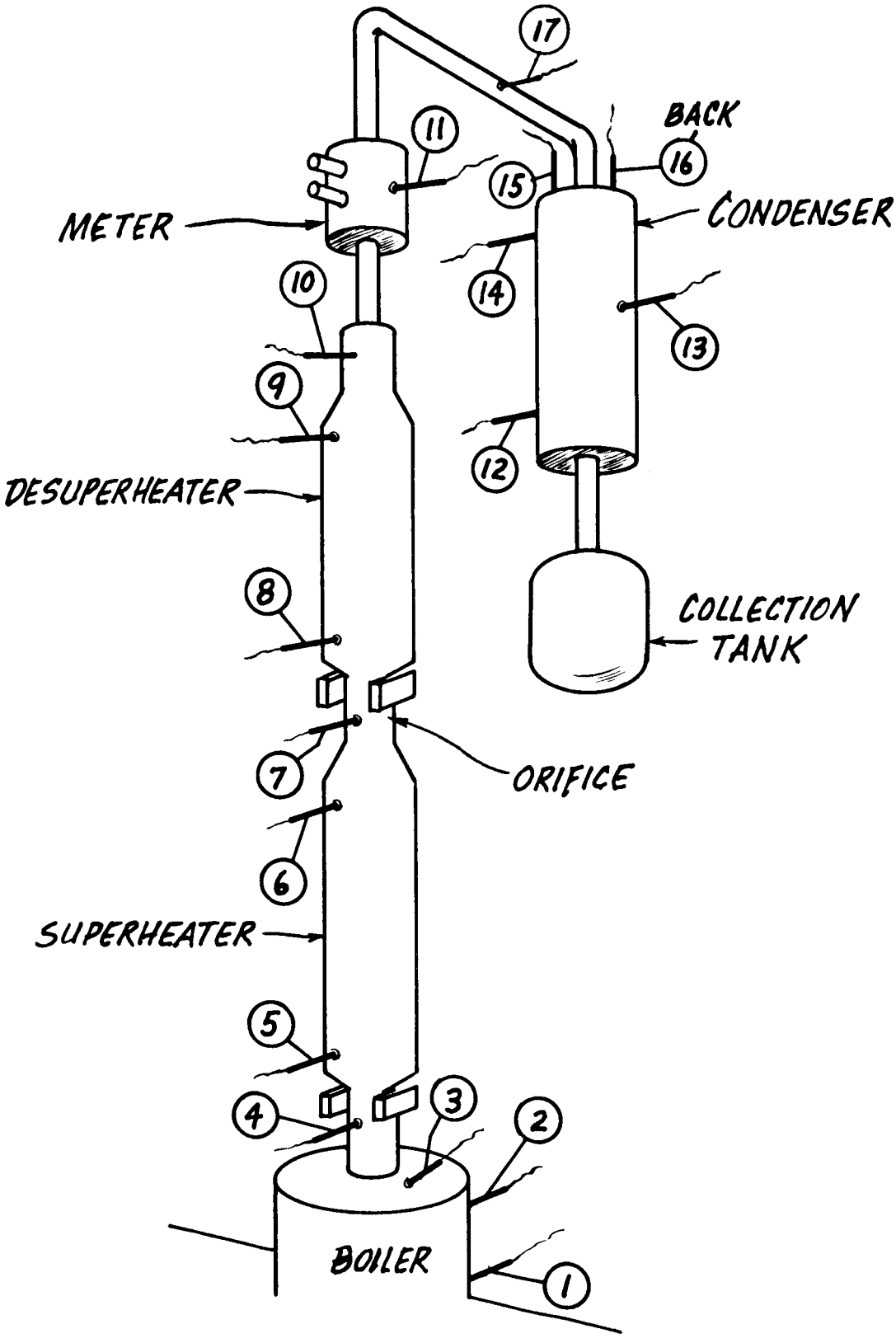

METER CALIBRATION SYSTEM

Figure A-3

All components were made from type 316 or 347 stainless steel. Connections were accomplished with Swagelok tubing fittings. Iron-constantan was the thermocouple selection. All valves in the system that experienced liquid metals above 300°F were bellows sealed needle valves. All other valves were Teflon packed regulating valves.

Pictures of the individual components that made up the system are shown in Figures A-4, A-5 and A-6. Watlow immersions heaters such as shown in Figure A-4 were used for powering each of the components.

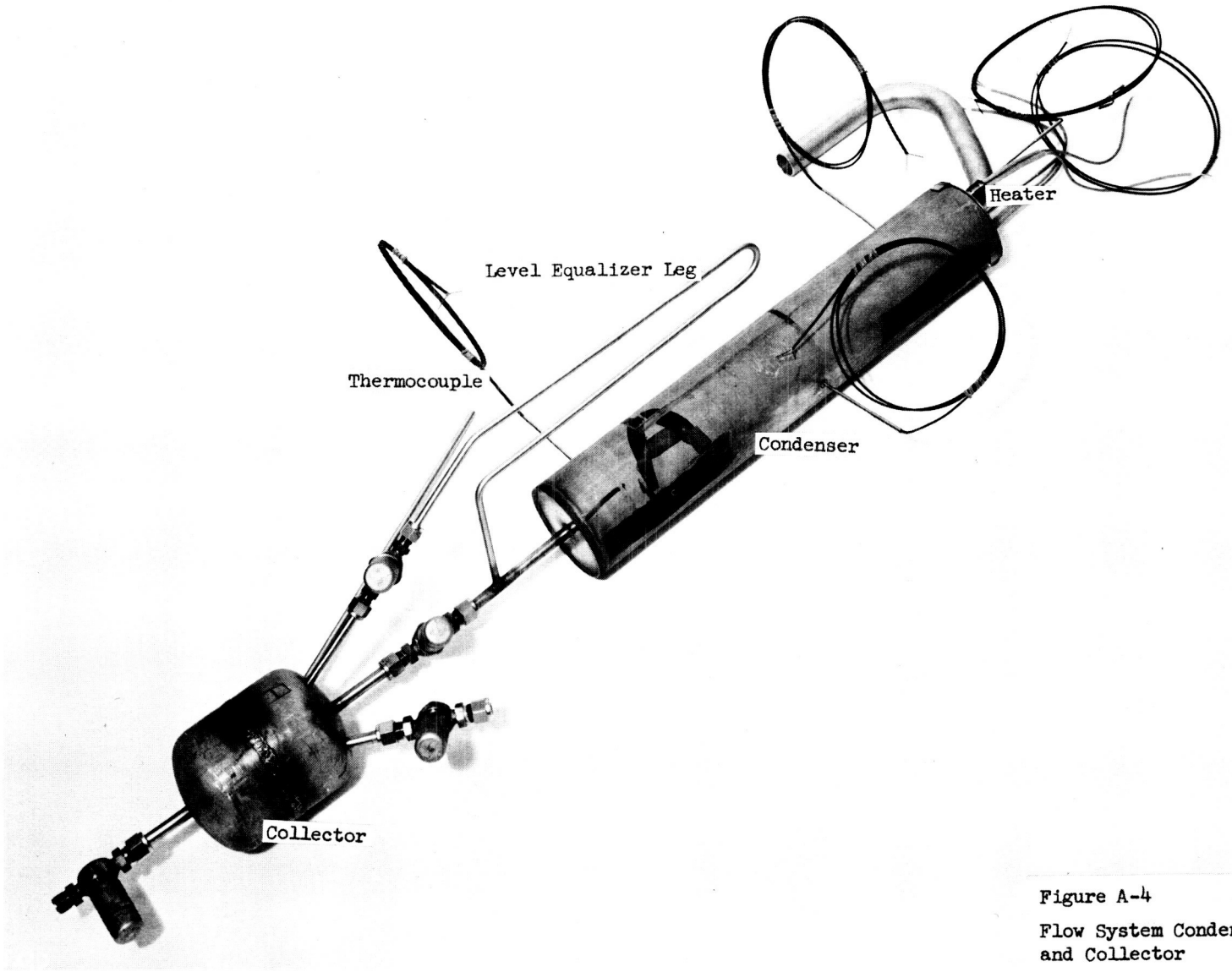

Figure A-4

Flow System Condenser and Collector

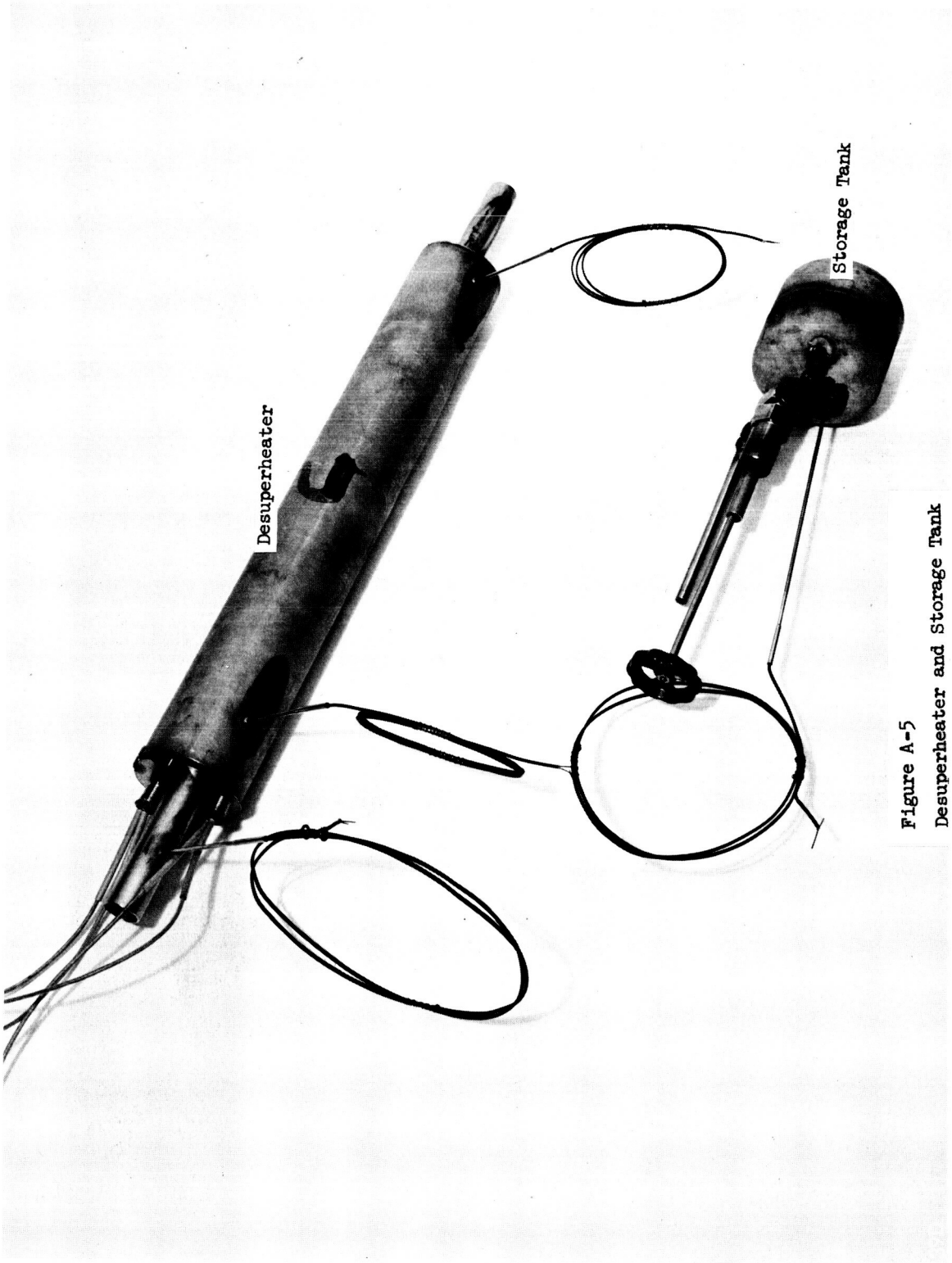

Figure A-5
Desuperheater and Storage Tank

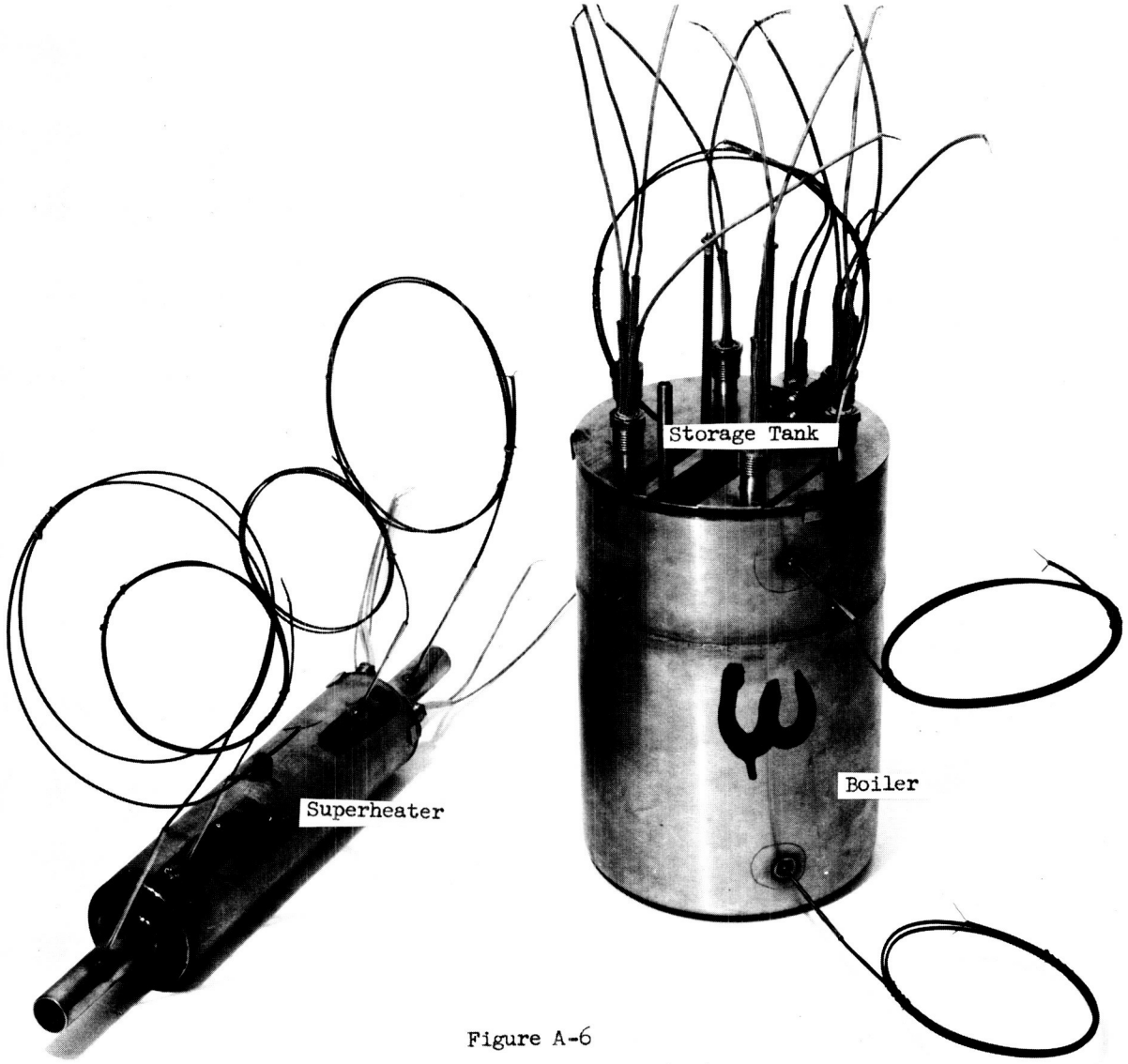

Figure A-6
Boiler and Superheater

APPENDIX B
CALIBRATOR RIG OPERATION

Two orifices were designed and built for the calibrator rig. The smaller one (0.016 inches diameter) is intended for use over the entire flow rate range (10^{-4} to 5 x 10^{-2} gms/sec) with mercury and over the 10^{-4} to 4 x 10^{-3} gms/sec range with cesium. The larger orifice (0.0440 inches in diameter) is intended for use with cesium over the mass flow range of 4 x 10^{-3} to 5 x 10^{-2} gms/sec. Details of how these orifice diameters were chosen and over what flow rate ranges they were to be used is discussed in Appendix C of this report.

Figures B-1 through B-4 are mercury and cesium calibration curves for each of the two orifices. The manner in which the curves were plotted and the procedure for taking the data is presented in detail in Appendix D of this report.

The operation procedure of the calibrator rig will be explained for use with mercury. However, the same procedure is also applicable with cesium. Because of the required meter pressure operation ranges (0.1 to 25 torr) the condenser temperatures necessary to obtain these pressures range from 180 to 800°F. For mercury operation, the condenser temperature range is from 180 to 250°F. For cesium, this range is from 500 to 800°F. Plots of experimental data showing condenser temperature level versus system operating pressure for both mercury and cesium flow conditions are shown in Figures B-5 and B-6.

During mercury operation the condenser is to be filled with a high temperature oil. A suitable salt is to be used for cesium tests.

System Operation Procedure

Filling of Condenser

1. Fill boiler with 100-150 cc of Hg; evacuate to 50 microns or less, and close boiler valves.
2. Evacuate entire calibrator rig to 50 microns or less pressure level.
3. Close condenser valve and condenser leg valve between collector and condenser.
4. Add 600 cc of Hg to collector.
5. Evacuate collector to 50 microns or less pressure level.

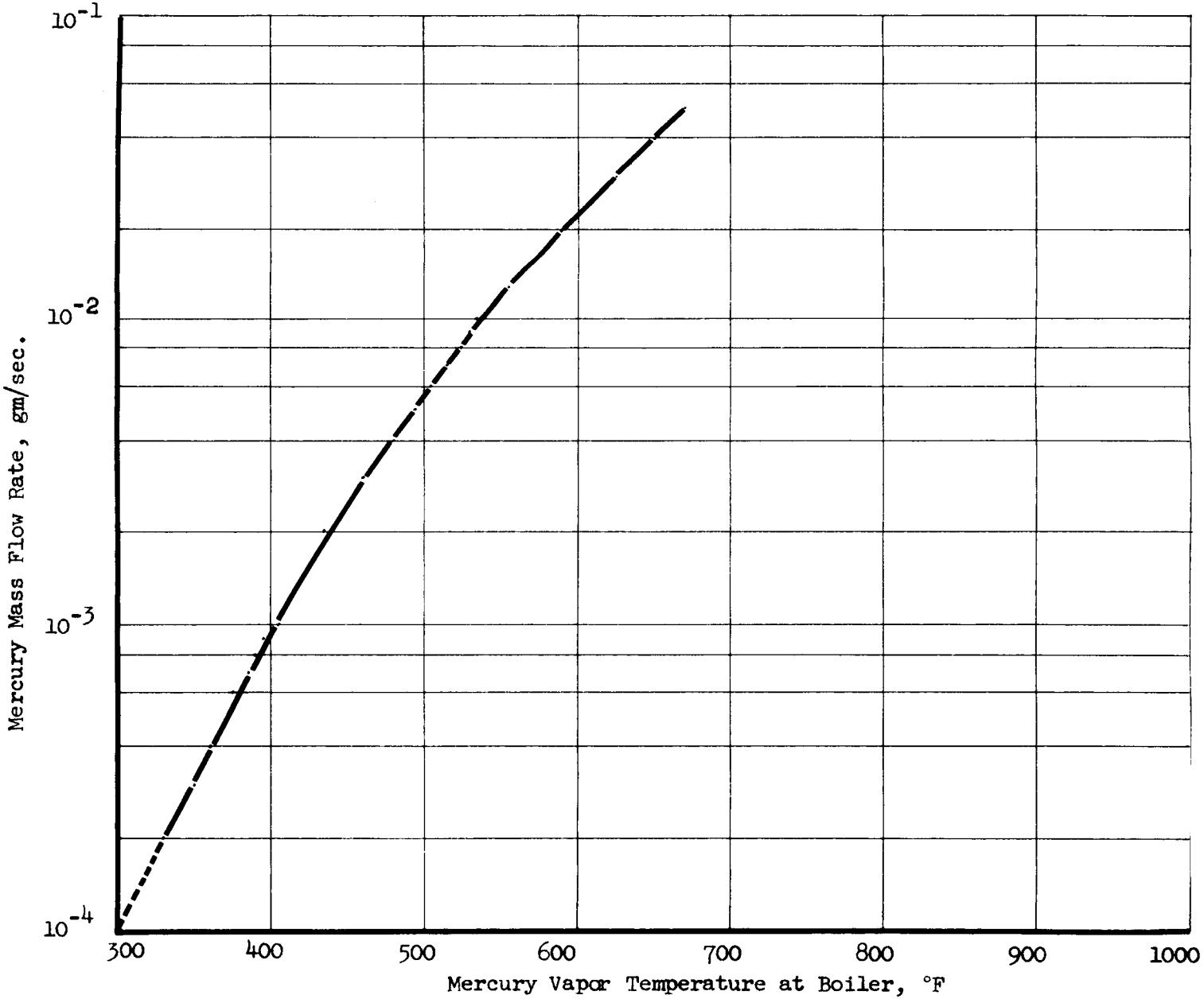

Figure B-1

Orifice Calibration Data for Mercury Mass Flow Rates
(Orifice Diameter 0.016 Inches)

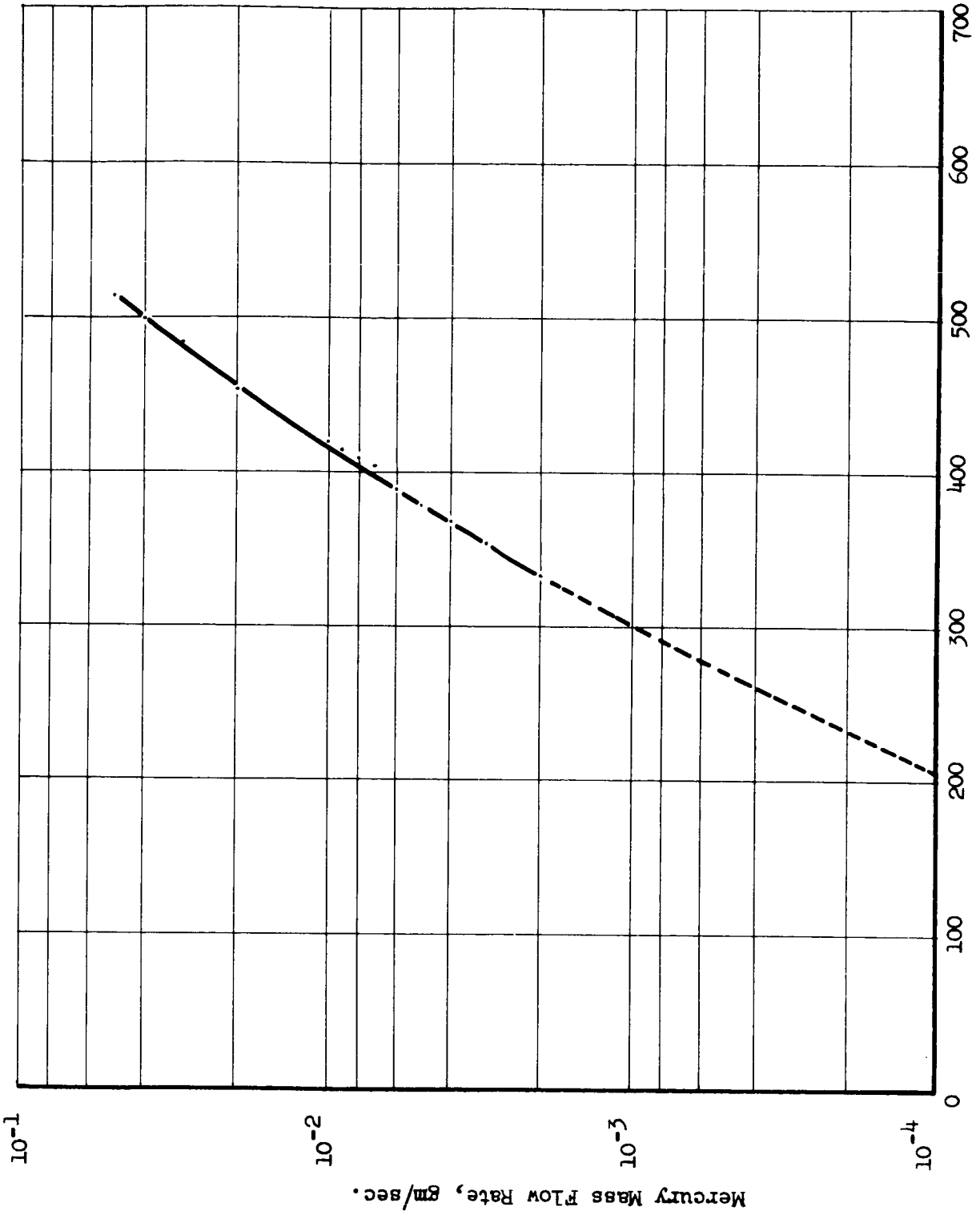

Figure B-2

Orifice Calibration Data for Mercury Mass Flow Rates
(Orifice Diameter 0.044 Inches)

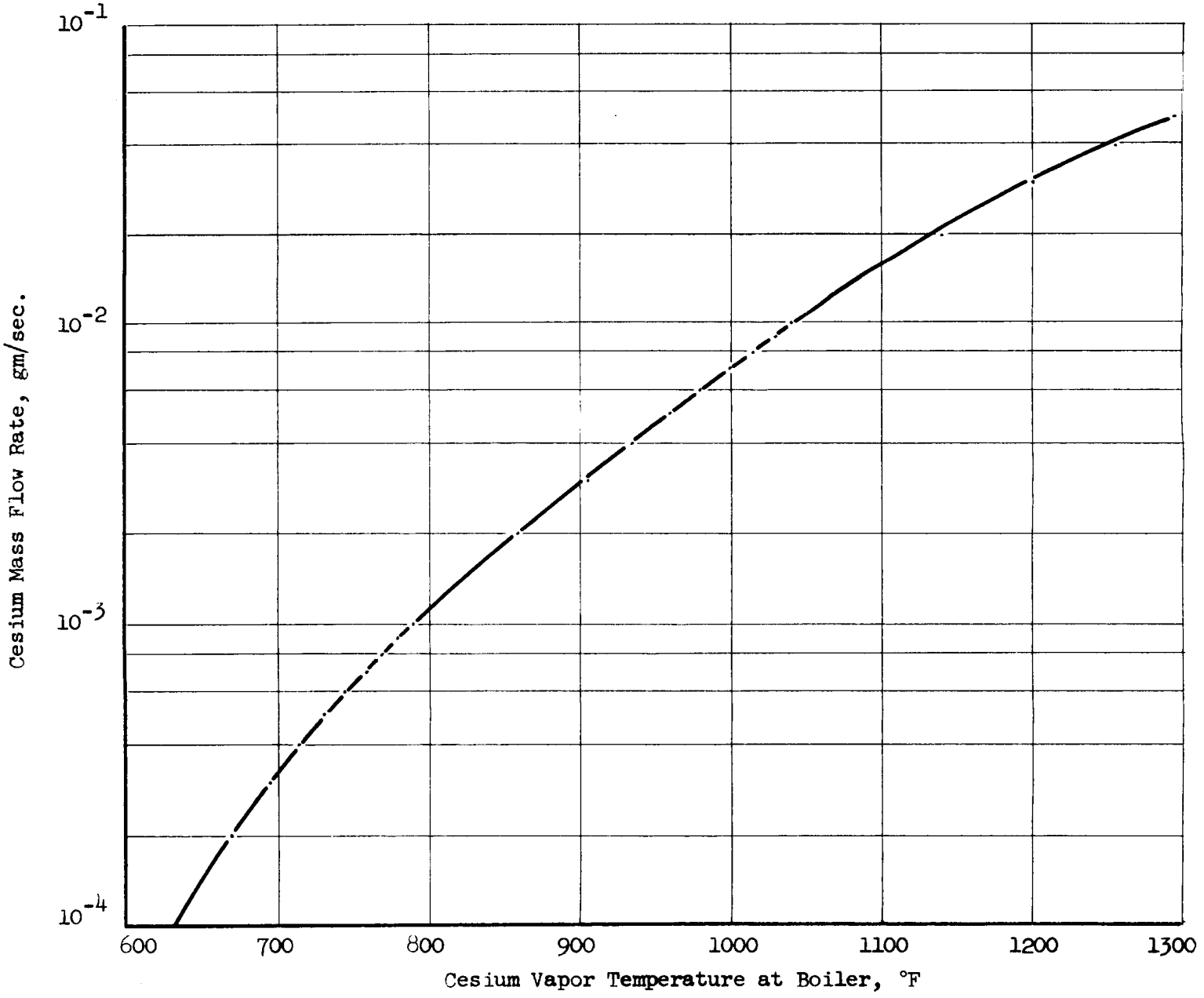

Figure B-3

Orifice Calibration Data for Cesium Mass Flow Rates
(Orifice Diameter 0.016 Inches)

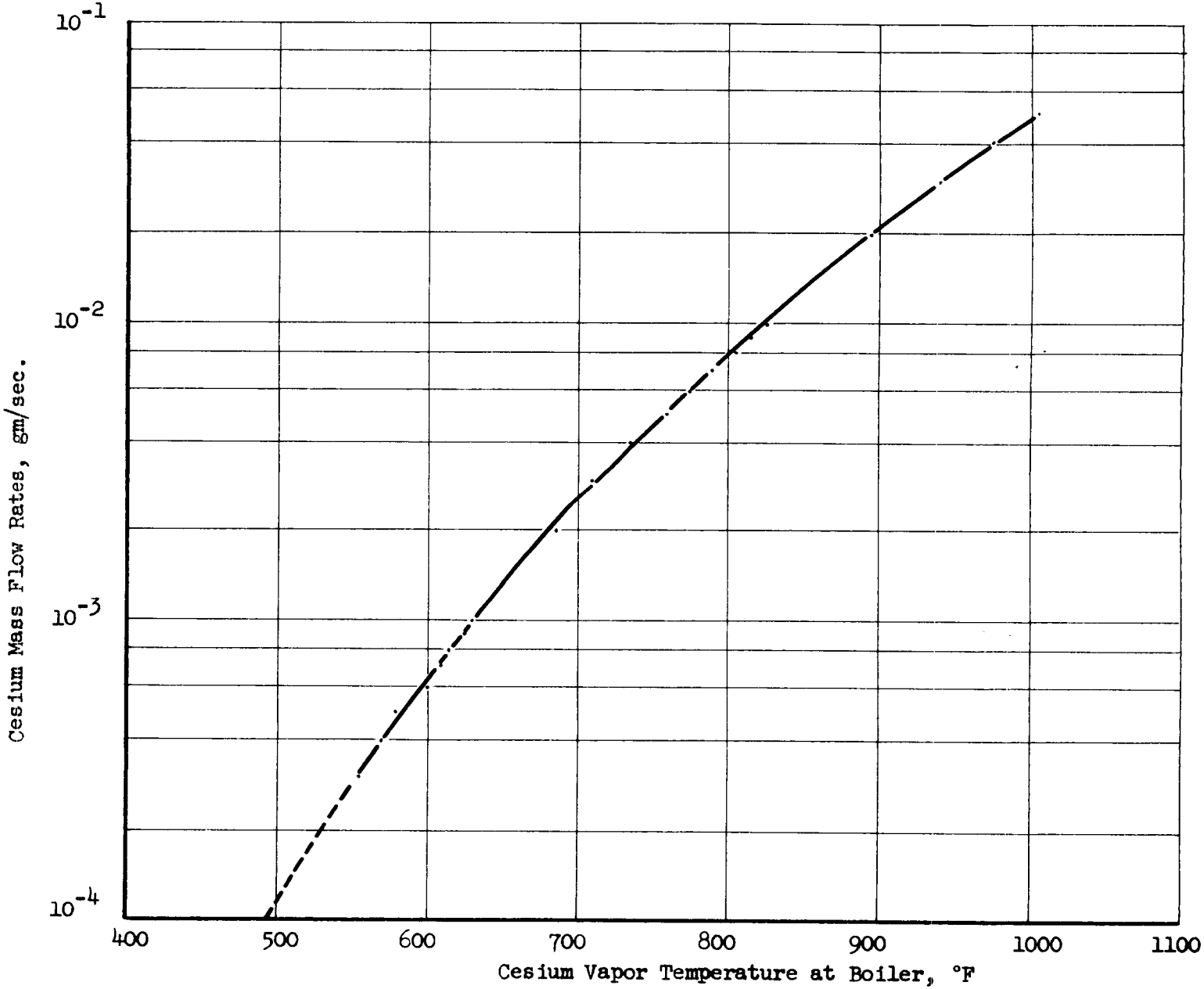

Figure B-4

Orifice Calibration Data for Cesium Mass Flow Rates
(Orifice Diameter 0.044 Inches)

Reference: WADC Technical Report 59-598

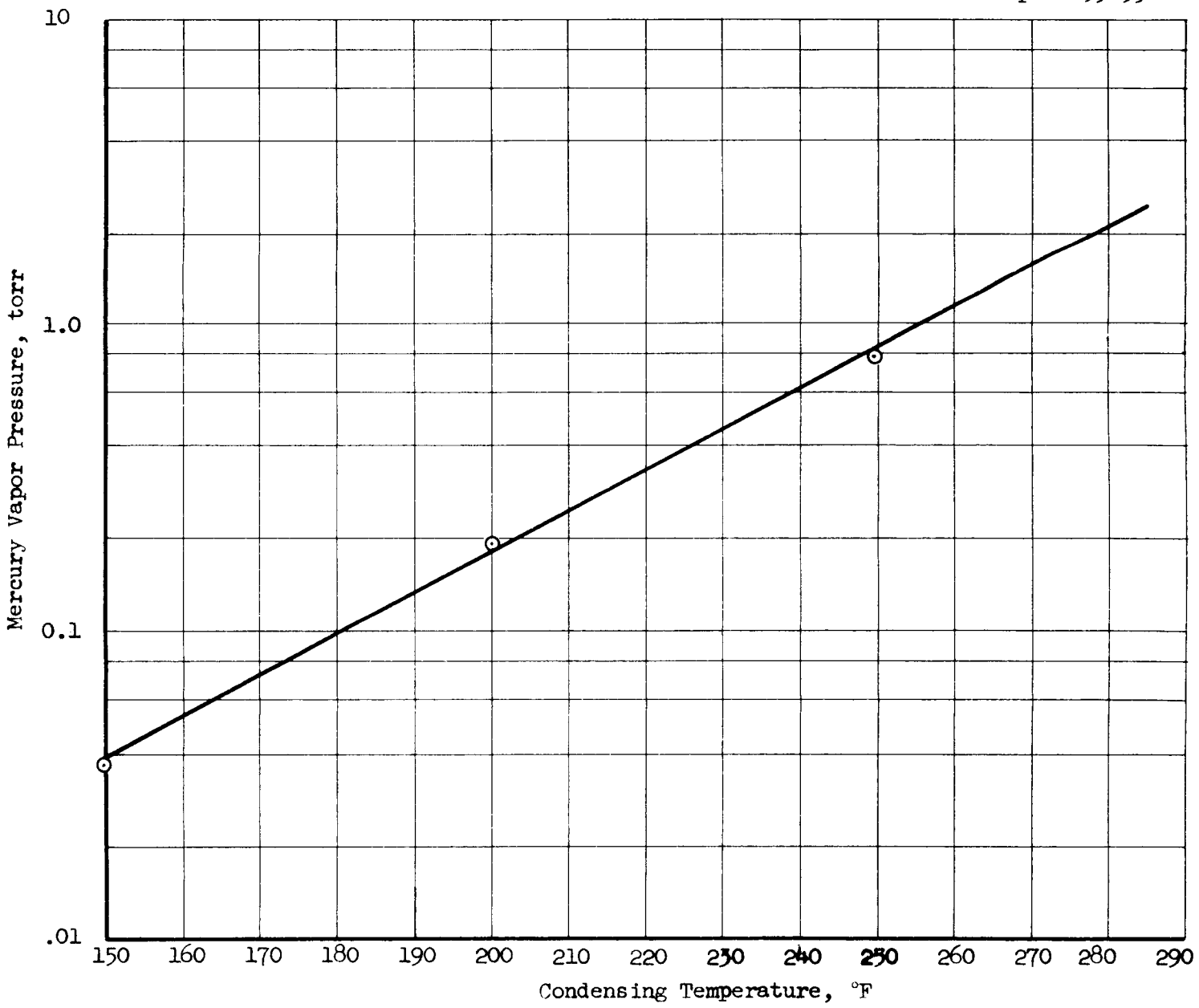

Figure B-5
Vapor Pressure Curve for Condenser Operation
(Flowing Vapor -- Mercury)

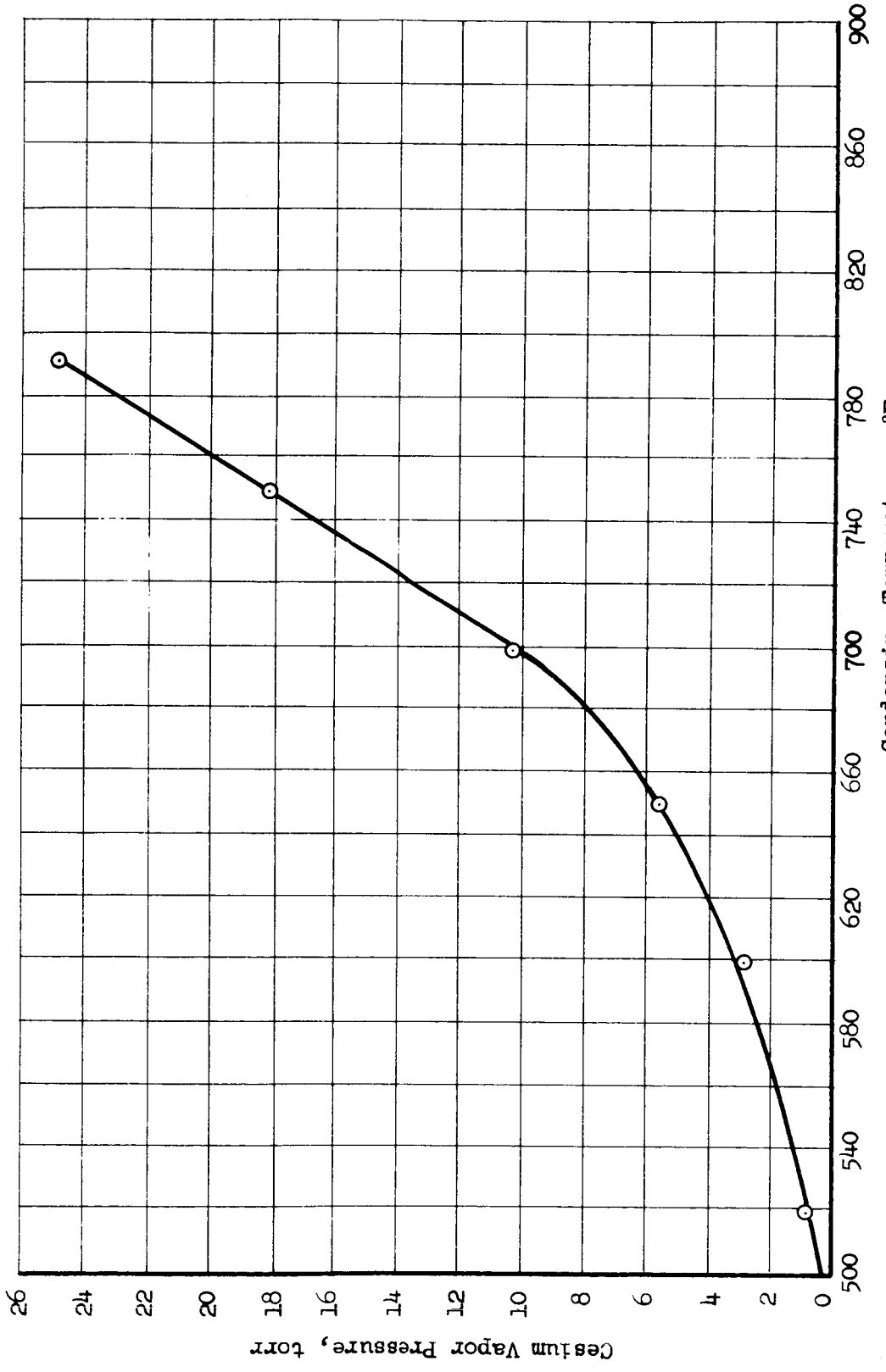

Reference: WADC Technical Report 59-598

Figure B-6

Vapor Pressure Curve for Condenser Operation
(Flowing Vapor -- Cesium)

6. Open condenser valve.
7. Pressurize collector with sufficient argon or air pressure to elevate a column of mercury one inch above the height of the condenser leg. (This is approximately 23 inches).

Note: For cesium operation only argon can be used.

8. Close condenser valve.
9. Drain excess of mercury out of collector.
10. Evacuate collector to 50 microns or less pressure level.
11. Open condenser leg valve and drain excess mercury from condenser into collector.
12. Close condenser leg valve, remove mercury from collector and evacuate collector to 50 microns or less pressure level.
13. Open condenser leg valve. The remaining mercury, about 240 cc, should stay in condenser and not be drained through the condenser leg. During rig operation the condenser leg valve should always be open and the condenser valve should always be closed. The condenser valve is only to be opened at the end of test to empty the condenser.

Component Temperature Settings

The following temperature levels are to be maintained at each of the rig components:

1. Boiler - The vapor flow rate is maintained by the boiler vapor temperature (thermocouple No. 3). This temperature magnitude may range from 300 to 1000°F, depending upon the flow media, orifice diameter in system, and desired flow rates. Reference is made to Figures B-1 through B-4 for the correlation between vapor temperature and cesium or mercury flow rate.
2. Superheater - Average temperature of 840°F (average of thermocouples 5 and 6) for mercury. For cesium this temperature will be 1000°F.
3. Desuperheater - Average temperature of 840°F (average of thermocouples 8 and 9) for mercury and cesium.
4. Anemometer - 840°F (thermocouple No. 11). This temperature is maintained by the salt bath controller. Coarse and fine adjustments of this unit is controlled with the indicated resistors on the back of the unit. The fine adjustment is turned counterclockwise until the

slip clutch no longer engages the resistor mechanism. When thermocouple No. 11 reaches 840°F, the coarse adjustment is turned counterclockwise until the heater-on light (white light) goes off. The fine adjustment is then turned clockwise until the heater-on light turns on again. The controller is now set and should need no further adjustments during the calibration run.

5. Condenser Inlet - 800°F
6. Condenser - The meter pressure is controlled by the condenser temperature. The average reading of thermocouples 15 and 16 should be interpreted as the condenser temperature. Reference is made to Figures B-5 and B-6 for the exact condenser temperature level for the flowing vapor and the desired meter pressure.

The components should be allowed to reach equilibrium temperatures before calibration tests begin. Temperatures should be recorded at every half hour interval during the warm-up times.

Anemometer Preparation

Once the anemometer salt bath has attained an equilibrium temperature the following procedure should be taken in preparing the anemometer for calibration.

1. Check the electrical continuity of the thermocouples on both the reference and heated anemometer fins, and the heated leads. These are the most fragile assemblies in the test system.
2. With a constant current source, supply 0.366 amps (DC) to the anemometer fin.
3. Connect the anemometer thermocouples, null balance system, and indicating microvoltmeter as shown in Figure 2-21.
4. Balance these two thermocouple outputs until a 0 microvolt signal is attained.

The meter is now ready for calibration. No further adjustment of the null system should be made during the remainder of the test.

Calibration Procedure

Following attainment of component temperature equilibrium and nulling of anemometer thermocouple outputs, the following procedure is used to calibrate the meter.

1. Open the boiler valve.
2. Record microvolt output as a function of time at the desired flow rate. Care should be taken to keep boiler temperature constant -- preferably for a half-hour time period at any one flow rate.
3. Change boiler temperature to other levels and repeat step 2. This calibration procedure should be repeated for at least 4 to 6 points over the prescribed flow rate range.

APPENDIX C
CALIBRATION RIG DESIGN

Introduction

One method considered for calibrating the vapor flow meter involved a condensing calorimeter. This instrument would sense the heat of condensation of the vapors and relate this to flow rate. The difficulty in applying this concept to the flow meter system arises from the wide ranges of condensation heat that must be sensed by the instrument. The heat loads vary from 0.115 BTU/hr (corresponding to the low mercury flow rate) to 108.4 BTU/hr for the high cesium flow rate. This is a condenser load variation of approximately 1000 to 1. Since one calorimeter is not sufficiently sensitive over this entire heat load range the following design parameters were chosen to determine the exact number of calorimeters required for this application:

1. The heat loss to the ambient was to be a maximum of 1/10 of the measured condensation heat.
2. The heat loss to the ambient was to be 1/2 per cent of the maximum measurable condensation heat.

This resulted in a need for three calorimeters to cover the required flow range.

The difficulty expected in accurately calibrating these calorimeters (especially the smallest one) plus some reliability problems that may be experienced with the thermopile sensing elements, resulted in further searches for other calibration systems.

A modification of the above mentioned calorimeter was considered whereby the entire heat load range could be sensed using one instrument. This required changing the condensing media as the flow rate range changes. This concept was also abandoned for the same reasons considered with the three individual calorimeters.

Another possible method of meter calibration was volume accumulation. However, using the lowest flow rates as an example it would take 158 seconds to accumulate a one inch buildup in a 0.003 inch diameter tube. A small change in condenser liquid hold-up would result in a large calibration error. Therefore, this idea was also abandoned.

The only approach which had no serious limitations to it, was a choked orifice. This could be calibrated with argon at or near design flow and the results extrapolated from the calibration temperature to the operating temperature of the meter.

In using this orifice flow system a boiler thermocouple will sense saturation temperature and indicate the orifice supply pressure. The superheater will help prevent liquid carry-over through the orifice. A desuperheater will bring the vapor temperature to the required 840°F. Meter pressure level is fixed by the condenser. The prime disadvantage to the orifice system lies in the calibration techniques. For the specified flow rates, collection methods for orifice calibration cannot be used. In its place, calibration must be accomplished with a different fluid, and then the results extrapolated to predict either cesium or mercury flow data. A schematic drawing of this system is presented as Figure C-1.

Orifice Design Calculations

The flow equation for a choked orifice can be written as:

$$G = \sqrt{\frac{gk}{R}\left(\frac{2}{k+1}\right)^{\frac{k+1}{k-1}}}\left(\frac{P}{\sqrt{T}}\ C_D A\right) \qquad \text{(C-1)}$$

where

G = flow rate, lb/sec.

g = dimensional constant, 32.2 lb_m ft/lb_{ft} sec^2

R = gas constant, lb_f ft/lb_m °F

k = C_p/C_v

C_p = specific heat at constant pressure, BTU/lb °F

C_v = specific heat at constant volume, BTU/lb °F

P = absolute orifice upstream pressure, lb/ft^2

T = absolute temperature of gas, °R

C_D = orifice coefficient

A = throat area of orifice, ft^2

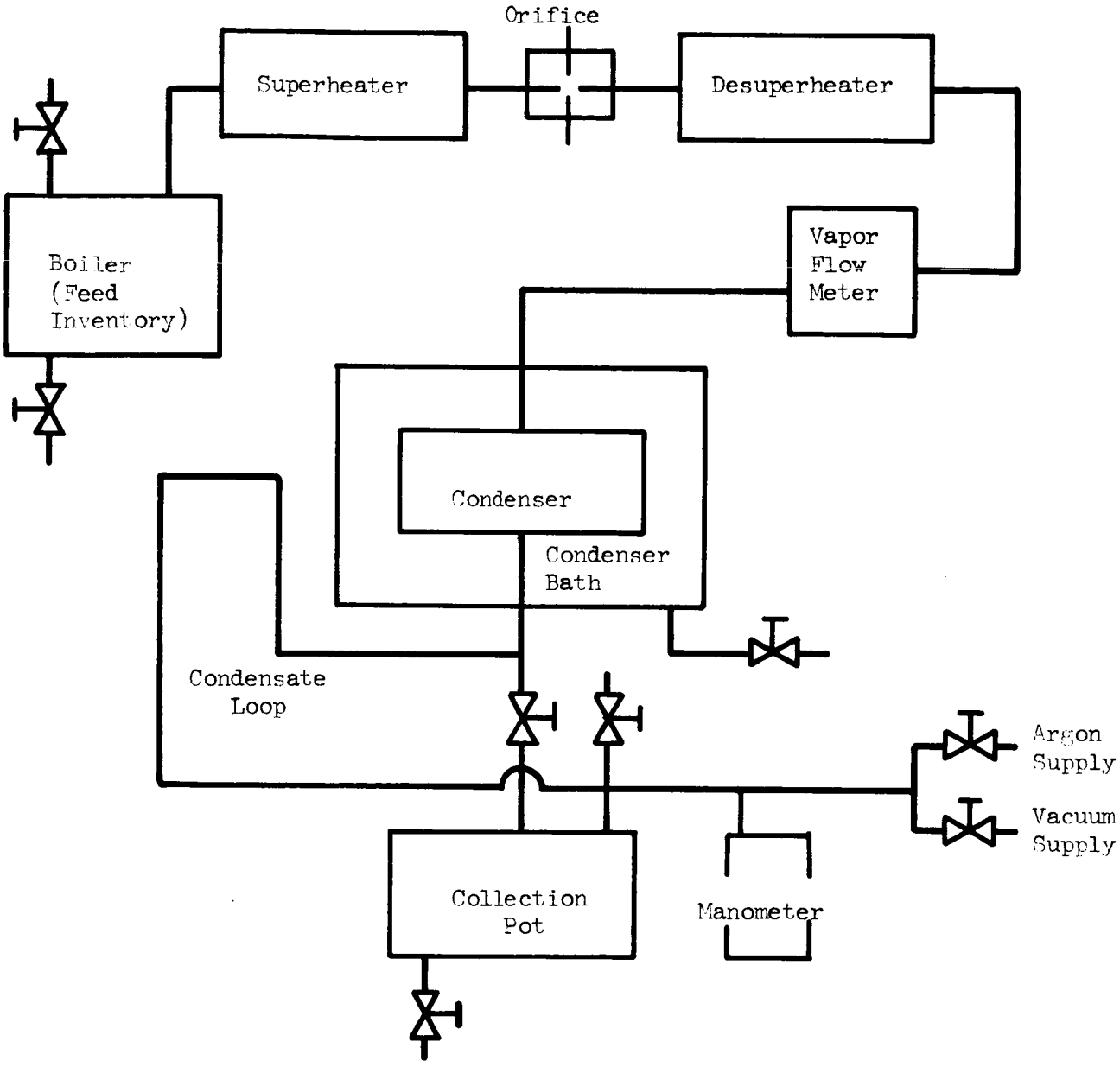

Figure C-1
Schematic Diagram
of
Vapor Flow System

All the properties for the vapors (both mercury and cesium) were taken from Report No. WADD TR 61-96.

For cesium equation (C-1) can be written as

$$\dot{m}_{Cs} = \frac{1.23\ PC_D A}{\sqrt{T}} \qquad (C\text{-}2)$$

and for mercury

$$\dot{m}_{Hg} = \frac{1.49\ PC_D A}{\sqrt{T}} \qquad (C\text{-}3)$$

Assume the average temperature across the orifice is 900°F (or 1360°R) and $C_D \approx 0.84$[1].

Equations (C-2) and (C-3) can be rewritten as:

$$\dot{m}_{Cs} = 0.192\ PD^2 \qquad (C\text{-}4)$$

and

$$\dot{m}_{Hg} = 0.233\ PD^2 \qquad (C\text{-}5)$$

where

$\dot{m}$ = flow rate, gm/sec.

P = upstream orifice pressure, torr

D = orifice diameter, in.

A plot of these equations for different orifice diameters is presented as Figure C-2. On the same curve the specified meter pressure lines are also drawn. By dividing the meter pressure by the required pressure ratio for a choked orifice $\left[2/k + 1\right]^{k/(k-1)}$, lines of minimum supply pressure can be drawn. In each case, the system operating pressures must exceed or be to the right of this minimum supply pressure line.

Because the minimum supply pressure for cesium are of greater magnitude than the minimum supply pressures for mercury, the orifice design for the cesium flow system is the controlling factor for the system orifice specifications.

---

[1] Shapiro, A. H., "The Dynamics and Thermodynamics of Compressible Fluid Flow", Ronald Press Company, p. 100, New York, New York, 1953.

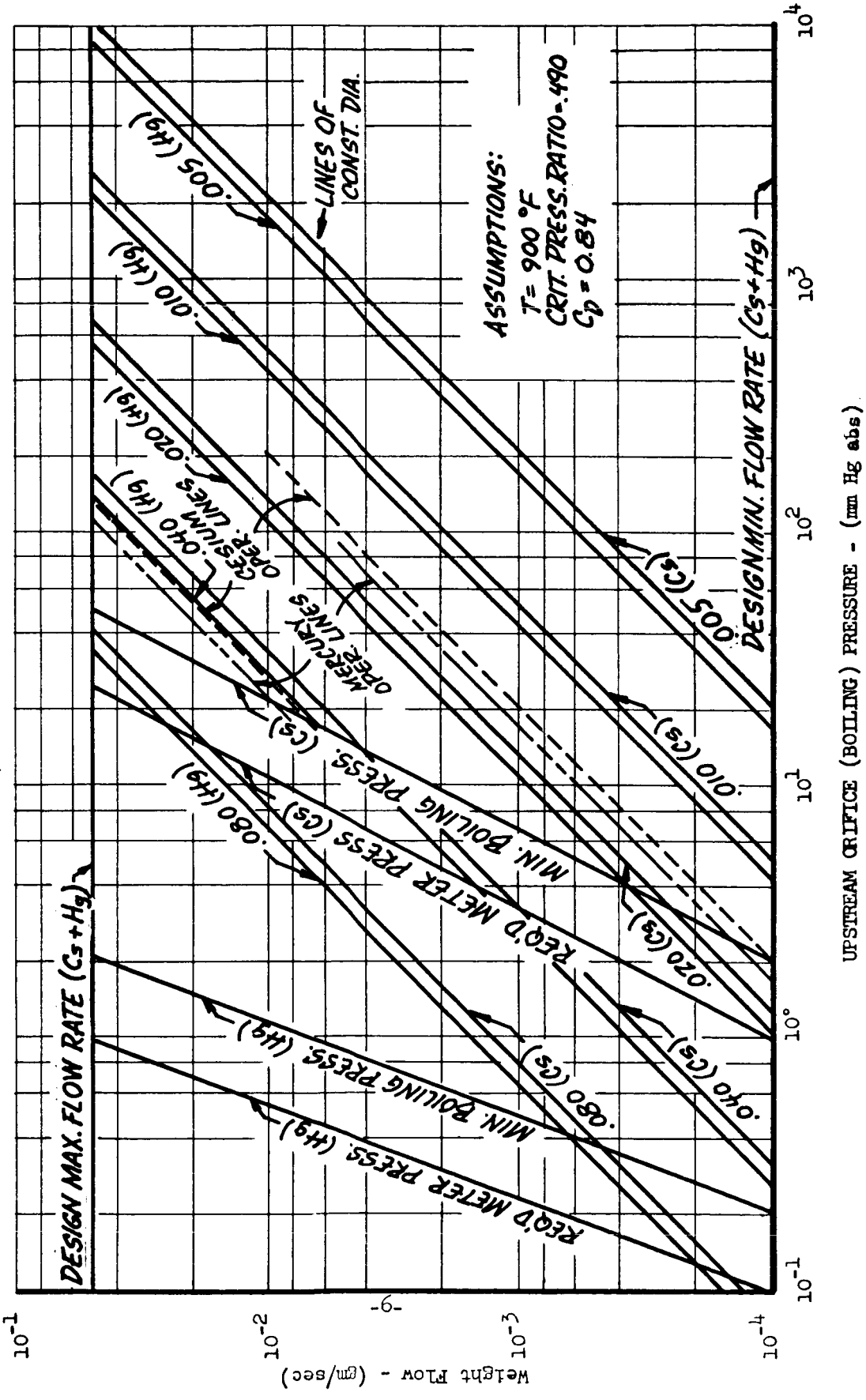

Figure C-2
ORIFICE-OPERATING PLOT FOR Cs AND Hg VAPOR

To use Figure C-2 as a design scale consider a system in which one orifice would be used to cover the entire flow range (i.e., from 5×10^{-2} to 10^{-4} gms/sec). A line is drawn parallel to the constant orifice diameter line until it intersects the minimum supply pressure at the minimum flow rate. For cesium the maximum boiler supply pressure (corresponding to the line intersection at the maximum flow rate) is approximately 1000 torr. This represents a boiling temperature of 1310°F. Because this is not a practical operating temperature more than one orifice must be used to cover the entire cesium flow range. If two orifices are used the maximum supply pressure can be reduced to 135 torr or a supply temperature of 980°F. These orifice diameters are 0.0440 and 0.0160 inches respectively. The larger orifice covers the cesium flow range from 5×10^{-2} gms/sec to 4×10^{-3} gms/sec. The smaller orifice covers the cesium range from 4×10^{-3} gms/sec to 10^{-4} gms/sec.

These orifice configurations for mercury operation results in a range of supply pressures of 116 torr (or a saturation temperature of 513°F) to 1.75 torr (or a saturation temperature of 281°F).

When considering the orifice system, the following points arise:

1. The high cesium vapor flow rate is generated at 980°F and then superheated somewhat above this temperature to assure no liquid carryover through the orifice. Since a 900°F temperature was assumed in plotting the operating lines on Figure C-2, experienced flow conditions will be somewhat different from those predicted from the graph.
2. The Knudsen number at the small diameter orifice indicated that slip flow may exist at the low mercury flow rate. The exact effect of this is not readily apparent. However, if calibration is conducted at the same Knudsen number, any discrepancy arising from slip flow conditions will not be apparent in the final testing results.
3. Figure C-3 is a plot taken from Shapiro of the sharp edged orifice discharge coefficient versus the pressure ratio. As this ratio approaches 0.4, the value of the coefficient changes from 0.84 to a lesser value. The operating lines in Figure C-2 were plotted under the assumption that $C_D = 0.84$ remained constant. From the above plot it is seen that this is not always the case. However, if the

Figure C-3
ORIFICE COEFFICIENT
versus
DOWNSTREAM TO UPSTREAM PRESSURE RATIO

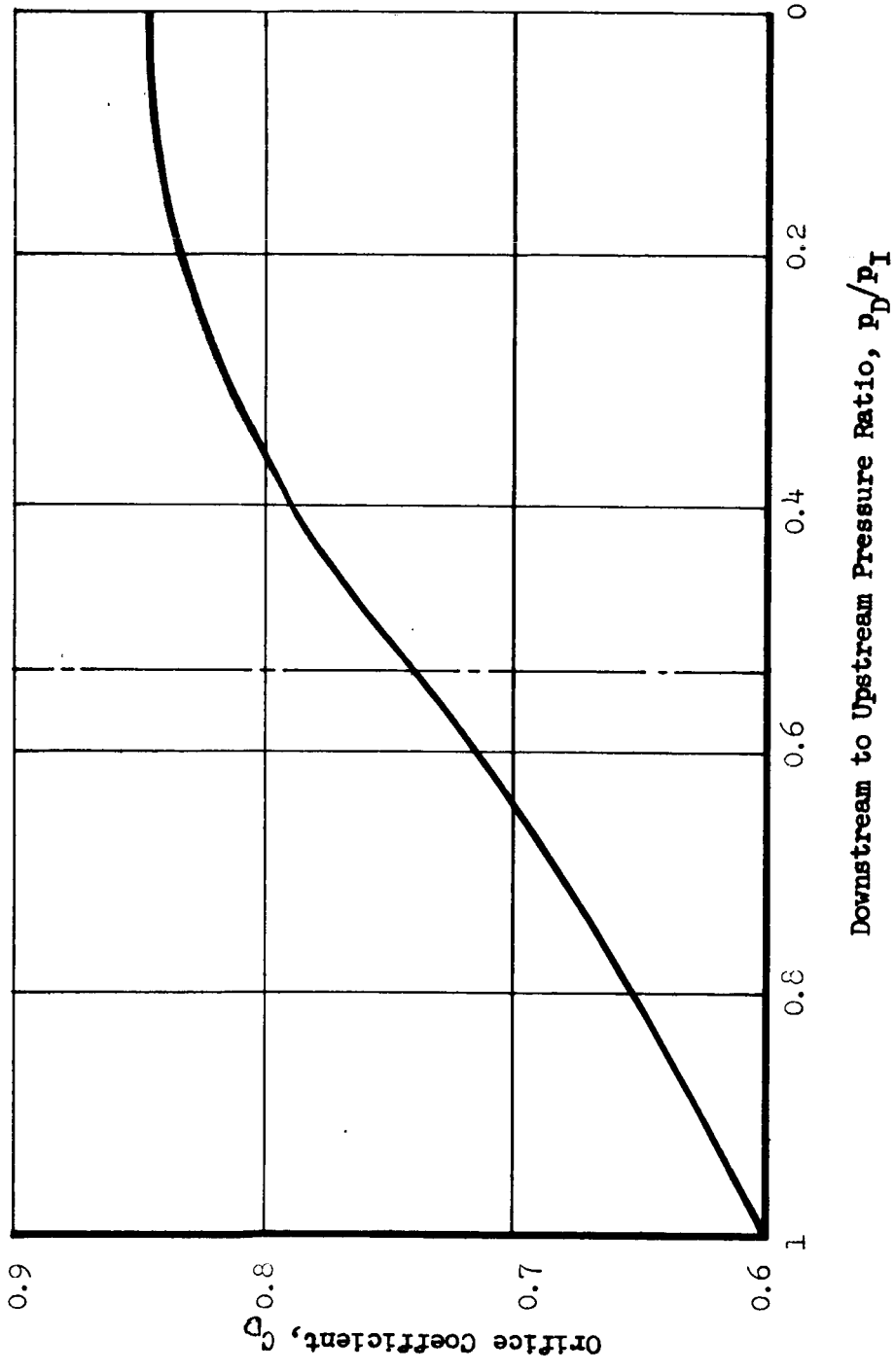

calibration is conducted at the same conditions that are experienced in actual meter operation, this changing value of C_D should not alter the accuracy of the calibration system.

Boiler Design Calculations

The boiler will be sized for the maximum volumetric flow (which corresponds to the high cesium flow rate). Furthermore, it is assumed that there will be eight hours of continual operation.

$$V = \frac{\dot{m}}{\rho} t$$

V = Tank volume, in^3

$\dot{m}$ = Flow rate, lb_m/hr

ρ = Fluid density, lb_m/in^3

t = Flow time, hr

$\dot{m} = 5 \times 10^{-2}$ gms/sec = 0.397 lb_m/hr

$$V = \frac{(0.397 \text{ lb/hr})(1728 \text{ in}^3/\text{ft}^3)(8 \text{ hr})}{(106 \text{ lb/ft}^3)} = 51.8 \text{ in}^3 \qquad \text{(C-6)}$$

This tank will be sized for a cylindrical geometry. Assume the diameter to be four inches diameter (D) by six inches high (h)

$$V = \frac{\pi D^2 h}{4}$$

$$V = \frac{\left[\pi(4)^2 \quad (6)\right]}{4} = 75.3 \text{ in}^3 \qquad \text{(C-7)}$$

A tank of these dimensions was used for the boiler, and was insulated with a one inch thick layer of Kaowool.

The heat loss = (C-8)

$$q = \frac{KA\Delta T}{\Delta X}$$

q = rate of heat loss, BTU/hr

K = thermal conductivity of Kaowool, BTU/hr ft °F

A = area of heat transfer, ft^2

ΔT = temperature difference causing heat transfer, °F

ΔX = distance through which heat transfer occurs, ft

K = 0.030 $BTU^{(2)}$/hr ft °F

$A = 2\left[\frac{\pi D^2}{4}\right] + \pi Dh = 2\left[\frac{\pi(4)^2}{4}\right] + (\pi\ 4 \times 6) = 101\ in^2$

$\Delta T = (T_2 - T_1)$

T_2 = highest temperature expected to be reached in the boiler = 980 °F

T_1 = temperature expected on the outside of the Kaowool = 100°F

ΔT = 980 - 100 - 880°F

ΔX = one inch

$$q = \frac{(0.030\ BTU/hr\ ft\ °F)\ (101\ in^2)\ (880°F)\ (12\ in/ft)}{(144\ in^2/ft^2)\ (1\ in.)}$$

q = 221 BTU/hr

$q_{total} = q_{latent\ heat} + q_{heat\ loss}$ (this assumes sensible heat is negligible)

q_{total} = 108 + 221 = 329 BTU/hr = 96.4 watts

This power input was obtained using a constant temperature salt bath.

Condenser Design Calculations

A condenser is required not only to condense the vapor which passes through the meter but also to maintain the specified meter pressure. Adding the line pressure drop from the condenser to meter establishes the pressure conditions within the meter. However, the line pressure drop can be shown to be minimal for all flow conditions with the exception of those that approach slip flow. Under continuum conditions, the meter pressure may be considered equal to the condenser pressure.

---

[2] Babcock and Wilcox, Kaowool Bulletin R-47

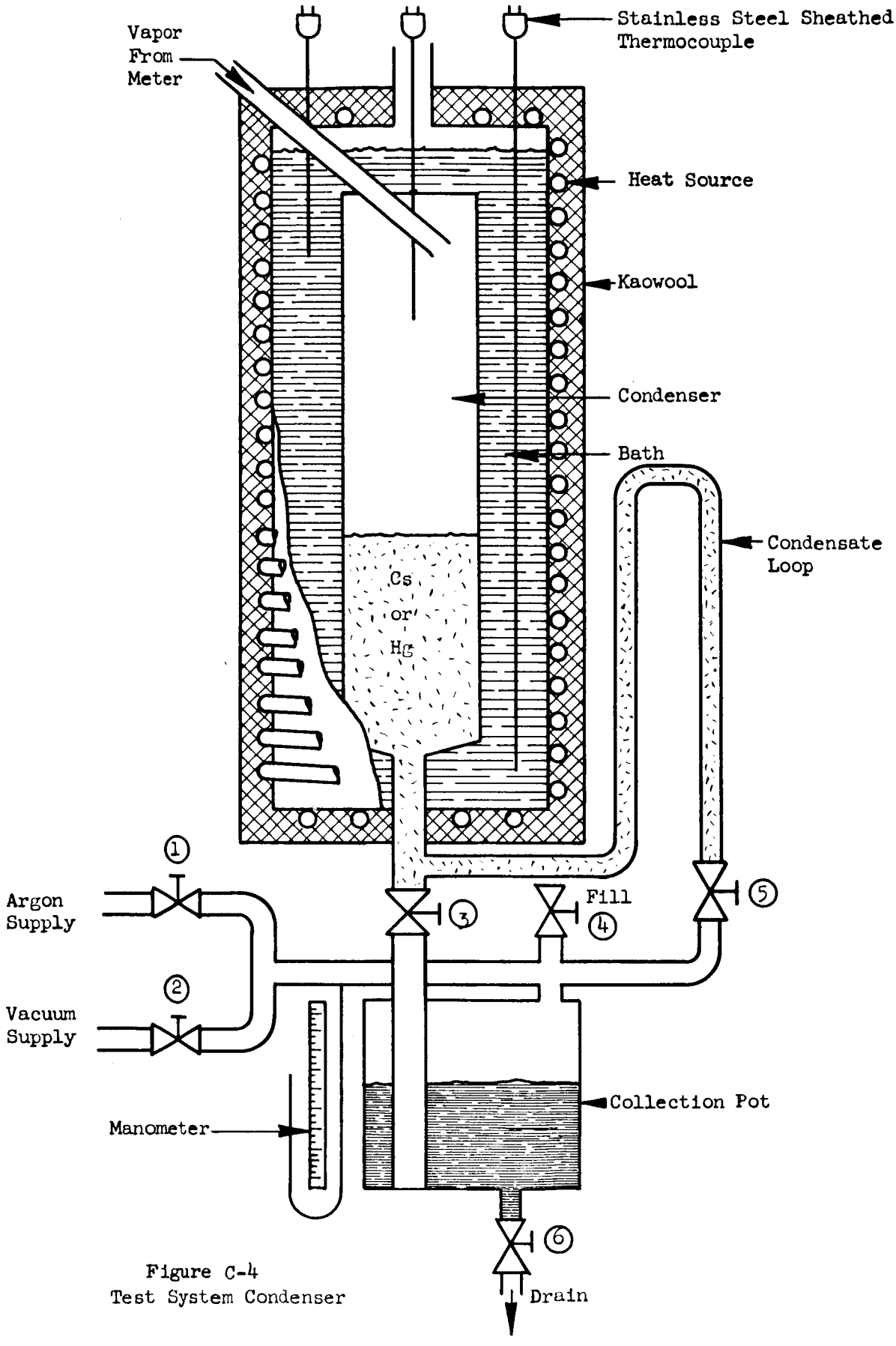

Figure C-4
Test System Condenser

For cesium these pressures range from 1 to 25 torr (corresponding to saturation temperatures of 530 to 78°F). For mercury the pressure range is 0.1 to 1 torr (corresponding to saturation temperatures of 179 to 259°F). A heat treat - high flash point oil is suggested for the mercury condenser operation. When cesium is flowing a heat treat salt is to be used.

A schematic drawing of the suggested condenser is shown in Figure C-4. The procedure for operating the numbered valves is included in Appendix B of this report.

The trap and condensate loop is necessary to stabilize the condensing interface. The required loop height is calculated from the maximum cesium pressure.

i.e.,

$$h = \frac{P}{\rho} = \frac{(25 \text{ torr})(0.0193 \text{ lb/in}^2 \text{ torr})(1728 \text{ in}^3/\text{ft}^3)}{(106 \text{ lb}_m/\text{ft}^3)}$$

$$h = 7.85 \approx 8 \text{ inches}$$

The temperature difference between the condensing vapor and the bath will be established as 10°F. To estimate the value of the overall heat transfer coefficient (U) for this system, reference was made to similar tests using water as the condensing media. Here a value of U = 60 BTU/hr ft^2 °F was found[3]. For a conservative design U = 60/3 = 20 BTU/hr ft^2 °F was used.

To calculate the heat transfer area required for the condenser the following relations were used:

$$q = \dot{m} \lambda \qquad (C\text{-}9)$$

and

$$q = UA\Delta T \qquad (C\text{-}10)$$

---

[3]Marks, L. H., "Mechanical Engineer's Handbook", Fifth Edition, McGraw-Hill Book Company, New York, New York, 1951.

where

q = rate of heat transfer, BTU/hr

$\dot{m}$ = flow rate, lb_m/sec

λ = latent heat of vaporization, BTU/lb

U = heat transfer coefficient, BTU/hr ft^2 °F

A = heat transfer area, ft^2

ΔT = the temperature drop from the condensing bath to the condensing vapors

Equating equations (C-9) and (C-10) and solving for A leaves

$$A = \frac{\dot{m}}{U\Delta T}$$

For mercury at the high flow rates, which requires the largest area

$$A = \frac{(5 \times 10^{-2} \text{ gm/sec})(3600 \text{ sec/hr})(127 \text{ BTU/lb})}{(454 \text{ gm/lb})(20 \text{ BTU/hr ft}^2/°\text{F})(10°\text{F})}$$

$$A = 0.252 \text{ ft}^2$$

$$Nu = 3.65 = hD/k$$

where

h = heat transfer coefficient, BTU/hr ft^2 °F

k = vapor thermal conductivity, BTU/hr ft °F

D = tube diameter, ft.

for cesium vapor at 1080°F, $k = 0.00308$ BTU/hr ft °F.

$$h = \frac{3.65\ k}{D} = \frac{(3.65)(0.00308 \text{ BTU/hr ft °F})(12 \text{ in/ft})}{(1 \text{ in})}$$

$$h = 0.135 \text{ BTU/hr ft}^2 °\text{F}$$

Heat input = $q = \dot{m}\ C_p \Delta T$

$$q = \frac{(5 \times 10^{-2} \text{g/sec})(3600 \text{ sec/hr})(0.0665 \text{ BTU/lb °F})(1080 - 980) \text{ °F}}{454 \text{ g/lb}} \qquad \text{(C-12)}$$

$$q = 2.64 \text{ BTU/hr}$$

The equation relating the heat transfer rate to the superheater area is

$$q = UA\Delta T_m \qquad \text{(C-13)}$$

where

ΔT_m = log mean temperature difference between the tube and vapor temperature

Assume the vapor and tube temperature profile to be as shown below:

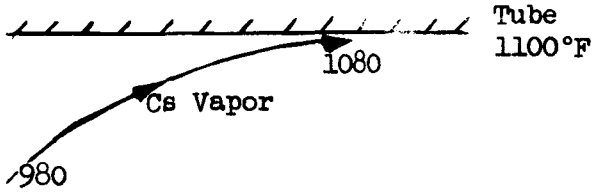

$$\Delta T_m = \frac{(1100 - 980) - (1100 - 1080)}{n(1100 - 980)/(1100 - 1080)} = 55.9$$

If the resistance of the tube wall is neglected, "U" in Equation (C-13) becomes equal to "h" in Equation (C-11).

$$A = \frac{q}{h\Delta T_m} = \frac{(2.64 \text{ BTU/hr})}{(0.135 \text{ BTU/hr ft}^2 \text{ °F})(55.9 \text{ °F})} = 0.350 \text{ ft}^2$$

Let L = the length of the superheater

$$L = \frac{A}{\pi D} = \frac{(0.350 \text{ ft}^2)(144 \text{ in}^2/\text{ft}^2)}{\pi (1 \text{ in.})} = 16.1 \text{ inches}$$

The required length will now be checked for the mercury flow system. For the maximum flow rate the superheat vapor range is 551 to 900°F.

$$h = \frac{3.65\ k}{D}$$

$$h = \frac{(3.65)(5.37 \times 10^{-3}\ \text{BTU/hr ft °F})(12\ \text{in/ft})}{(1\ \text{in.})} = 0.235\ \text{BTU/hr ft}^2\ \text{°F}$$

The temperature distribution will be assumed as

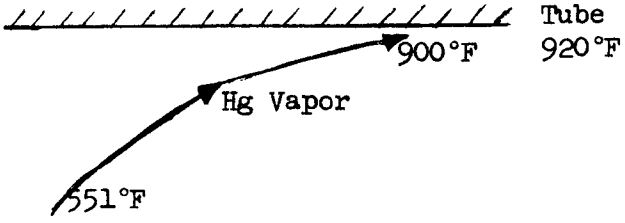

$$\Delta T_m = \frac{(920 - 551) - (920 - 900)}{\ell n\ (920 - 551)/(920 - 900)} = 130$$

$$q = \dot{m}\ C_p \Delta T = \frac{(5 \times 10^{-2}\ \text{gm/sec})(3600\ \text{sec/hr})(0.0249\ \text{BTU/lb °F})(900 - 551)}{454\ \text{gm/lb}}$$

$$q = 3.45\ \text{BTU/hr}$$

$$A = \frac{q}{h \Delta T_m} = \frac{(3.45\ \text{BTU/hr})}{(0.235\ \text{BTU/hr ft}^2\ \text{°F})(130\ \text{°F})}$$

$$A = 0.113\ \text{ft}^2$$

$$L = (\text{length of superheater}) = A/\pi D$$

$$L = \frac{(0.113\ \text{ft}^2)(144\ \text{in}^2/\text{ft}^2)}{\pi\ (1\ \text{inch})}$$

This cesium superheater length was the size actually used in the system.

To calculate the heat input into the superheater, it is assumed that a one inch layer of Kaowool is used as an insulation medium, and the insulation outside temperature will be 100°F.

$$q_{loss} = \frac{2\pi kL\ T}{\ell n\ r_o/r_i}$$

Where r_i = the radius from the center of the tube to the outside wall

r_o = the radius from the center of the tube to the outside of the insulation.

L = 24 inches (or 2 ft) will be used for this calculation to obtain the maximum heat loss expected.

$$q_{loss} = \frac{2\pi(0.030\ \text{BTU/hr ft °F})(1080 - 100)\text{F}\ (2\ \text{ft})}{\ell n\ (1.5)/(5)}$$

$$q_{loss} = 335\ \text{BTU/hr} = 98.5\ \text{watts}$$

This is the maximum heat input that must be supplied to the superheater to have it effectively operate within the design range.

Desuperheater Design Calculations

The purpose of the desuperheater will be to cool the cesium vapor from 1080 to 840°F (under some flow conditions), and both cesium and mercury vapors from 900 to 840°F under other flow conditions.

The maximum temperature drop will be 1080 - 840°F = 240°F. The desuperheater will be designed for this requirement.

$$q = \dot{m}\ C_p \Delta T \qquad \text{(C-12)}$$

$$q = \frac{(5 \times 10^{-2}\ \text{gm/sec})(3600\ \text{sec/hr})(0.0665\ \text{BTU/lb °F})(240\text{°F})}{(454\ \text{gm/lb})}$$

$$q = 6.34\ \text{BTU/hr}$$

This is the rate of heat loss that the desuperheater must accommodate.

If the heat transfer coefficient (h) = 0.135 BTU/hr ft^2 °F and a one inch tube is used, the length of the desuperheater (L) is:

$$L = A/\pi D$$

$$A = Q/h\triangle T_m$$

or

$$L = q/h\triangle T_m \pi D$$

To calculate $\triangle T_m$, the following temperature profile will be assumed.

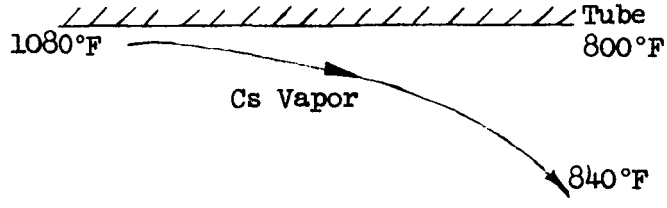

$$\triangle T_m = \frac{(1080 - 800) - (840 - 800)}{\ln (1080 - 800)/(840 - 800)}$$

$$L = \frac{(6.34 \text{ BTU/hr})(144 \text{ in}^2/\text{ft}^2)}{(0.135 \text{ BTU/hr ft}^2 \text{ °F})(1238)\ \pi\ (1 \text{ in.})} = 17.6 \text{ inches}$$

If either this length of the desuperheater, or the superheater length is physically too long to handle, the superheat temperature can be lowered from 1080°F to 1000°F. This will result in a shorter superheater and desuperheater length.

Condenser Collection Pot Design Calculations

The largest volume to be attained reasonably in the condenser would correspond to a height of 8 + 1 = 9 inches. For a two inch diameter cylindrical vessel this volume corresponds to:

$$V = \frac{\pi D^2}{4} h \qquad (C\text{-}7)$$

$$V = \frac{\pi(4)(9)}{7} = 28.4 \text{ in}^3$$

The tank was arbitrarily made four inches in diameter and four inches high. The volume corresponds to:

$V = \pi(16)(4)/4 = 50.3 \text{ in}^3$ which is more than that actually required.

Summary of Calibration Rig Design

This section of the report considers the design of a flow system to test and to calibrate the vapor flow meter over a flow range of 5×10^{-2} to 10^{-4} gm/sec. The pressure range for the cesium system is 25 to 1 torr and for the mercury system is 1 to 0.1 torr.

The flow system chosen for this purpose utilizes a pot boiler, superheater, orifice, desuperheater, and a condenser. For mercury one orifice with a 0.0160 inch diameter is applicable. This orifice as well as one with a 0.0440 diameter is required for the cesium tests. The system pressures (upstream of the orifice) will vary from 135 torr to 1.75 torr. Figure A-1 is a schematic diagram of the flow system.

APPENDIX D
ORIFICE CALIBRATION PROCEDURE

System Requirements

A system of critical orifices was selected to serve as a means of continuous calibration for the anemometer vapor flow meter. The orifice must monitor cesium and mercury vapor at flow rates ranging from 10^{-4} gm/sec to 5×10^{-2} gm/sec at temperatures of 840°F and pressures ranging from 0.1 to 1 torr for mercury and 1 to 25 torr for cesium.

The metering orifices chosen for this requirement operate with choked flow, where the mass flow rate is dependent upon the upstream pressure and temperature. The pressure ratio across the orifice must be:

$$P_D/P_I \leq \left(\frac{2}{k+1}\right)^{k/(k-1)} \qquad \text{(D-1)}$$

where P_I = inlet or upstream pressure, lb_f/ft^2

P_D = discharge or downstream pressure, lb_f/ft^2

$k = C_p/C_v$

C_p = heat capacity at constant pressure, $BTU/lb_m\ °F$

C_v = heat capacity at constant volume, $BTU/lb_m\ °F$

For an ideal gas (which includes cesium and mercury superheated vapor)

$$C_p/C_v = 1.67 = k$$

and

$$P_D/P_I = 0.485$$

The mass flow rate of a gas across an orifice designed for choked flow is:

$$\dot{m} = \sqrt{\frac{gk}{R}\left(\frac{2}{k+1}\right)^{(k+1)/(k-1)}}\ \frac{P_I}{\sqrt{T}}\ AC_D \qquad \text{(D-2)}$$

where $\dot{m}$ = mass flow rate, $lb_m/sec.$

g = dimensional constant, 32.2 ft lb_m/lb_F sec^2

R = gas constant, lb_f ft/lb_m °F

T = absolute gas temperature, °R

A = orifice area, ft^2

C_D = orifice discharge coefficient

With reference to Figure C-3, it may be seen that the orifice coefficient (C_d) is not a constant number. For P_D/P_I equal to, or less than 0.2, the numerical value of C_D remains essentially constant. As the ratio increases from 0.2 to 0.485 (the maximum pressure ratio for a critical system) the C_D value changes approximately 15 per cent. Therefore, it is important that the flow conditions experienced in the calibration system be the same as those expected in the meter test system.

Over the entire mercury flow range the maximum P_D/P_I ratio is less than 0.2; therefore, in calibrating the orifice it is only necessary to maintain the pressure ratio at a maximum of 0.2. Detail measurements of this number are not necessary.

Over the cesium flow range the P_D/P_I ratio will range from 0.485 to less than 0.2. Here the orifice coefficient will vary and it is necessary in the calibration procedure to maintain the same pressure conditions across the orifice as are expected to exist in the meter system.

Calibration Measurements

Equation (D-2) for mercury can be written as:

$$\dot{m}_{Hg} = C_{Hg} \frac{P_{Hg}}{\sqrt{T_{Hg}}} A C_D \qquad \text{(D-3)}$$

where $$C_{Hg} = \sqrt{\frac{g k_{Hg}}{R_{Hg}} \left(\frac{2}{k_{Hg} + 1}\right)^{(k_{Hg} + 1)/(k_{Hg} - 1)}}$$

P_{Hg} = Mercury vapor pressure at the orifice inlet

T_{Hg} = Absolute temperature of the mercury vapor

For the calibration procedure, argon was used as the test fluid. Equation (D-1) for argon is then written as:

$$\dot{m}_A = C_A \frac{P_A}{\sqrt{T_A}} AC_D \qquad \text{(D-4)}$$

where the argon symbols here have the same denotation as those indicated for mercury in equation (D-3).

Dividing equation (D-3) by equation (D-4) results in:

$$\dot{m}_{Hg}/\dot{m}_A = \frac{C_{Hg} P_{Hg} \sqrt{T_A}}{C_A P_A \sqrt{T_{Hg}}} \qquad \text{(D-5)}$$

If in the calibration procedure the pressure of the argon is set equal to the mercury pressure, (i.e., $P_A = P_{Hg}$) (D-6)

Equation (D-5) is reduced to:

$$\dot{m}_{Hg}/\dot{m}_A = \frac{C_{Hg} \sqrt{T_A}}{C_A \sqrt{T_{Hg}}} \qquad \text{(D-7)}$$

or

$$\dot{m}_{Hg} = \dot{m}_A \frac{C_{Hg} \sqrt{T_A}}{C_A \sqrt{T_{Hg}}} \quad \text{or} \quad \dot{m}_{Hg} = \dot{m}_A K \frac{\sqrt{T_A}}{\sqrt{T_{Hg}}} \quad \text{where } K = C_{Hg}/C_A$$

A similar flow equation relating cesium to argon flow rates can also be written as:

$$\dot{m}_{Cs} = \dot{m}_A \frac{C_{Cs} \sqrt{T_A}}{C_A \sqrt{T_{Cs}}} \qquad \text{(D-8)}$$

where $P_{Cs} = P_A$ (D-9)

Evaluation of Constants

The numerical evaluation of constants presented in Equations (D-6) and D-7) are evaluated as follows:

For mercury:

$$C_{Hg} = \sqrt{\frac{gk}{R}\left(\frac{2}{k+1}\right)^{(k+1)/(k-1)}}$$

$k = 1.67$

$R = 1545/M$

M = gas formula weight = 201

$R = 1545/201 = 7.68\ lb_f\ ft/lb_m\ °F$

$$C_{Hg} = \sqrt{\left[\frac{(32.2)(1.67)}{(7.68)}\right]\left[\frac{2}{(1.67+1)}\right]^{(1.67+1)/(1.67-1)}}$$

$C_{Hg} = 1.52$

The temperature of the mercury vapor flowing across the orifice will be 840°F:

$$\sqrt{T_{Hg}} = \sqrt{840 + 460} = 36$$

For argon:

$k = 1.67$

$R = 1545/39.9 = 38.8\ lb_f\ ft/lb_m\ °F$

where $M_A = 39.9$

$$C_A = \sqrt{\left[\frac{(32.2)(1.67)}{(38.8)}\right]\left[\frac{2}{(1.67+1)}\right]^{(1.67+1)/(1.67-1)}}$$

$C_A = 0.659$

Equation (D-7) is then reduced to:

$$\dot{m}_{Hg} = \dot{m}_A \frac{(1.52)\sqrt{T_A}}{(0.659)(36)} = 0.0643\ \dot{m}_A \sqrt{T_A} \qquad \text{(D-10)}$$

or

$$\dot{m}_{Hg} = 6.43 \times 10^{-2}\ \dot{m}_A \sqrt{T_A}$$

For cesium:

$$k = 1.62^{(1)}$$

$$M = 140$$

$$R = 1545/140 = 11.0\ \text{ft/°R}$$

$$C_{Cs} = \sqrt{\left[\frac{(32.2)(1.62)}{(11.0)}\right]\left[\frac{2}{(1.62+1)}\right]^{(1.62+1)/(1.62-1)}}$$

$$C_{Cs} = 1.24$$

The temperature of the cesium vapor across the orifice will be 1000°F or 1460°R.

$$\sqrt{T_{Cs}} = \sqrt{1460} = 38.2$$

This reduces Equation (D-8) to:

$$\dot{m}_{Cs} = \dot{m}_A \frac{(1.24)\sqrt{T_A}}{(0.659)(38.2)}$$

$$\dot{m}_{Cs} = 4.93 \times 10^{-2}\ \dot{m}_A \sqrt{T_A} \qquad \text{(D-11)}$$

During the argon calibration tests, the gas flow rate ($\dot{m}_A$), gas temperature (T_A), and upstream orifice pressure (P_A) will be recorded. This data will be plotted in the form of:

---

[1] Data taken from WADD TR 61-96

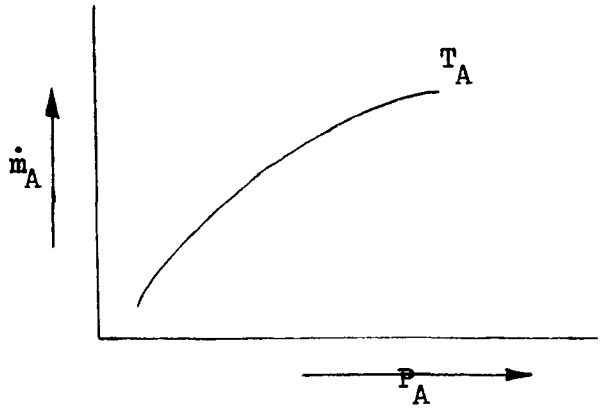

Experimental Procedure

A schematic diagram of the experimental apparatus is presented in Figure D-1. A pictorial diagram of this apparatus is shown as Figure D-2. The following procedure was used to calibrate the orifice:

1. Initially valves 5, 4, 3, 2, 12, 13, 10, 8 and 7 are opened and the vacuum pump is turned on to remove all the air from the lines.
2. All valves with the exception of No. 4 are closed. Valve No. 4 serves as a vernier regulator for controlling argon flow rate from the pressure tank to the orifice. Vapor flow through the orifice is stopped or started by opening or closing valve No. 3.
3. The argon supply is fed into the pressure tank by opening valve No. 1. The pressure level to which the tank is filled is governed by anticipated upstream and downstream orifice pressure levels. These will vary from 135 torr upstream pressure to 0.1 torr downstream pressure. (Reference Appendix C)

The tank pressure must be sufficiently higher than the upstream orifice pressure so that during the calibration run the argon pressure supply is not depleted to the extent that a minimal pressure difference exists between the orifice inlet and argon tank. If this was to occur a constant velocity and upstream orifice pressure would not be maintained and the calibration experiment would be meaningless.

There is also a maximum pressure level to which the tank can be filled. The mass flow rate through the system is obtained from the following expressions.

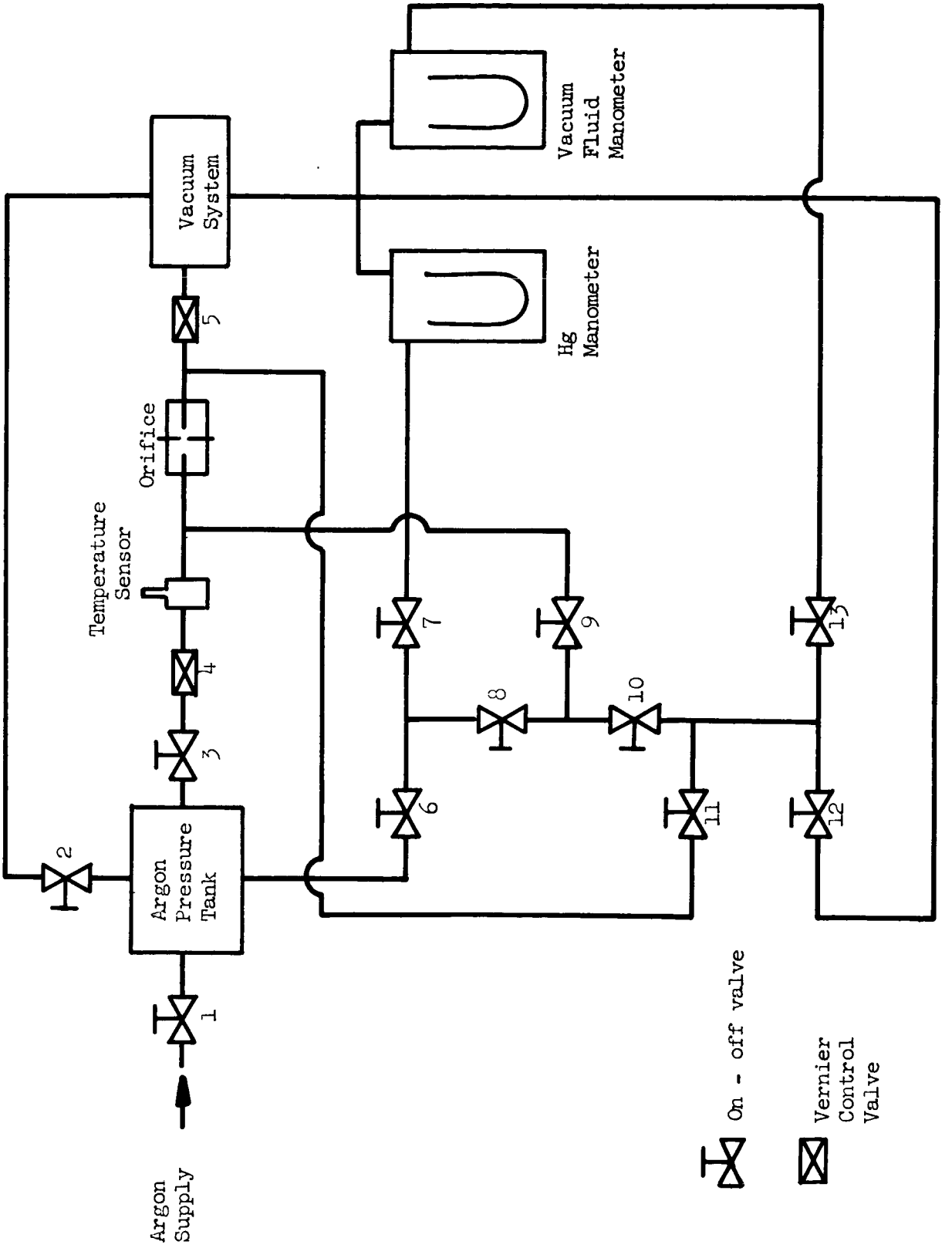

Figure D-1
Calibration System Schematic Diagram

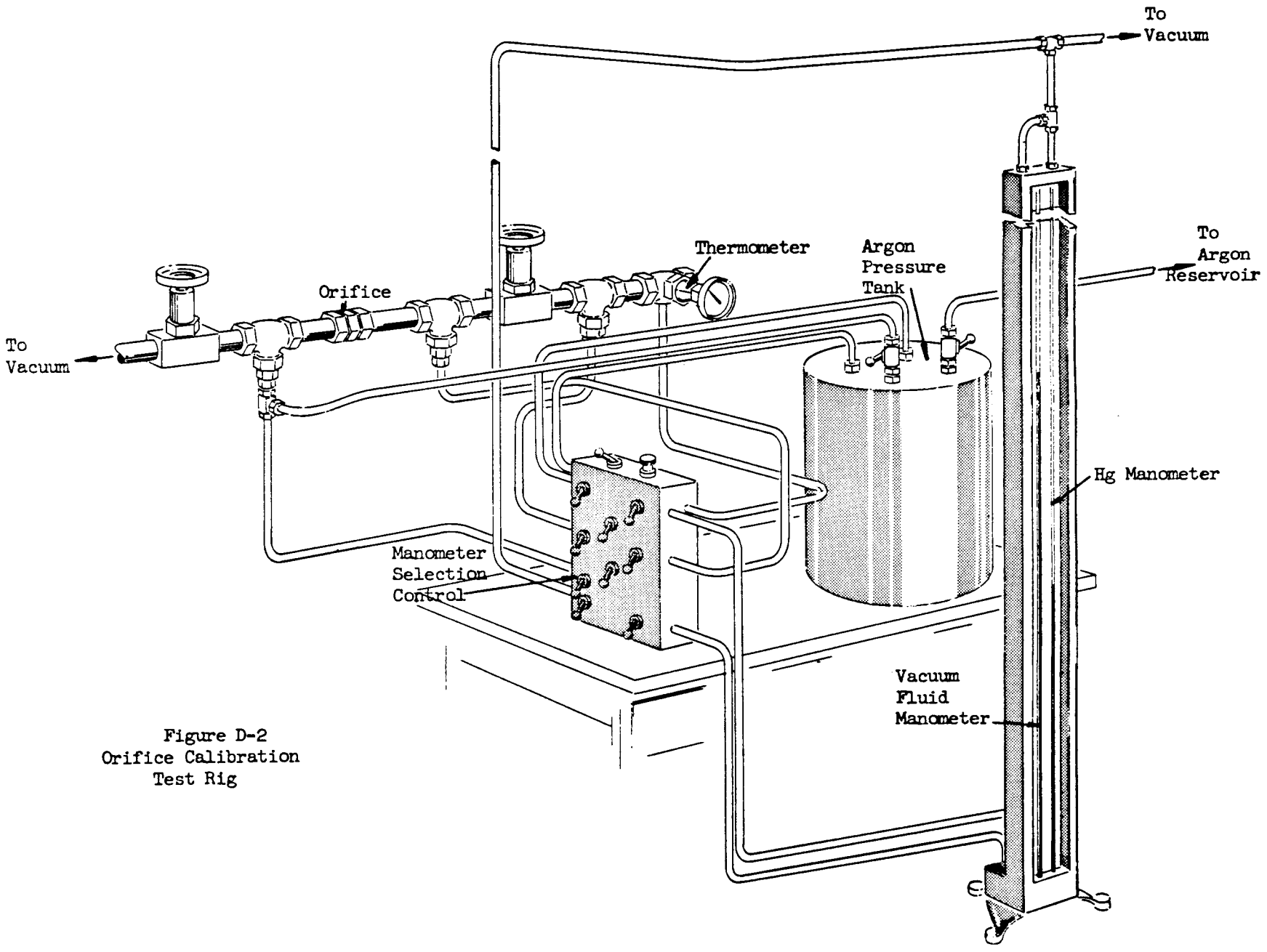

Figure D-2
Orifice Calibration
Test Rig

$$P_i = \frac{n_i RT}{V}$$

where P_i = initial tank pressure, lb_f/ft^2

n_i = initial number of lb moles of gas present

R = gas constant, lb_f ft/lb_m mole °R

T = absolute gas temperature, °R

V = tank volume, ft^3

and

$$P_f = \frac{n_f RT}{V} \qquad \text{(D-13)}$$

where P_f = final tank pressure, lb_f/ft^2

n_f = final number of lb moles of gas present

$$P_i - P_f = (n_i - n_f)\, RT/V$$

or

$$n_i = n_f = \frac{(P_i - P_f)\, V}{RT} \qquad \text{(D-14)}$$

If this process is carried out over a finite period of time (t) equation (D-14) becomes

$$\frac{n_i - n_f}{t} = \frac{(P_i - P_f)\, V}{RT\, t} = \dot{w} \qquad \text{(D-15)}$$

where $\dot{w}$ = mass flow rate in lb moles/unit time.

$$\dot{w}\, M = \dot{m} \qquad \text{(D-16)}$$

where M = gas formula weight

$\dot{m}$ = mass flow rate, lb_m/unit time

If the numerical value of $P_i - P_f$ is small (which may occur if there is a large quantity of gas initially present) the accuracy of this measurement, and the subsequent accuracy of the calculated flow rate, will be considerably reduced. Therefore, in filling the argon tank, the pressure must be between these two discussed limits. The numerical values of these limits is dependent upon the desired upstream orifice pressure.

For each calibration run, the initial quantity of argon may have to be determined experimentally. Valve No. 2 serves as a bleed off outlet, to help regulate the argon tank pressure.

4. Measure the argon pressure in the tank using either the mercury manometer or the vacuum fluid manometer.

Both test manometers for this system are of the well type -- each having one indicating leg. The mercury manometer will operate over a pressure range of 0 to 2560 torr, and the vacuum fluid manometer is applicable over a 0 to 188 torr range. By arranging the proper combination of valves either the high pressure or the low pressure manometer can be set to read the argon tank pressure, upstream orifice pressure, or downstream orifice pressure.

5. Arrange valve combinations so that either the mercury manometer or the vacuum fluid manometer will indicate upstream orifice pressure.
6. Open valve 3, and adjust 4 to the desired upstream pressure.
7. Rearrange manometer valve settings for downstream orifice pressure indication.
8. Adjust valve 5 for proper downstream pressure. (It may be necessary to repeat steps 6, 7, and 8 several times so that upstream and downstream orifice pressures are at prespecified levels).
9. Close valve 3, and proceed to take data in the following manner:
   a. At the beginning of the experiment the pressure level in the argon tank is measured and recorded.
   b. Valve 3, is opened and the upstream and downstream orifice pressures are recorded.
   c. Make note of gas temperature.

d. For the length of the run (which will tentatively be for five minutes) valve 4 is continually adjusted so that the upstream orifice pressure remains constant during the length of the test. As long as the downstream pressure is sufficiently low that:

$$P_D/P_I = \frac{2}{k+1}^{k/(k-1)} \qquad \text{(D-1)}$$

the critical flow condition will remain across the orifice and equation (D-2) can be used to calculate the orifice coefficient (C_D).

e. At the end of the test period valve 3 is closed and the pressure level in the argon tank is again recorded. The difference in the measurements between steps a and e is the measurement of the mass flow.

f. Using equations (D-7) or (D-8) the mass flow rates of either mercury or cesium is calculated for the specific orifice in the test system.

A graphical presentation of this data for both mercury and cesium flow rates is presented in Appendix B of this report.

Design Calculations for Argon Pressure Tank

$$P\,V = nRT$$

where P = system pressure, lb_f/ft^2

V = system (tank) volume, ft^3

n = number of lb moles of gas present

R = universal gas constant

1.55×10^3 (lb_f/ft^2) $ft^3/°R$ lb mole

T = system temperature, °R

For design calculations a flow rate of 5×10^{-2} gm/sec will be used.

The formula weight of argon is 39.9

$$\dot{w} = \frac{5 \times 10^{-2} \text{ gm/sec}}{(4.54 \times 10^{2} \text{ gm/lb})(3.99 \times 10)} = 0.277 \times 10^{-5}$$

$$\dot{w} = 2.77 \times 10^{-6} \text{ lb moles of argon/sec}$$

$$T = 70°F = 530 \text{ °R}$$

The system will be designed to deliver a 100 torr pressure drop over a calibration period of five minutes.

Let P_1 = the initial pressure of the system

P_2 = the final pressure of the system

$$P_1 - P_2 = (n_1 - n_2) \frac{RT}{V} = 100 \text{ torr}$$

$$n_1 - n_2 = (2.77 \times 10^{-6} \text{ lb moles/sec})(5 \text{ min})(60 \text{ sec/min})$$

$$n_1 - n_2 = 833 \times 10^{-6} = 8.33 \times 10^{-4} \text{ lb moles}$$

$$P_1 - P_2 = (100 \text{ torr})(2.78 \text{ lb/ft}^2 \text{ torr})$$

$$P_1 - P_2 = 2.78 \times 10^{2} \text{ lb}_f/\text{ft}^2$$

$$V = \frac{(n_1 - n_2) RT}{P_1 - P_2}$$

$$V = \frac{(8.33 \times 10^{-4})(1.55 \times 10^{3})(5.30 \times 10^{2})}{(2.78 \times 10^{2})} = 24.7 \times 10^{-1}$$

$$V = 2.47 \text{ ft}^3 \ (1.728 \times 10^{3} \text{ in}^3/\text{ft}^3) = 4.28 \times 10^{3} \text{ in}^3$$

The tank will be designed for a cylindrical geometry.

$$V = \frac{\pi D^2 h}{4} \qquad \text{(D-17)}$$

where D = tank diameter

h = tank height

Assume D = 16 inches

$$h = \frac{4V}{\pi D^2} = \frac{4\ (4.28 \times 10^3)}{\pi (16)^2}$$

h = 21 inches

A cylindrical tank 16 inches in diameter by 21 inches high was constructed for the argon pressure tank vessel.

Summary

A system of critical orifices has been chosen as a means of calibrating the heated fin anemometer vapor flow meter. For the mercury vapor flow range, one orifice (with a 0.0166 inch diameter) was used. This orifice plus one with a 0.044 inch diameter is required for the cesium flows.

To use an orifice it is necessary that its flow coefficient be known. An experimental system using argon gas is described which will provide the necessary data to calculate this number. Detail design concepts of the system and experimental operating procedures are also included.

APPENDIX E
LIST OF SYMBOLS

A = area, ft^2

B = convective heat transfer coefficient, BTU/hr ft^2/°F

c = circumference, ft

C = constant

C_D = orifice coefficient

C_p = specific heat, BTU/lb/°F

C_v = specific heat at constant volume, BTU/lb/°F

d = sphere diameter, ft

d_w = lead wire diameter, ft

D = support post diameter, ft

F = radiative view factor

g = dimensional constant (32.2 ft lb_m/lb_f sec^2)

G = flow rate, lb/sec

h = heat transfer coefficient, BTU/hr ft^2/°F

h = incremental height, ft

h_r = radiation heat transfer coefficient, BTU/hr ft^2/°F

i = current, amps

k = thermal conductivity, BTU/hr ft/°F

k = compressibility factor

k_f = vapor thermal conductivity, BTU/hr ft/°F

k_p = anemometer fin thermal conductivity, BTU/hr ft/°F

k_s = support post thermal conductivity, BTU/hr ft/°F

k_w = wire thermal conductivity, BTU/hr ft/°F

k_v = vapor thermal conductivity, BTU/hr ft/°F

K = thermal conductivity, BTU/hr ft/°F

K_1 = radiation constant, $°R^3$

ℓ = extension length, ft

L = length, ft

$\dot{m}$ = mass flow rate, gm/sec or lb/sec

M = formula weight

n = moles, lb_m/lb-molecular weight

Nu = Nusselt number

P = pressure, lb/ft^2

Pr = Prandtl number

q = heat transfer rate, BTU/hr

Q = radial flux, BTU/hr

Q = heat input, BTU/hr

Q_{gen} = heat generation in fin, BTU/hr

$Q_{w\ gen}$ = heat generation in wire, BTU/hr

r_i = inside annular radius, ft

r_o = outside annular radius, ft

R = gas constant, ft/°R

Re = Reynolds number

R_p = fin resistance, ohms

R_w = wire resistance, ohms

t = thickness, ft or in.

t = flow time, hrs

Δt = temperature change, °F

T = temperature, °F

T_v = vapor temperature, °F

ΔT_m = log mean temperature, °F

U = heat transfer coefficient, BTU/hr ft^2/°F

v_f = vapor velocity, ft/sec

V = linear vapor velocity, ft/sec

V = volume, ft^3

w = anemometer fin width, ft

$\dot{w}$ = mass flow rate, lb-moles/hr

x = characteristic linear dimension, ft or in.

x = increment anemometer fin length, ft

X = heat transfer distance, ft

z = anemometer fin thickness, ft

β = thermal expansion coefficient, $°R^{-1}$

θ = time, hrs

λ = latent heat, BTU/lb

μ = vapor viscosity, lb/ft/sec

μ_f = vapor viscosity, lb/ft/sec

ρ = vapor density, lb/ft^3

ρ_m = electrical resistivity, ohm-ft

σ = Stefan-Boltzman constant (1.73×10^{-9} BTU/hr $ft^2/°R^4$

ψ = heat flux product, BTU/hr/°F

APPENDIX F

REPORT DISTRIBUTION LIST FOR CONTRACT NO. NAS3-2515

NASA Lewis Research Center (1)
Spacecraft Technology Procurement Section
21000 Brookpark Road
Cleveland, Ohio 44135
Attention: John H. DeFord

NASA Lewis Research Center (1)
Technology Utilization Office
21000 Brookpark Road
Cleveland, Ohio 44135
Attention: John Weber

NASA Marshall Space Flight Center (1)
Huntsville, Alabama
Attention: M-RP-DIR/Dr. E. Stuhlinger

NASA Headquarters (2)
FOB-10B
600 Independence Avenue, Southwest
Washington, D. C. 20546
Attention: RNT/James Lazar

Commander (1)
Aeronautical Systems Division
Wright-Patterson Air Force Base, Ohio
Attention: AFAPL (APIE)/Lt. Robt. Supp

Jet Propulsion Laboratory (1)
4800 Oak Grove Drive
Pasadena, California
Attention: J. J. Paulson

Electro-Optical Systems, Inc. (2)
125 North Vinedo Avenue
Pasadena, California
Attention: R. C. Speiser

General Electric Company (2)
Flight Propulsion Laboratory
Cincinnati, Ohio 45215
Attention: M. L. Bromberg

Ion Physics Corporation (2)
Burlington, Massachusetts
Attention: Dr. S. V. Nablo

Space Technology Laboratories (2)
8433 Fallbrook Avenue
Canoga Park, California
Attention: Dr. D. Langmuir

AFWL (2)
WLPC/Capt. C. F. Ellis
Kirtland Air Force Base
New Mexico

NASA Lewis Research Center (1)
21000 Brookpark Road
Cleveland, Ohio 44135
Attention: Reports Control Office

North American Aviation, Inc. (1)
12214 Lakewood Avenue
Downey, California
Attention: Technical Information Office
Department 4096-314

NASA Lewis Research Center (2)
Library
21000 Brookpark Road
Cleveland, Ohio 44135

Aerojet-General (2)
Nucleonics Division
San Ramon, California
Attention: Mr. J. S. Luce

Hughes Research Laboratories (2)
Malibu Canyon Road
Malibu, California
Attention: Dr. G. R. Brewer

NASA Lewis Research Center
Spacecraft Technology Division
21000 Brookpark Road
Cleveland, Ohio 44135
Attention: J. H. Childs (2)
R. Hieber (7)

United Aircraft Corporation (2)
Research Laboratories
East Hartford 8, Connecticut
Attention: R. J. Meyerand, Jr.

NASA Lewis Research Center
Electromagnetic Propulsion Division
21000 Brookpark Road
Cleveland, Ohio 44135
Attention: W. R. Mickelsen (1)
W. Moeckel (2)

Westinghouse Astronuclear Laboratories (2)
Pittsburgh, Pennsylvania 15234
Attention: Electric Propulsion Lab.
Mr. W. H. Szymanowski

NASA Scientific and Technical Information Facility (6 + 1 Reproducible Master)
Box 5700
Bethesda, Maryland 20014
Attention: NASA Representative RQT-2448

Aerospace Corporation (2)
P. O. Box 95085
Los Angeles, California 90045
Attention: Library Technical Documents Group

TRW Electromechanical Division (1)
Thompson Ramo Wooldridge, Inc.
23555 Euclid Avenue
Cleveland, Ohio 44117
Attention: R. T. Craig